Design, Fabrication, and Testing of an Apparatus for Mechanical Properties Characterization of Nb_3Sn Superconducting Wires

Submitted By
David Bader

In partial fulfillment of the requirements for the degree of

MASTER OF SCIENCE IN MECHANICAL ENGINEERING

School of Engineering
Tufts University
Medford, Massachusetts

May 2012

Author: David Bader
Department of Mechanical Engineering
Tufts University

Certified By: Dr. Luisa Chiesa
Assistant Professor
Department of Mechanical Engineering
Tufts University
Research Advisor

Certified By: Dr. Makoto Takayasu
Research Scientist
Plasma Science and Fusion Center,
MIT

Certified By: Dr. Gary Leisk
Lecturer and Research Assistant
Professor
Department of Mechanical Engineering
Tufts University

ABSTRACT

Multifilament Nb_3Sn superconducting wires are of interest for building high-magnetic field superconducting magnets. The superconducting A15 phase Nb_3Sn is formed after applying one or more heat treatments with a temperature above 650°C. This phase is very brittle and failure of the filaments occurs. This results in degradation of the performance characteristics of the wire and the superconducting magnet. Finite element analysis (FEA) is used to predict the behavior of a full-size cable comprised of thousands of individual wires. Due to the complex composite structure of a wire and the varying stages of plasticity of each material, mechanical property estimations such as the rule of mixtures (ROM) are not accurate. Experimental tensile testing is required for accurate measurements of the mechanical properties of the composite. This thesis discusses the design, fabrication, and testing of a tensile testing apparatus for characterizing the mechanical properties of Nb_3Sn strands and cables. Measurements were performed on Nb_3Sn strands from different manufacturers at room temperature, but the device has the capability of measuring properties of multi-strand cables and can be used at cryogenic temperatures. From the stress-strain curves of the tested wires, the following mechanical properties were evaluated: modulus of elasticity, proof strength, tensile strength, and elongation to fracture. The scatter of the measured values was analyzed to measure the COV, the standard deviation divided by the average, and compared against similar superconducting wire tensile testing machines from literature.

ACKNOWLEDGMENTS

I would first like to thank my advisor, Professor Luisa Chiesa, for all of her guidance and support. She has taught me so much about designing and executing experiments and presenting academic work effectively. The two years I spent under her guidance have tested me and taught me valuable lessons about myself. Working with her has given me confidence that with dedication and hard work I can be very successful.

I would also like to thank my other committee members, Makoto Takayasu and Professor Gary Leisk. Their advice and comments helped shape my research and thesis work and helped me to consider new challenges and solutions for my work.

Thanks are also due for everyone, students and staff, at Bray Laboratory for their support and advice. Without Vinny Miraglia and James Hoffman, my apparatus would never have been completed in time. My lab mates in the superconducting lab Phil, Tiening, Joe, Amy, and Nate were essential to my mental sanity during the last stressful moments of the thesis. They were always available to offer good conversation and encouraging words of support.

Lastly, I owe many great thanks to my friends and family for encouraging and motivating me through my graduate studies. Without you, this process would have been almost much more difficult to handle. Special thanks go to my wonderful girlfriend, Alex, for all her support and encouragement and for being willing to listening to me talk about my research nonstop for the past many months.

This work was supported in part by the U.S. Department of Energy under GRANT DE-SC0004062

TABLE OF CONTENTS

LIST OF TABLES

LIST OF FIGURES

Design, Fabrication, and Testing of an Apparatus for Mechanical Properties Characterization of Nb_3Sn Superconducting Wires

1.0 Introduction

Superconductivity was discovered in the early 1900s and since its discovery physicists have searched for applications that could be improved with the integration of superconducting magnets. One such application that is gaining much attention today is fusion reactors. Fusion energy production has been sought after since the first fusion experiments in the 1930s, but no reactor has ever been able to reach the "breakeven point" – the point at which more energy is expelled than it consumes. Today, in an attempt to demonstrate the viability of nuclear fusion for energy production, seven major countries are cooperating on an international project to construct a 500 MW output fusion reactor in Cadarache in southern France [1–3]. The ITER project will utilize a tokamak – a donut shaped vacuum vessel – to confine and heat a plasma of deuterium and tritium ions to achieve nuclear fusion. The design requires many large, powerful superconducting magnets to circulate the plasma and to keep it away from the walls of the containment vessel. Conventional resistive copper magnets could be used for this purpose, but would require inordinate amounts of electric power and structural support to produce a large enough magnetic field. The ITER project is the motivation for much of the research surrounding superconducting materials today, including the work presented here.

The superconducting material selected for these electromagnets is niobium-tin, Nb_3Sn, because of its ability to sustain high magnetic fields. Current-carrying performance of Nb_3Sn, however, is very susceptible to strain and can result in a

magnet being unable to reach the magnitude of magnetic field it had been designed for. There are currently many investigations into various forms of strain that Nb_3Sn must handle during magnet operation, including axial strain, bending strain, and transverse strain [4–8]. Finite element analysis (FEA) is used to predict the amount of strain on a wire under a set of given conditions. However, in order to accurately predict the material behavior, the models used in FEA must be provided with accurate mechanical material properties of the cable [9]. This can prove to be difficult because of the complex structure of the cable.

A typical cable is composed of thousands of strands, each of which is complex unto itself. Approximations can be made to attempt to analytically determine the overall properties of the cable, however, the accuracy of these approximations becomes suspect when the complexity of the cable structure is considered. A cable is a multi-stage, composite structure with a non-constant cross-section, components that may vary position along the length of the cable and may exhibit elasto-plastic behavior. Experimental testing offers a simpler and more assured way of characterizing the mechanical properties of these wires. Experimental testing is not without its own challenges too; Nb_3Sn becomes very brittle in its superconducting A15 phase and there are currently no established standard test procedures for testing this material.

1.1 Thesis goal

This work seeks to design, validate, and test a tensile testing apparatus for the purpose of accurately determining the material properties of Nb_3Sn single strands

and three-strand triplets at cryogenic temperatures. While the apparatus will be designed to meet all of these goals, the testing performed in the scope of this thesis will only include single strand samples at room temperature.

1.2 Scope

In the following section, a background on superconductivity, mechanical properties testing, Nb_3Sn wires, and a discussion of similar testing that has been performed by other research groups will be provided. Next, the test apparatus designed for these experiments, including the design requirements, major component details, and validation with reference material will be discussed. Lastly, results from preliminary tests conducted on superconducting wire samples and compare them to results from other research groups will be presented. These tests were limited to single strands of Nb_3Sn wire at room temperature.

2.0 Background

2.1 Brief History of Superconductivity

Superconductivity is a property exhibited by some materials in which the material has zero electrical resistance. Superconductivity was first discovered by Kamerlingh Onnes in 1911 when he discovered that the resistivity of mercury dropped to practically zero when chilled to a temperature below 4.2 K. Compared to their resistive equivalents, superconducting magnets have much less resistive losses and higher current density capacity. A copper wire of 1 mm^2 cross-section can carry about 5 Ampere of current, while a superconducting wire of the same size might carry 1000 Ampere or more – 200 times greater than copper. Reasons such as these make superconductors ideal for large magnetic field applications. Superconductors are not without their drawbacks; however. Superconducting materials only exhibit this resistance-free behavior below certain conditions of temperature, applied magnetic field, and current. These conditions describe what is called a "critical surface (Figure 1)". When the critical surface is breached -- either by exceeding any of the critical conditions individually or combined-- the material returns to a normal resistive state [2].

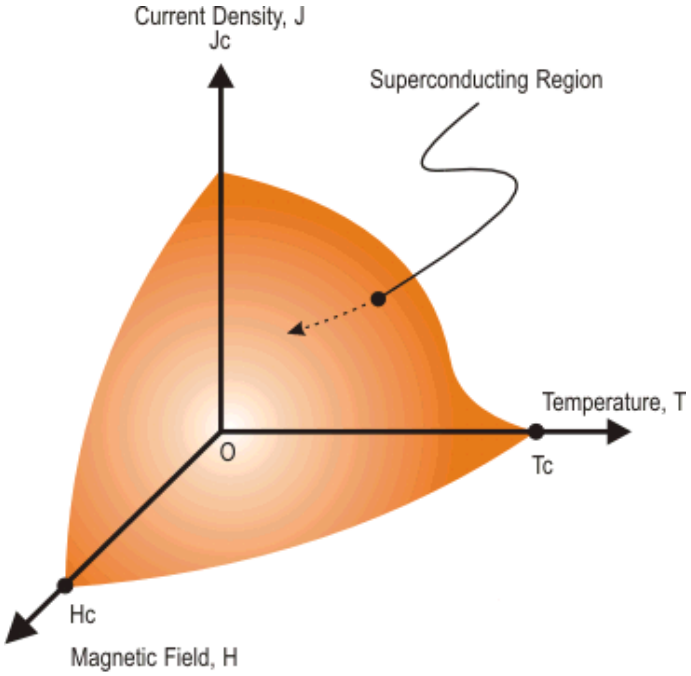

Figure 1: Critical surface defined by current, temperature, and field

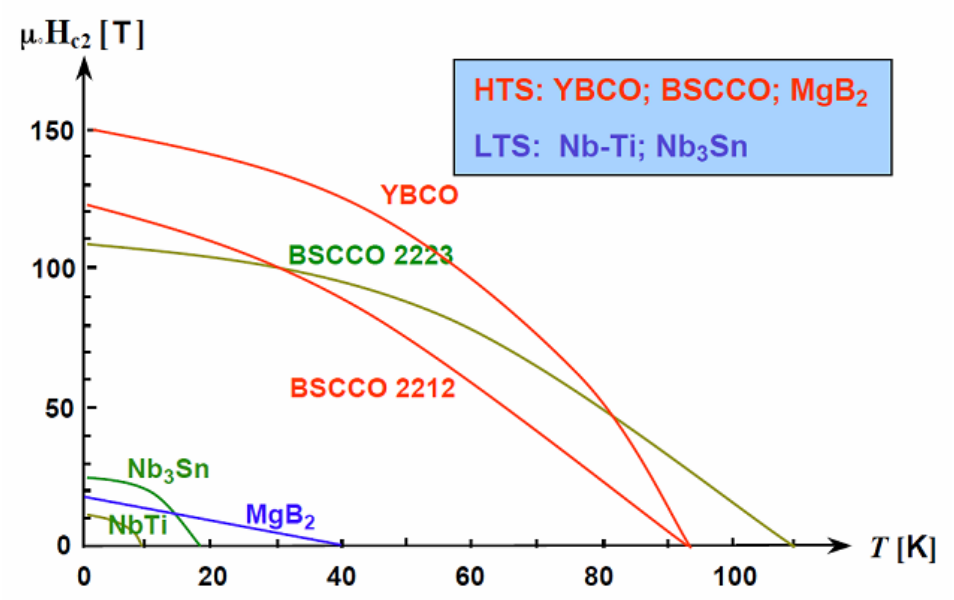

Figure 2 : Critical Surface at zero current [10].

Superconducting materials are classified into two fields, those that have a critical temperature above 77 K and those that have one below 77 K. The former are called high temperature superconductors, HTS, and the latter, low temperature superconductors, LTS. The distinction is made at 77 K because this is the boiling temperature of liquid nitrogen. Once in its liquid form, nitrogen will never reach a temperature above its boiling point. This makes it an ideal environment to operate high temperature superconductors. A cryogen with a lower boiling point is required to achieve temperatures low enough to meet the superconducting critical temperatures of LTS materials. Liquid helium has a boiling point of 4.2 K and is the cryogen of choice for many LTS applications.

Superconductors can be broken up into two types: Type I and Type II. Type I superconductors transition immediately from a superconducting to a normal resistive state as the applied magnetic field around it increases (Figure 3).

Alternately, Type II superconductors enter a "mixed state" where they are both partially superconducting and normal (Figure 4). This mixed state does also transition to a normal resistive state, but occurs gradually and at higher magnetic fields. This means that a Type II superconductor is able to maintain superconductivity up to higher magnetic fields than a Type I superconductor and is more useful for magnet applications [11].

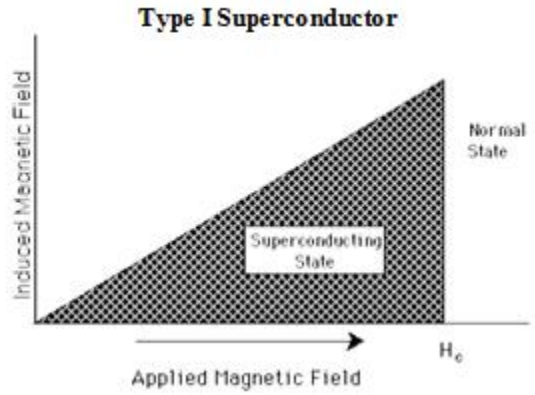

Figure 3: Type I superconductor behavior in applied magnetic field

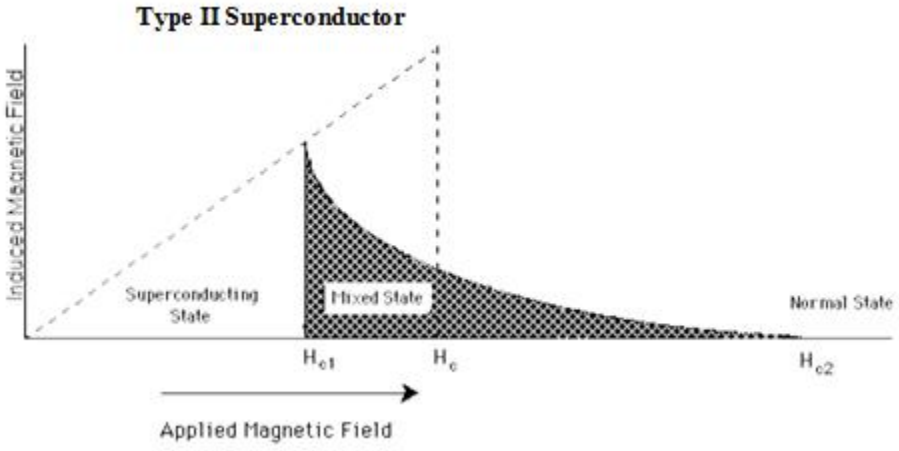

Figure 4: Type II superconductor behavior in applied magnetic field

2.2 ITER Project

The ITER Project is a multinational effort to build a nuclear fusion reactor in Cadarache, which is located in southern France. Hydrogen ions, deuterium and tritium, will be fused together in a fusion reaction that produces helium, neutrons and energy. This reaction requires extremely high temperatures to occur, near 150 million degrees Celsius. At such extreme temperatures, gas becomes plasma, a hot, electrically charged gas. To confine the plasma, powerful superconducting electromagnets are used to suspend the plasma away from the walls of the reactor core. This is possible because the helium nuclei produced in the fusion reaction is electrically charged and can be influenced by magnetic fields. The plasma is confined in a donut-shaped vacuum vessel called a tokamak (Figure 5).

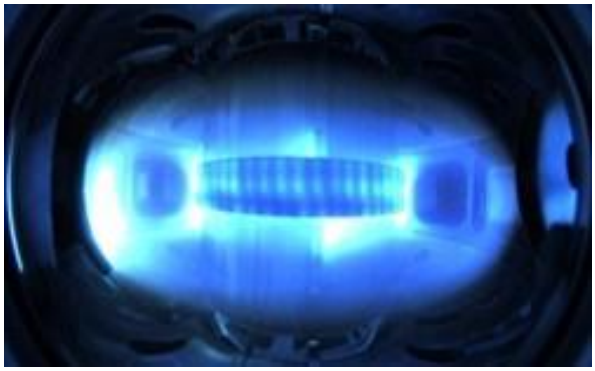

Figure 5: Tokamak plasma confinement

2.3 Superconducting magnets

Two superconducting materials of interest for magnet design are niobium-titanium, NbTi, and niobium-tin, Nb_3Sn. Previously, NbTi has been favored over Nb_3Sn in superconducting magnet design because its performance is independent of strain, unlike the latter. The magnets that confine the plasma in ITER's tokamak core require magnetic fields higher than the critical field of NbTi.

Therefore, the magnets will need to use Nb_3Sn. The critical field for Nb_3Sn is 24.5 T at 4.2 K, while that of NbTi is 10.5 T.

2.4 Superconducting Cables

Superconducting cables are not made of bulk material; rather their geometry is a complex series of windings of composite wire material. A cable is made of more than 1000 strands, each strand about 1mm in diameter. Each strand is composed of superconducting material filaments 3-50 μm in diameter embedded in a copper matrix. The copper matrix provides structural support to the superconducting filaments and draws away current to protect the superconductor from overheating in case superconductivity is lost. The strands are twisted when manufacturing the cable to reduce coupling currents and AC losses.

2.4.1 Wire Design

There are several ways to manufacture Nb_3Sn wires. The most common methods are Bronze route, Internal Tin, and Powder in Tube (PIT). All three of these methods combine niobium filaments and tin in a copper casing and require a heat treatment process to chemically react the niobium and tin to form the superconducting compound, Nb_3Sn.

2.4.1.1 *Bronze route*

The Bronze route process (Figure 6) involves embedding niobium filaments in a matrix of bronze, hence its name. Tin elements within the bronze react with the niobium during heat treatment. The diffusion process in contained by a barrier of tantalum and structural support is provided by a copper sheathing.

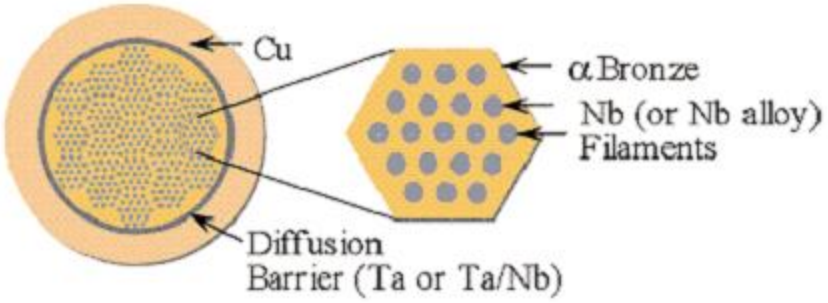

Figure 6: Bronze process [12]**.**

2.4.1.2 *Internal tin*

In the Internal tin process (Figure 7), niobium filaments are placed in a copper matrix around a filament of tin. Like the bronze route, a tantalum barrier is used to control diffusion. Tantalum may be placed around all the filaments together, like in the bronze route process, or around each filament sub-bundle individually.

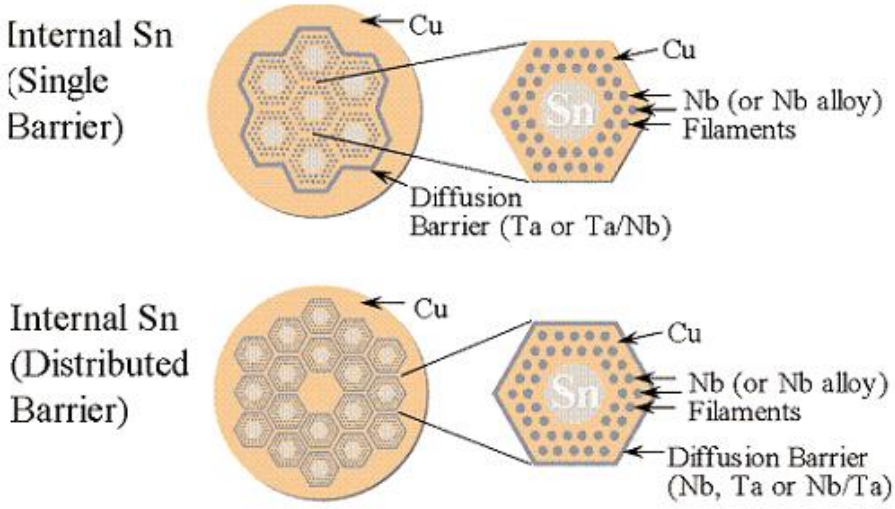

Figure 7: Internal Tin method [12]

2.4.1.3 *Powder in tube*

Unlike the previous two methods, the Powder in Tube (PIT) method uses niobium for the bulk of each filament tube (Figure 8). Each niobium tube is filled with a

tin-rich powder and acts as a diffusion barrier, making tantalum unnecessary for this process.

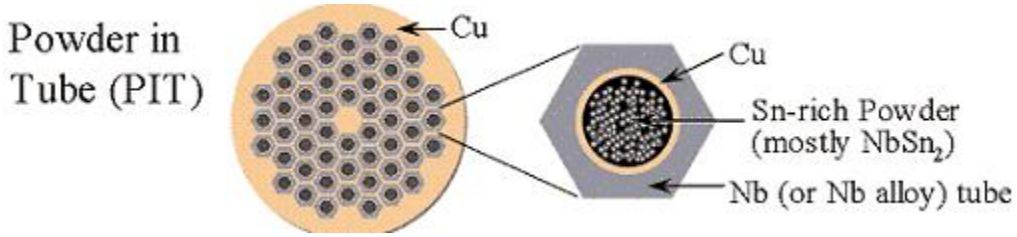

Figure 8: Powder in Tube process [12]

2.4.2 Cable-in-Conduit Conductor

ITER uses a cable design called Cable-In-Conduit Conductor, CICC (Figure 9). The CICC manufacturing process starts by taking 3 strands and winding them together. Three of these "triplets" are then wound together and then 5 triplets to form a subcable. Finally, 6 subcables are bundled together around a circular channel which is used to cool the superconducting strands to maintain the cryogenic temperature. The deformed barriers of each subcable can be seen in the figure.

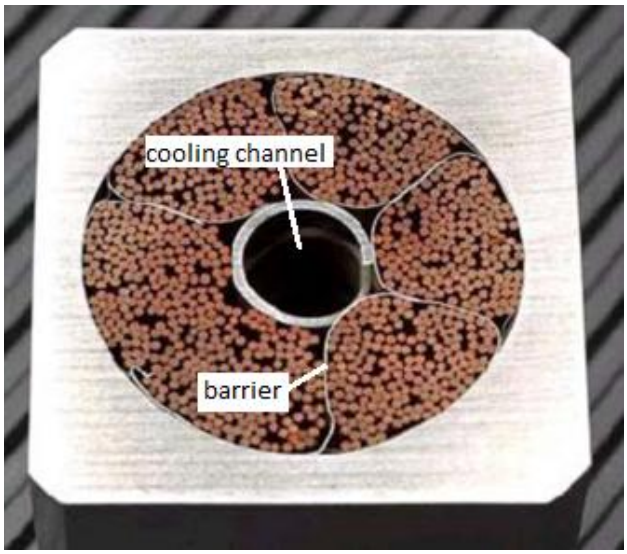

Figure 9 : Cable in Conduit Conductor (CICC) [12]

2.4.3 Strain-Related Performance Degradation

The final stage of a CICC cable may include more than 800 superconducting strands and, each strand composes thousands of individual filaments. These complex geometries undergo a complex combination of strains that affect their performance. Strain is defined as relative deformation (1).

$$\varepsilon = \Delta l / l \qquad (1)$$

Where Δl is the change in length of an element and l is its original length.

Strains can be caused within the cable from mechanical loads, thermal effects, and magnetic forces. Mechanical loads can include those from handling, hoop stresses, and contact between strands within the cable. Thermal effects become significant because the material undergoes massive temperature changes when moving from the heat treatment environment (~650°C or 923 K) to operational temperatures (4.2 K). Differences in the thermal expansion coefficient of each of the materials incorporated in the superconducting strand cause some of the materials to expand or contract more than the others. Lastly, the current passing through the cable to produce a magnetic field is itself acted upon by the field. A Lorentz force – equal to the product of the current and field – acts on the wire perpendicular to the direction of the field. These strains can be classified by the direction of their action on the wire; axial (along the length), transverse (across the width), and bending. As mentioned previously, Nb_3Sn is very susceptible to strain and predicting these strains is critical to the performance of a superconducting Nb_3Sn cable, i.e. the amount of current it can carry.

2.5 Finite Element Analysis for Full-Scale Behavior

In order to properly design superconducting magnets for their applications, we must be able to accurately predict the operational performance of the Nb_3Sn cables used in the magnets. Full-scale experimental testing is difficult to perform because the full-size cables can be very large and expensive to produce. To simplify the experiments, tests are performed with single strands, triplets, and sometimes subcables. The benefits to performing tests on the smaller stages of the cable are that these stages are easier and cheaper to produce, specific strain behaviors (e.g. bending strain) can be isolated to study their effects, and the resources (namely current) required to operate tests are much less significant.

These small-scale performance behavior tests are used to predict the amount of performance degradation to a sample from a given amount of strain. Finite element analysis (FEA) is used to simulate strain distributions and understand how the strains manifest themselves in the complex geometry of the cable. However, no useful information can be gained without knowing how to correlate this strain information with the conditions that cause the strain, namely the forces acting on the wires.

2.6 Mechanical Material Properties

The strain behavior of a material under load is described by its mechanical properties. The Young's modulus, also called the elastic modulus, relates the stress on a material to the elastic deformation caused by the force, given as (**2**).

$$E = \frac{\sigma}{\varepsilon} \quad (2)$$

However, modeling each of the thousands of filaments in a superconducting wire individually would be far too complicated. Complicated areas must be simplified by estimating the overall behavior of the combined materials. One way to achieve this is to homogenize the filament areas using the rule of mixtures (ROM), (3). In this manner, the many strands within a wire, including Nb_3Sn filaments, tantalum barrier, and copper matrix can be treated as a single entity.

$$E_{cl} = E_m * V_m + E_f + V_f \quad (3)$$

Where E_m is the Young's modulus of the matrix material, V_m is the volume fraction of the matrix material, E_f is the Young's modulus of the fiber material, and V_f is the volume fraction of the fiber material, in this case the superconductor. However, the rule of mixtures is only valid when the materials are elastic. It was found that during cool-down from heat treatment, the copper in the superconducting wire is at or near plastic behavior. This leaves it to experimentation to characterize the true overall mechanical properties of the wire.

2.7 Tensile Testing

There are multiple methods to measure the Young's modulus, but the typical method is a tensile test. ASTM E8 Standard Test Methods for Tension Testing of Metallic Materials outlines standards for tensile tests. A typical tensile test will use a rectangular cross section specimen with a narrow middle section. This shape

is often referred to as a “dog bone” for its resemblance to the object. This geometry is preferable because it induces failure in the smaller cross section at the middle, causing repeatable failures at this location. This makes it easier to measure the elongation of the sample after the test and reduces the influence of stress concentrations at the grip ends. This is not an option for superconducting wire because it cannot be made into this geometry.

Tensile testing can be performed on wires, but the task becomes more difficult. Smaller specimen dimensions are more difficult to measure and may introduce error into stress and strain calculations. Additionally, stress concentrations at grip ends become more pronounced. One way to prevent this is to use capstan grips (Figure 10). Capstan grips utilize a spool on which the wire is wound several times before the wire end is fixed with a set screw. Friction between the wire and spool performs like a winch, preventing any slipping along the grips.

Figure 10: Capstan grips (Instron)

While this method is appropriate for many wire samples, it cannot be used for heat treated Nb_3Sn wire due to its brittle nature. Currently, an official testing standard, outlining what equipment and test methods to use, does not exist. The International Electrotechnical Commission is currently in the process of developing a standard and a preliminary draft, modified from a standard for NbTi measurement [13,14].

2.8 IEC/TC90 WG5 61788

The International Electrotechnical Commission has a superconductivity committee working to develop a set of test procedures relating to Nb_3Sn testing, including tensile testing procedures for determining its Young's modulus. This standard, IEC/TC90 WG5 61788-16 [13], is still in a draft form as of the writing of this document. The next phase of the draft is expected 8/2013.

This draft was modified from the standard IEC 61788-6 for testing Cu/Nb-Ti wire to include recommendations on handling Nb_3Sn, gathered from preliminary round-robin experiments and analysis [14–16].

This draft lays out specifications and recommendations for:

- Specimen length
- Sample grips
- Extensometers
- Testing speed
- Determining cross-sectional area

- Unloading
- Test validation

These specifications will be discussed in more detail in the Design Requirements section.

2.9 Measuring Young's Modulus

The Young's modulus of some materials can be very difficult to consistently and accurately measure. Nb_3Sn has an especially short linear elastic loading line, sometimes ending before 0.02% strain. This may be owing to the fact that upon cool down from heat treatment, the copper component of the wire may be close to or already plastically deformed. With very little additional strain, the wire diverges from linear elastic behavior.

A solution to this problem is to strain-harden the material and then unload the applied force from the sample during the experiment. While undergoing unloading, the material behaves elastically until returning back up to the strain level at which unloading began. This provides a more reliable, linear line on which the modulus can be calculated. To differentiate between the two modulus measurements, the initial modulus and unloading modulus are named E_0 and E_u.

During the round-robin testing (RRT), it was shown that this method yielded more reliable results for the Young's modulus. It is recommended in the IEC draft to perform these unloads between 0.3% and 0.5% strain. Following the example set in the RRT, during these experiments three unloads were performed at 0.3%, 0.4%, and 0.5%, respectively. The unloading modulus calculated from these

points are named $E_{u,0.3}$, $E_{u,0.4,}$ and $E_{u,0.5}$. More details are provided on how the unloading is performed in the Experimental Procedure section.

3.0 TENSILE TESTING APPARATUS

The tensile testing apparatus was designed to accurately measure the mechanical properties of superconducting wire at cryogenic temperature. The cryogenic environment required a custom-built machine in lieu of a commercially-bought tensile testing machine. To meet the cryogenic temperatures required to match the operational environment of the wires, the test apparatus needs to operate inside a cryogenic dewar. The key components of the apparatus include: motor, actuator, structural members, sample grips, and measurement devices (load cell and extensometers). More detail about each component will be provided in subsequent sections.

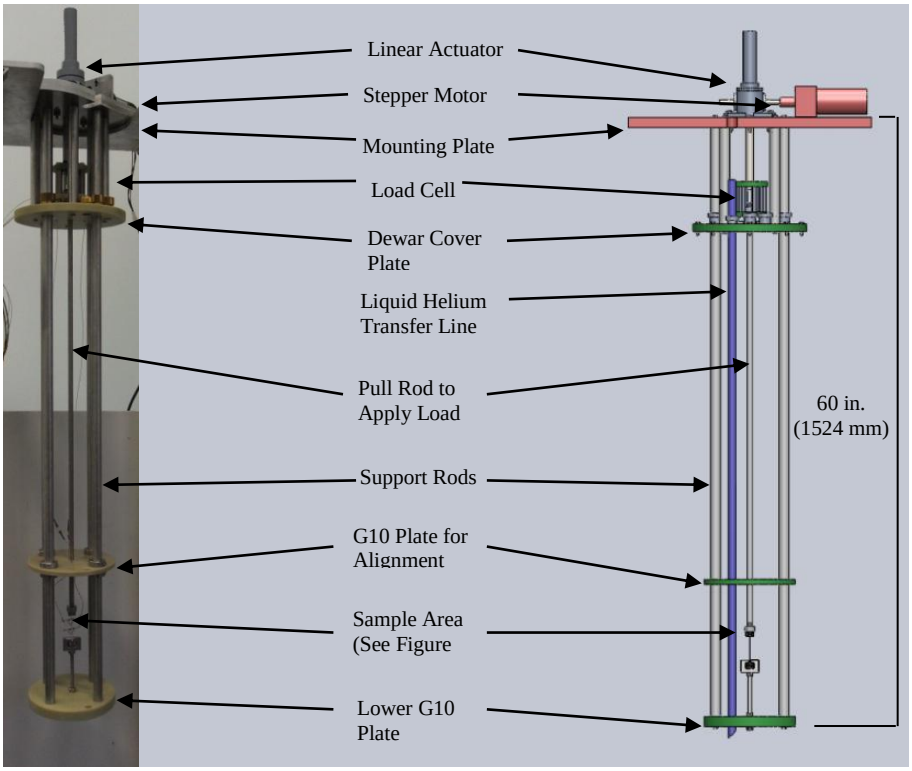

Figure 11: Overview of Apparatus Assembly

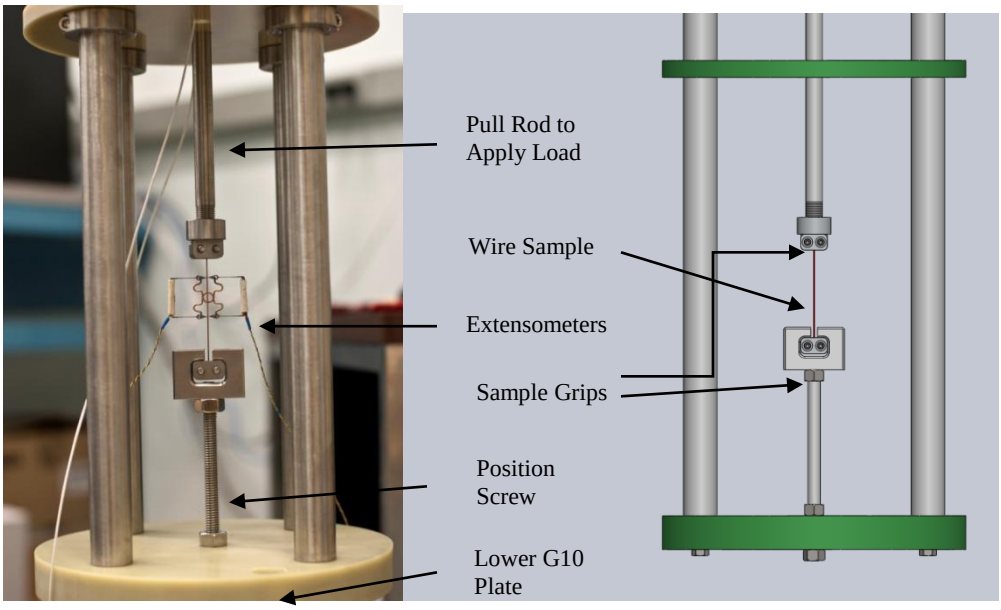

Figure 12: Overview of Sample Area

3.1 Design Requirements

For successful operation the apparatus needed to fulfill the following requirements:

- Apply up to 5 kN load; sufficient to achieve up to 1% strain to single and triplet samples of Nb_3Sn (0.8mm and 2 mm, respectively)
- Operate in range of stroke rate of 0.1 – 0.5 mm/min, controllable and reversible
- Operate between room temperature (300K) and liquid helium boiling point (4.2K)
- Fit into commercially available cryogenic research dewar
- Allow access for liquid helium transfer lines
- Minimize liquid helium boil off
- Precisely measure load applied
- Precisely measure strain of sample

- Minimize vibrational and electrical noise to measurement devices
- Capability to mount samples with minimal disturbance to specimen
- Magnetically neutral materials

3.2 Materials

The design used primarily type 316 stainless steel and G10-FR fiberglass epoxy. Both of these materials were selected for their high-strength and magnetically neutral properties. Magnetic susceptibility is very important for any future tests that may be run in a background magnetic field. Additionally, the electrical conductivity of G10-FR fiberglass epoxy is low, so it provided an easy way to electrically isolate the measurement devices from the motor.

The difference in thermal expansion coefficient is important to consider in the design of the apparatus. As the apparatus is cooled from room temperature to 4.2 K, some materials will contract more than others. From room temperature (~300 K) to liquid helium boiling point (4.2 K), stainless steel, Nb_3Sn, and G10 fiberglass epoxy contract by 0.265%, 0.165%, and 0.713%, respectively. This results in a thermal expansion of 6 μm between the sample grips and -0.149 mm of the sample material. A 2 mm gap is provided at the lower sample grip to allow for the net contraction of 0.155 mm between the ends of the sample grips (Figure 12).

3.3 Structural support

Structural support for the apparatus includes all components of the device that carry significant amounts of load during operation. This primarily means all the

components involved in reacting the load applied to the sample back to the mounting plate at the base of the machine.

3.3.1 **Buckling**

Four stainless steel support rods run the full length of the machine, from the sample area to the mounting plate. During tensile testing, these rods are in compression as they react the load applied to the sample. Under compression, these rods are susceptible to failure by buckling well below the ultimate compressive stress of the material. The Euler buckling equation (4) was used to determine the minimum diameter of the support rods:

$$F_{cr} = \frac{FS * F}{\mathrm{N}} = \frac{\pi^2 EI}{(KL)^2} \quad (4)$$

$$I = \frac{\pi * d^4}{64} \quad (5)$$

Where F_{cr} is the force at which buckling occurs, *FS* is the factor of safety, *F* is the design load, *N* is the number of rods, *E* is the elastic modulus of the rod material, *I* is the area moment of inertia (5), *K* is the column effective length factor, and *L* is the unsupported length of the column. Applying a factor of safety, *FS = 2*, length, *L=58 in. (1473 mm)*, the minimum diameter of the rods for structural stability was found to be 0.86 in. (21.9 mm). This calculation is based on a worst-case, fixed-free end condition for a rod under compression. It does not take into consideration the added robustness gained from joining the rods at the bottom of the apparatus with the lower G10 plate.

3.3.2 Liquid helium boil-off

During cryogenic testing, the sample area of the apparatus will be submerged in liquid helium in order to cool the superconducting wire to its operating temperature. Even with a well-insulated dewar, liquid helium consumption is a concern when designing a cryogenic probe. The following equation (5) was used to calculate the heat conducted through the stainless steel rods from 300 K to 4.2 K:

$$\dot{q} = \frac{A}{L}\int_{4\,K}^{300\,K} \lambda(T)dT \qquad (5)$$

Where A is the cross-sectional area of the material, L is the length of the rod from the lower G10 plate to the mounting plate, λ is the thermal conductivity of the material, and $\dot{q}$ is the heat loss due to conduction. As the area of the rods decrease to zero, heat loss is minimized. Therefore, in the interest of helium consumption, it is preferred to keep the diameter of the support rods as small as possible. An estimate for the liquid boil off will be given in Section 3.3.6. Additionally, Quikonnect vacuum couplings were used to seal gaps around any openings in the dewar top plate to prevent loss of helium gas and reduce boil off.

3.3.3 Acceptable footprint positioning

The support rods and lower G10 plate must be small enough to fit within the inner bore of the cryostat, while also providing sufficient space for the sample grips and extensometers. The bore of the cryostat is 9 inches in diameter (See 3.6 Cryostat) and the extensometers and sample grips extend at most 23.5 mm from the center

axis of the apparatus (See 3.8 Extensometers). The allowable space for the support rods is between 114.3 mm (4.5 in.) and 23.5 mm (0.9 in.) from the center axis.

3.3.4 **Lower G10 plate**

The lower G10 plate (Figure 13) connects the sample area to the support rods. Under tensile testing, the lower G10 plate is in bending. The following equations (6) & (7) are used to determine the minimum plate thickness required to prevent structural failure:

$$\sigma_F = \mathrm{FS} * \frac{3FL}{2bd^2} \qquad (6)$$

$$d = \sqrt{FS * \frac{3FL}{2b\sigma_F}} \qquad (7)$$

Where F is the load applied to the plate, L is the distance between supports (Figure 13, left), and b and d are the width and depth of the cross section (Figure 13, right).

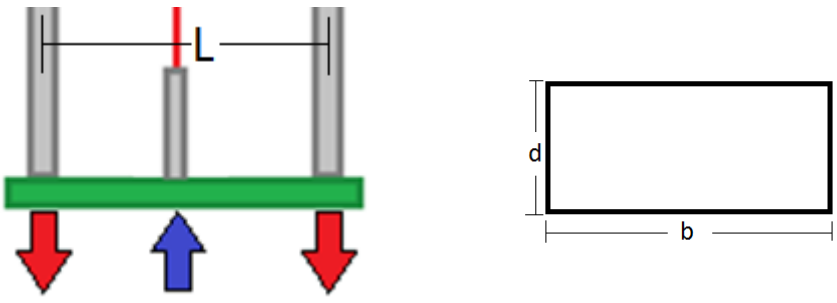

Figure 13: Schematic of the forces acting on the lower G10 plate (left), the rectangular cross section used to approximate the plate (right).

The plate has been approximated as a rectangular beam for simplicity with the dimensions shown in Figure 13 (right). Given a flexural strength of 448 MPa [17] for G10 fiberglass epoxy, a load of 5 kN, and a factor of safety, FS = 2, the minimum thickness required for the lower G10 plate is 7 mm (0.28 in.).

Furthermore, equation (8) can be applied to determine the maximum deflection in the middle of the plate. To keep the overall compliance of the apparatus low, it is better to keep the deflection of the plate small. The plate is approximated as a rectangular beam again for simplicity.

$$y = \frac{FL^3}{48EI_m} \quad (8)$$

Where y is the maximum deflection, E is the Young's modulus, and I_m is given by (9).

$$I_m = \frac{bd^3}{12} \quad (9)$$

The Young's modulus of G10 fiberglass epoxy is 16.5 GPa [17]. If the deflection limit is chosen as 0.2 mm (8 mils), the minimum thickness of the plate is 25.1 mm (0.98 in.).

The thickness of the plate selected is 1 inch (25.4 mm). This thickness should keep the deflection of the plate to an appropriately small amount and provide a high factor of safety against failure while applying load.

3.3.5 Adjustment screw

The adjustment screw (Figure 14) connects to the lower G10 plate and provides more flexibility for sample lengths. The adjustment screw is a stainless steel threaded rod that can be raised and lowered to fit sample lengths from 90 mm to 190mm, depending on the length of the screw installed. The machine is currently outfitted with two screw lengths of 3 and 6 inches, respectively.

The adjustment screw must resist 5 kN of tensile load. A 3/8-16 threaded, type 316 stainless steel rod was selected and has a safe working load of 49,000 lbs (21.8 kN).

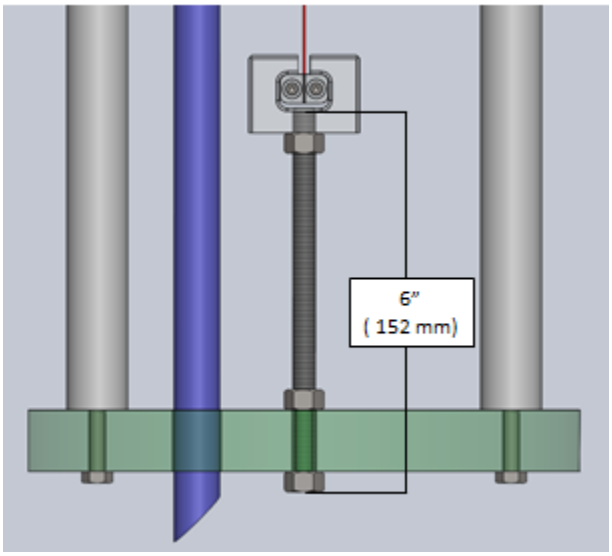

Figure 14 : Adjustment screw

3.3.6 Structural support summary

The support rods selected for the apparatus are four 1 in. diameter type 316 stainless steel rods. This diameter provides a high factor of safety and should guarantee a robust design sufficient to load triplet strands to failure.

These rods will allow an estimated 0.67 L/h of boil off. At an estimated cost for liquid helium of $5/L, the apparatus will cost less than $3 per hour to operate. Given that the experiments are not overly lengthy and do not require a large volume of liquid helium to operate, this cost is reasonable for the operation of the tensile testing apparatus.

3.4 Linear Actuator

This machine was designed to test single and triplet strands up to 5 kN of tensile load in the recommended test speed range of 0.1 – 0.5 mm/min. A Duff Norton 10 kN anti-backlash machine screw actuator with a gear ratio of 20:1 was selected for this purpose (Figure 15).

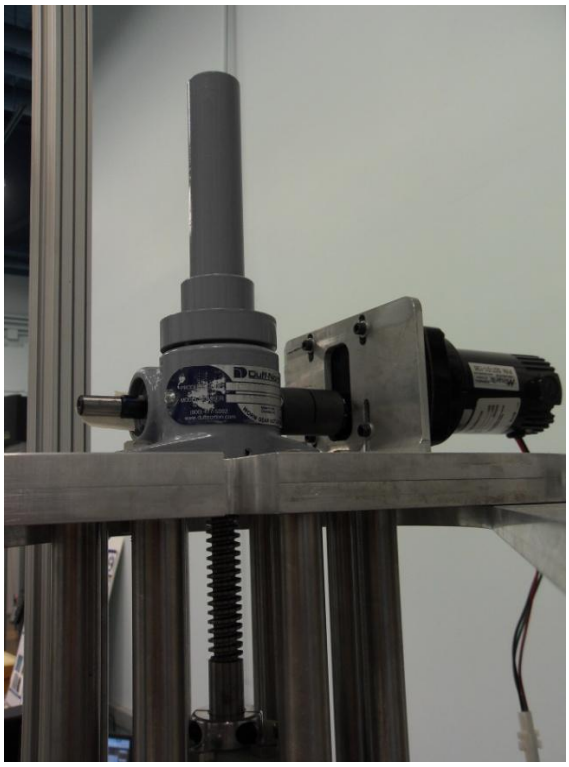

Figure 15: Linear actuator installed on apparatus

This crosshead of the actuator displaces 0.25 mm per revolution of the input shaft. To achieve the required displacement speed, the input shaft must be rotated at less than 2 rpm. A typical DC motor (See 3.5 Electric Motor) operates at much higher speeds, in thousands of rpm. A large gear ratio provides an economical way to shrink the size of the motor and to more closely match the typical operating speeds of DC motors.

The actuator input shaft requires 3.7 Nm (510 oz in.) of torque to operate at full load capacity of 10 kN. Due to the low operation speeds, the power required for operation is very low, 1e-3 hp.

3.5 Electric Motor

In order to provide the force required of our testing, the motor must provide a torque of 3.7 Nm at 2 rpm. The motor used is a Bison 1/40 hp PMDC (permanent magnet DC) motor (Figure 16). A DC gearmotor was selected in this design for its high-torque and low-speed capabilities. The motor is speed controllable and reversible and is operated manually by a Minarik controller (Figure 17). It was necessary to gear down the motor significantly (702.1:1) to provide a high-torque and low speed necessary to operate the linear actuator at the required testing speed. The motor has a maximum torque of 100 in-lb. (11.3 Nm) and a maximum speed of 2.6 rpm.

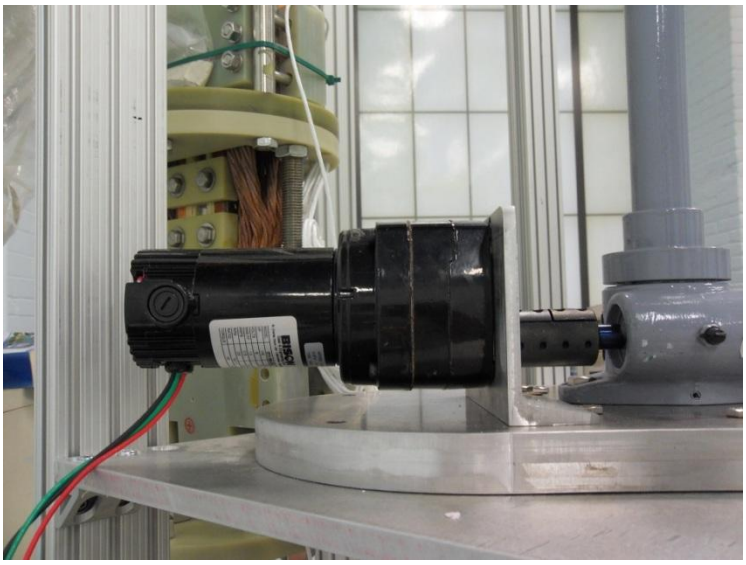

Figure 16: PMDC motor installed on apparatus

Figure 17: Motor controller for electric motor

3.6 Cryostat

The cryostat is a highly-insulated research dewar used to contain the cryogen used during testing. It is important that the dewar is well-insulated to avoid

unnecessary boil-off of the liquid cryogen. Even with the best insulation, ambient heat gradually penetrates to the cryogen and causes boil-off through conduction out the top and through radiation. For these reasons, it is important to make sure that the dewar is well-sealed, conduction is limited through the top opening, and the bore size is minimized to maximize the effectiveness of the volume of cryogen at the bottom of the dewar.

The dewar selected to contain the probe was the commercially available 9VSRD model from Janis. This dewar has a 9 inch inner bore, sufficient space for the sample holder area and support structure. The inside length of the dewar is 50 inches.

3.7 Sample Grips

Two different sample grip methods are recommended in the IEC draft [13] (Figure 18). One method uses a flanged cylinder soldered around the end of the wire (left). The other uses two pressing plates with v-shaped groove to seat the wire.

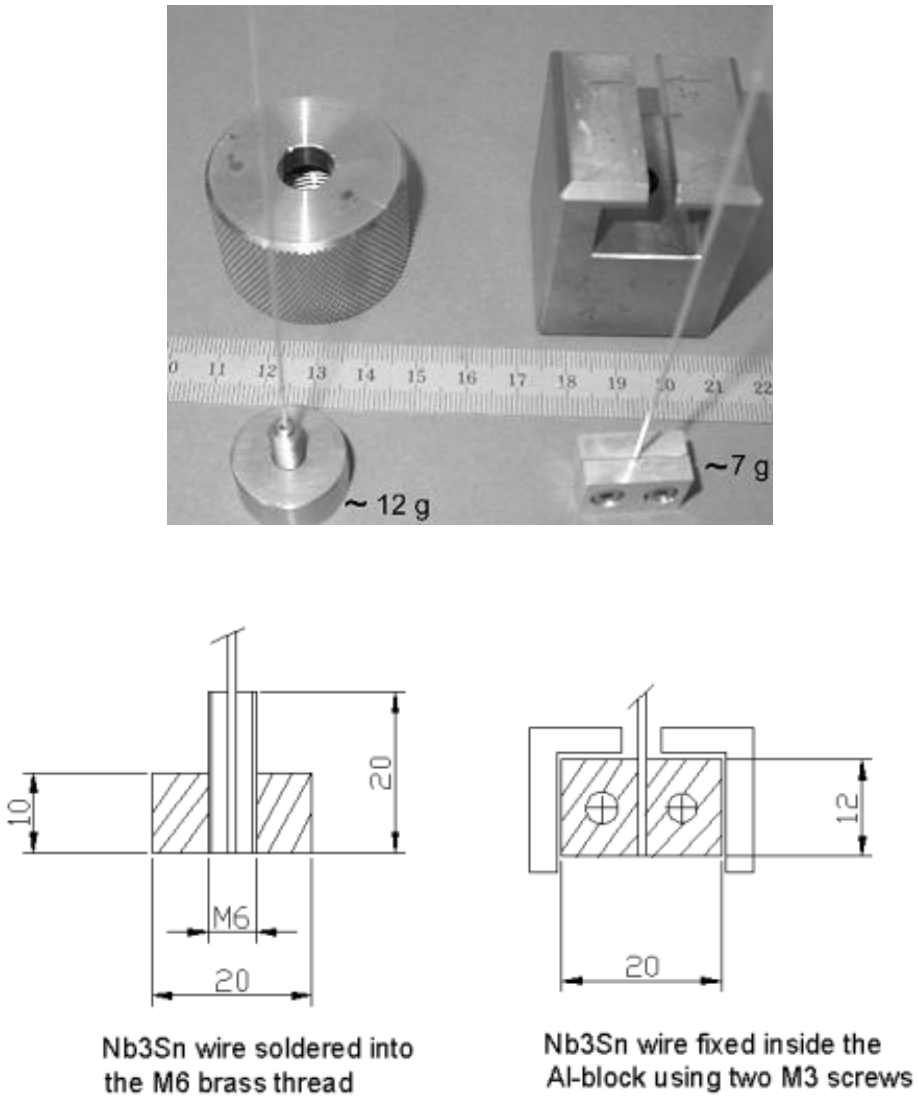

Figure 18: Two sample grip methods recommended from IEC; photo (top), dimensions (bottom)

This apparatus incorporated the v-groove clamping method as described in the IEC draft. Each end of the sample sits in a shallow v-groove between matching type 316 stainless steel plates which are held together with stainless steel screws (Figure 18, bottom right).

3.7.1 **V-Groove**

Although the IEC draft recommended dimensions for the overall size of the sample grips, no recommendations for the size of the v-groove were given. The v-groove was initially designed to be 0.018 inches deep, assuming up to 30% deformation of the sample cross section. However, sample slipping was found to be a problem during initial testing of reference materials. The grips were modified by sandblasting the v-grooves to create more friction against the wire surface and by shortening the depth of the v-grooves to 0.015 inches to provide more space to deform the wire cross section. Following these modifications, the grips did not show any slipping during testing. These grips performed up to a maximum of 750 N of load. This maximum was found during the stainless steel material testing and it could not be exceeded even with excessive tightening of the clamping screws.

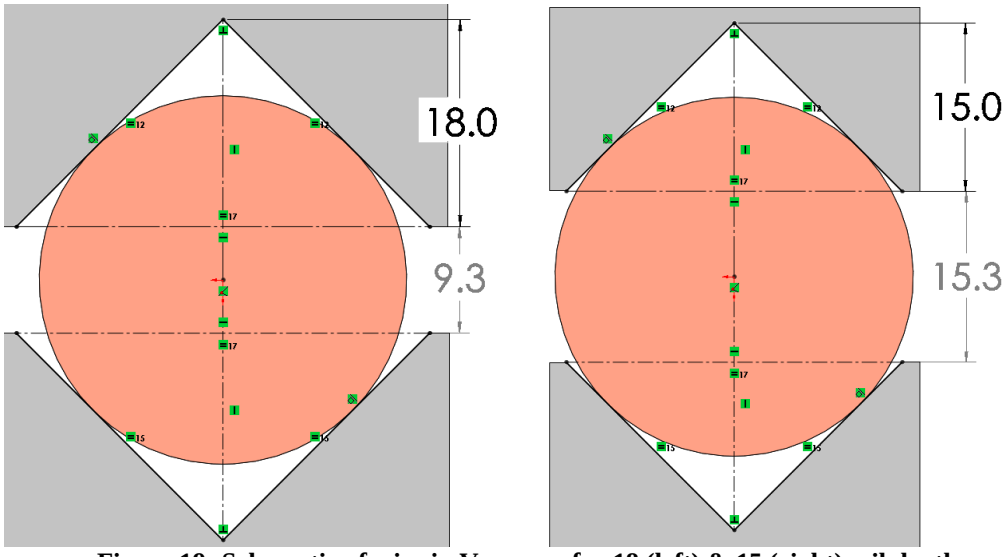

Figure 19: Schematic of wire in V-groove for 18 (left) & 15 (right) mil depth

3.8 **Extensometers**

Material testing necessitates a method for measuring the strain of the samples. In order to capture the small elastic region of the Nb_3Sn samples, a very precise strain measurement system must be used that can successfully operate in the hostile cryogenic environment. The extensometers must not damage the wire in such a way as to affect the test. Additionally, the extensometers must be signal conditioned with a low-noise amplification system prior to data acquisition to provide reliable and useful data with high accuracy. The system that was used in this setup was designed by Arman Nyilas [18] for this specific purpose and has been used successfully by many other research groups for the stress-strain measurements of Nb_3Sn wires.

The frames of the extensometers are electro discharge machined out of a single piece, with no welding or bolting, to ensure a consistent zero return position [19]. The frame is designed to be the strain sensing object, flexing during operation and returning a signal from strain gauges mounted to the frame. The frame must be made of a material with low Young's modulus to provide sufficient flexure for a high working range, but to provide little return spring force. There are two titanium alloys that are currently used for this task: Ti-6Al-4Zr-2Mo-2Sn and Ti-6Al-4V.

The double extensometer system compensates for any bending errors. The system has a very low mass (~3g) so as not to impart any extra loading on the wire apart from the load applied by the actuator. Dimensions are shown in Figure 20.

The extensometers are mounted by holding the extensometers together with two precipitation hardened Be-Bronze springs (Figure 20). They have a safe working range up to 10% strain.

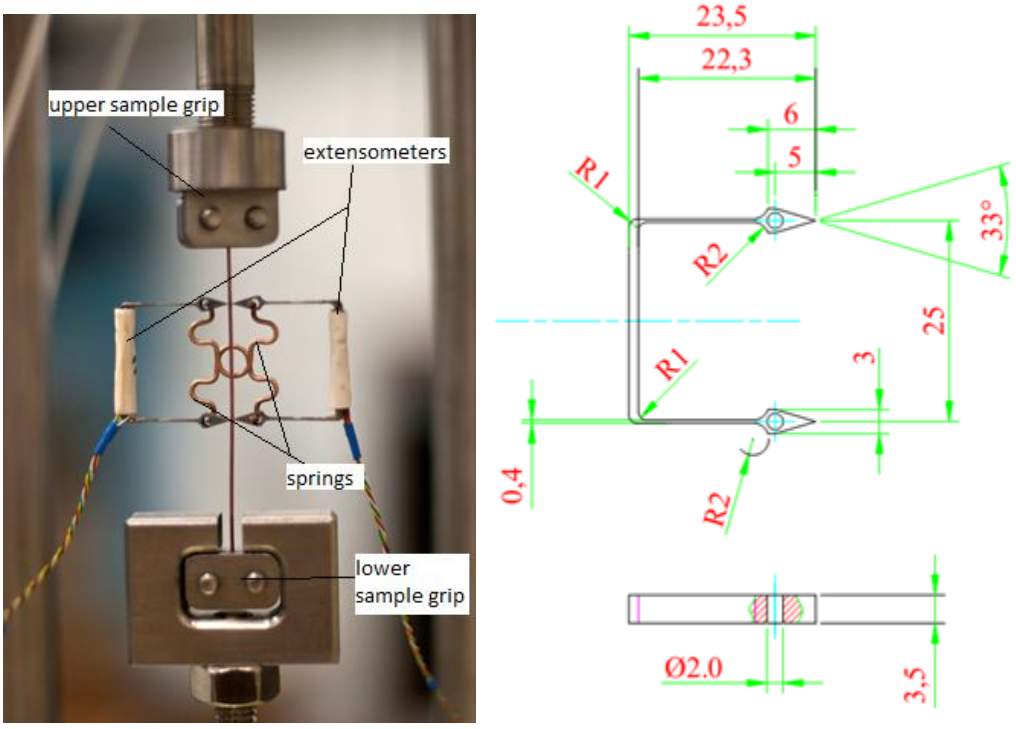

Figure 20: Extensometers mounted on sample wire (left), extensometer dimensions (right)

3.8.1 Extensometer Calibration

As displacement is applied to the sample and the strain gauges flex, a voltage is read across the data acquisition system. In order to be made useful data, this voltage must be converted to an engineering value. Prior to testing, the extensometers are calibrated using a precision micrometer to determine the correlation between displacement and voltage reading (Figure 21). The extensometer system requires a dc power source between 12 – 15 VDC and has three sensitivity levels, 1V, 2V, 5V to return on average about 0.6 V/mm, 1.2 V/mm, and 3 V/mm, respectively.

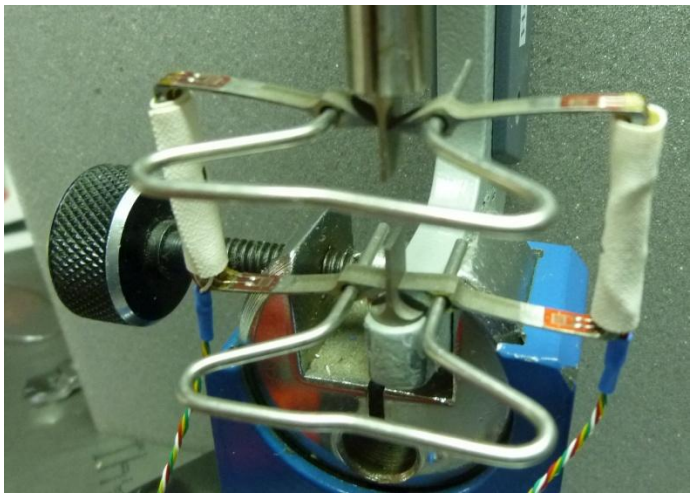

Figure 21: Extensometers mounted on micrometer with large springs for calibrating

During preliminary testing, the extensometers were calibrated prior to each test. During calibration, the extensometers would be mounted to the micrometer (Figure 21) and a known displacement applied from 0 to 2.5 mm (the full working range). The voltage was recorded for each extensometer at each displacement increment. The voltage generally scaled linearly with displacement. The linear fit of the data collected provided a conversion rate between displacement and voltage. Individually, these rates were shown to deviate less than 1% from the average and therefore the average was used for all superconducting tests for consistency.

It is still recommended that periodically, the extensometers are calibrated to ensure that they are still operating close to the expected behavior.

3.9 Load cell

The load cell provides a system to accurately measure the force applied to the sample during testing. Similarly to the extensometers, the load cell has strain

gauges mounted on an engineered rib to return a voltage signal when flexure is sensed. Unlike the extensometers, because the load cell is not mounted inside the cryogenic environment, no signal conditioner is necessary to pre-process the signal.

The tensile testing apparatus was originally designed to include a 2000 lb load cell by Sensing Systems Corporation (Figure 22, right). However, for better resolution at lower load ranges, this load cell was substituted for the LTH350 model from Futek (Figure 22, left). A comparison of the load cell resolution is provided in Section 5.2. The Futek load cell has a capacity of 250 lb (1.1 kN) with a maximum error of 0.041%. The load cells can be easily switched to modify the system for larger load testing, that is, for triplet samples.

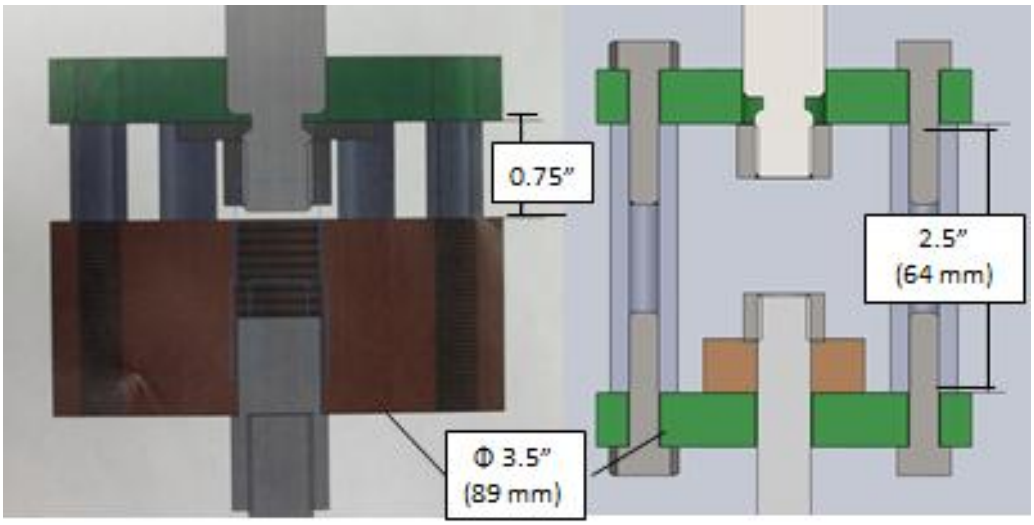

Figure 22: Load cell assembly with 250 lb capacity (left) and 2000 lb capacity (right)

3.10 **Data Acquisition**

Power supplies by KEITHLEY and Agilent provide 10 V and 14 V excitation voltages to the extensometers and load cell, respectively (Figure 23). The measurement signals from these devices are read using KEITHLEY 2000 model series multimeters and nanovoltmeter. The signal from the extensometers is also passed through a signal conditioner to reduce noise created from the cryogenic environment. The data is then recorded to a PC using a GPIB interface and Labview computer software. A Labview code provided by the National High Magnetic Field Lab (NHMFL, Tallahassee, FL) interfaces with the data acquisition system and collects data samples at 0.025 second intervals (40 pts per second).

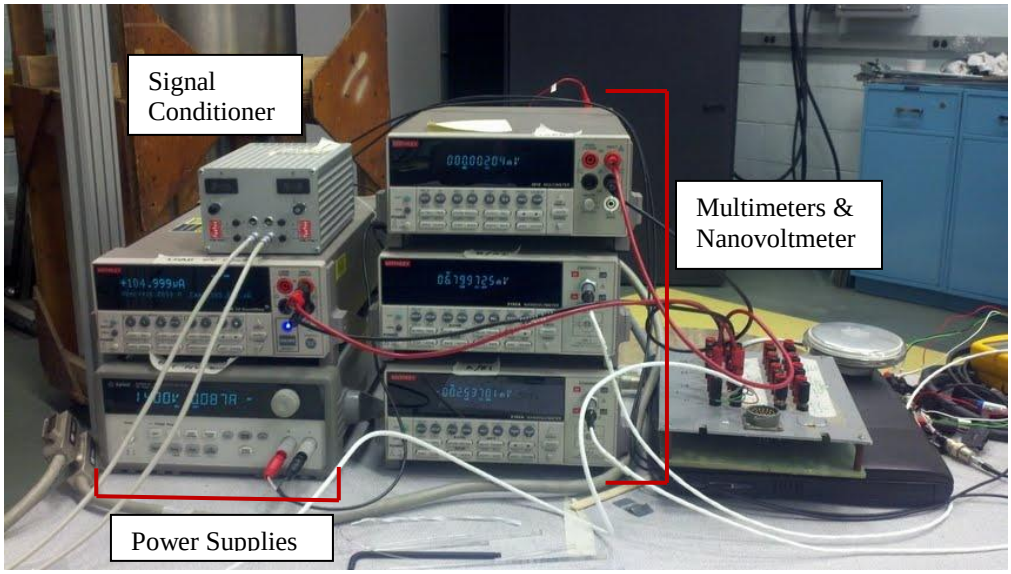

Figure 23: Data Acquisition System Setup

4.0 Experimental Procedure

The following section will discuss the materials that were tested and the procedure used to conduct the stress-strain experiments.

4.1 Materials Tested

Two rounds of testing were performed for this thesis work. The first round of testing used known materials as references to confirm the apparatus would yield expected results. That is, that the results would match expected values for elastic and plastic properties. The second round of testing used superconducting Nb_3Sn wires to confirm that the procedure was appropriate for the brittle, heat-treated wires, to characterize the elastic modulus and other mechanical properties of the wires, and to compare these results with those previously done by the International RRT [14].

4.1.1 Reference Materials

To confirm that the machine is operating properly, several known reference materials were tested to compare their experimentally-collected Young's modulus to their expected values. The materials tested and their expected values are listed in Table 1. It should be noted that manufacturing specifications for the materials did not completely describe the mechanical properties of the materials. Only the bolded values in Table 1, primarily ultimate tensile strength, have been certified by the manufacturer. The other values listed are representative of the approximate material behavior, but may vary depending on its temper. All of these materials were purchased in wire form with diameters and elastic properties similar in range

to that of the Nb_3Sn wires. These materials were selected as reference materials based on recommendations from [18] and [13].

Table 1: Reference Materials and Expected Values (Bolded values have been provided by manufacturer certifications, others are textbook values)

Material	Diameter	Young's Modulus (10^9 N/m^2, GPa)	Ultimate Tensile Strength (10^6 N/m^2, MPa)	Yield Strength (10^6 N/m^2, MPa)	Elongation (%)
OFHC Copper	0.82 mm	117	220	70	
Titanium Grade 2 Annealed	0.031 in.	110	**496**	**324**	**23**
316 Spring Stainless Steeel	.032 in.	180	**1640**	502	
1100 Soft Aluminum	0.0321 in.	69	**103**	95	**38.88**

4.1.2 Superconducting Materials

Superconducting Nb_3Sn wires from 4 different manufacturers (Oxford, Hitachi, EAS, and Luvata) were selected for preliminary testing. Both unreacted and heat treated samples were tested. All these wires were approximately 0.81 mm (0.032 in.) in diameter.

4.2 Sample Preparation

Before testing, any insulation material coating must be removed to avoid influencing the material properties calculated during the test. Some of the superconducting wires had a chrome layer that needed to be removed. This coating can be removed chemically with hydrochloric acid, but care should be taken to not damage the surface of specimen.

The length of the sample is measured to ensure that the sample meets the testing requirement for space between grips to allow sufficient space to mount the extensometers and to compare the length of the sample following the test. The diameter of the sample is measured to later calculate the tensile stress applied. The diameter of the sample is measured twice at orthogonal points around the sample and the average of these values is used to calculate the area. This is done to compensate for any non-uniformities in the wire geometry.

4.3 Sample Mounting

After the wire dimensions are calculated, it is carefully mounted in the lower sample holder. The sample should sit in the v-groove of each clamping plate and should lie along the full length of the channel without protruding much past the end of the grips (

Figure 24). The grips should also be held as close to even as possible when securing; any uneven shearing applied to the top of the grips during testing could result in loosening of the bolts and slipping of the sample prior to completion of the test.

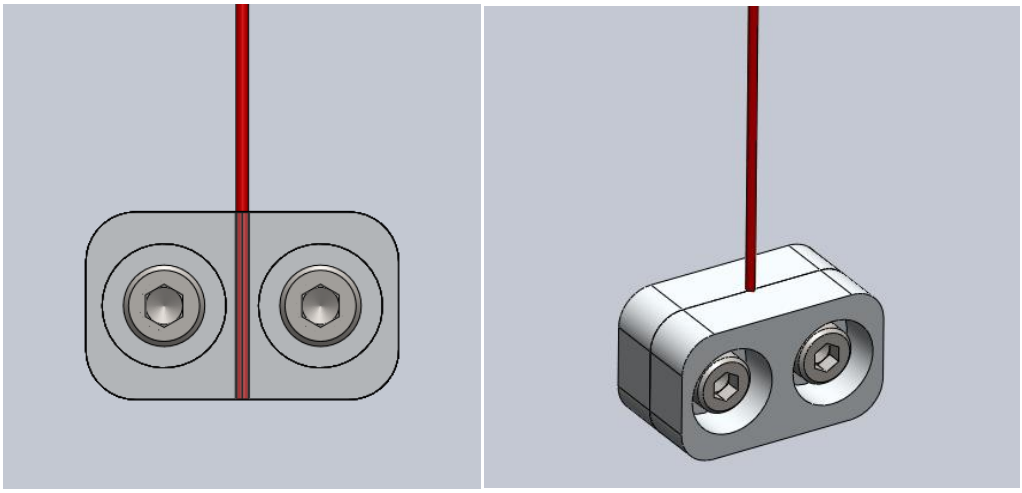

Figure 24: Wire mounted in lower sample grips

When tightening the screws, one should be careful not to undertighten the screws or the sample could slip before the test is complete. On the other hand, overtightening could cause premature failure of the sample at the grips. This second point is especially important for heat treated samples. When mounting heat treated samples, 5 in. lbs of torque were applied to two sample grip screws with a torque wrench. This torque was sufficient to prevent slipping. It was found that for ductile, unreacted samples that required more load to reach failure, 12 in. lbs. of torque was sufficient to prevent any sample slipping. The upper sample grip should be mounted in a similar manner (

Figure 25).

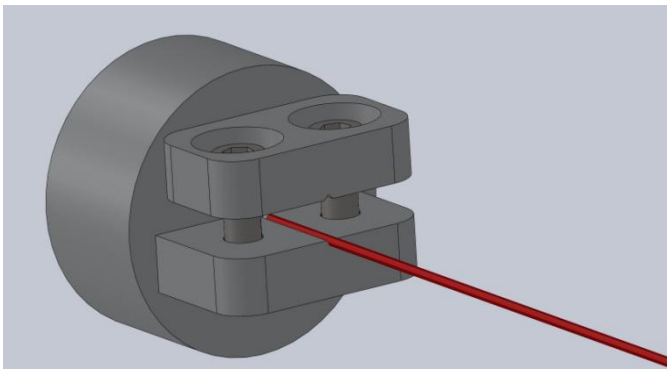

Figure 25: Sample mounted in upper sample grips

4.4 Extensometer Mounting

At this point, the sample should be mounted in both the upper and lower sample grips. Before mounting the extensometers, the operator should make sure that the lower sample grip is free-hanging; that is, it is not sitting on the lower part of the holder block and it is not contacting the upper part of the holder block and applying stress (Figure 26). This ensures that any disturbances made while mounting the extensometers do not cause damaging stress to the samples. The extensometers should be fitted with the Be-bronze springs and mounted vertically in the middle of the sample. Most heat-treated superconducting samples are kept straight in quartz tubes during heat-treatment, but if a sample is not straight, either from defects in the quartz tube or other reason, the extensometers should be mounted in the plane of the bend to compensate for the straightening effect during the beginning of the test. The tips of the extensometers should be as close to even as possible to avoid causing shear stress to the sample. After mounting, the extensometers should be zeroed on the signal conditioner to prepare for data collection.

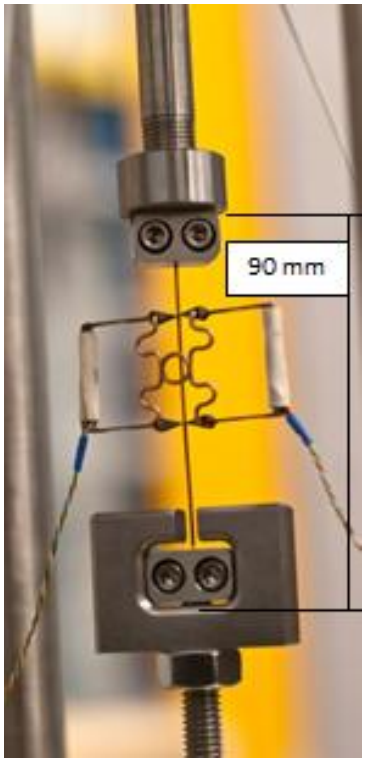

Figure 26: Sample mounted in apparatus

4.5 Testing Speed

As mentioned earlier, the speed of the test is required to be at a constant stroke rate between 0.1-0.5 mm/min. The motor has a rated maximum speed of 2.6 rpm at 90V (100%). The linear actuator crosshead displaces 0.25mm per revolution.

Table 2 shows the motor's performance and the resultant stroke rate as a function of the voltage applied, as governed by the control box. The range of speeds that meet the requirements for the testing speed are also indicated in red. All the tests that were performed in the scope of this thesis used a constant stroke rate of 0.3 mm/min, equivalent to 46% of the maximum voltage of the motor.

Table 2: Motor performance

Theoretical		
% Voltage	rpm	mm/min
0	0.00	0.000
10	0.26	0.065
20	0.52	0.130
30	0.78	0.195
40	1.04	0.260
50	1.30	0.325
60	1.56	0.390
70	1.82	0.455
80	2.08	0.520
90	2.34	0.585
100	2.60	0.650

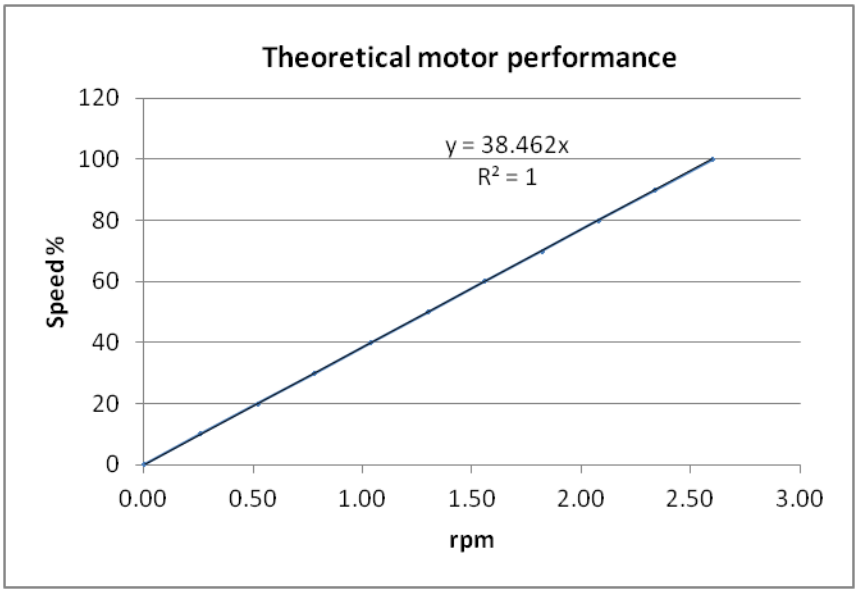

Figure 27: Theoretical motor performance

4.6 Unloading

At 0.3%, 0.4%, and 0.5% strain the sample is unloaded to 30-40% of the load from the point of unloading and reloaded, as indicated by the testing standards. Aside from reversing direction, the stroke rate should not be changed during the

test. The operator should be sure to brake the motor before reversing direction to prevent damage to the motor.

The unloading points, 0.3%, 0.4%, and 0.5%, correspond to average extensometer voltages of 43.3 mV, 57.8 mV, and 72.2 mV, respectively. When the average of the extensometer readings reaches each of these values, the motor should be braked and reversed until the load reaches 30-40% of its reading at the moment of braking.

5.0 DISCUSSION

5.1 Post-processing Data

The raw data collected from the load cell and extensometers were voltages. In order to convert them to useful engineering data, the voltages were converted with their respective calibration rates. The calibration rate applied to the extensometers was averaged over 30 runs to 578.5 mV/mm with a COV% of 3%. The load cell has an output value of 2.0127 mV/V at full load (250 lb). With a 10 VDC power source, the load cell returns 18.099 µV/N.

Matlab was used to convert the raw voltages to engineering units of displacement (mm) and force (N) using the above calibration factors. A stress strain curve was then built taking stress to be

$$\sigma = \frac{F}{A}$$

where F is the applied force and A is the cross sectional area of the wire. Strain was calculated as

$$\varepsilon = \frac{\Delta l}{l}$$

Where Δl is the displacement measured by the extensometers and l is the gauge length of the extensometers.

5.1.1 Calculating Young's Modulus

The Young's modulus can be calculated by finding the slope of the first order linear regression line of the linear portions of the stress-strain curve. To ensure good linearity, a coefficient of determination, R^2, value greater than 0.99 is desired. The linear portion of the initial loading line for Nb_3Sn is relatively small, ending below 0.02% in some cases [16].

Unloading is performed at 0.3%, 0.4%, and 0.5% strain for subsequent Young's modulus calculations. During unloading, the applied load is reduced by 30-40%. Previous experiments [13,20] have recommended measuring the Young's modulus of the unloading line from 99% to 90% of the load at which unloading begins (Figure 28). In the figure, it can be clearly seen that the unloading line makes a sharp transition at the point of unloading.

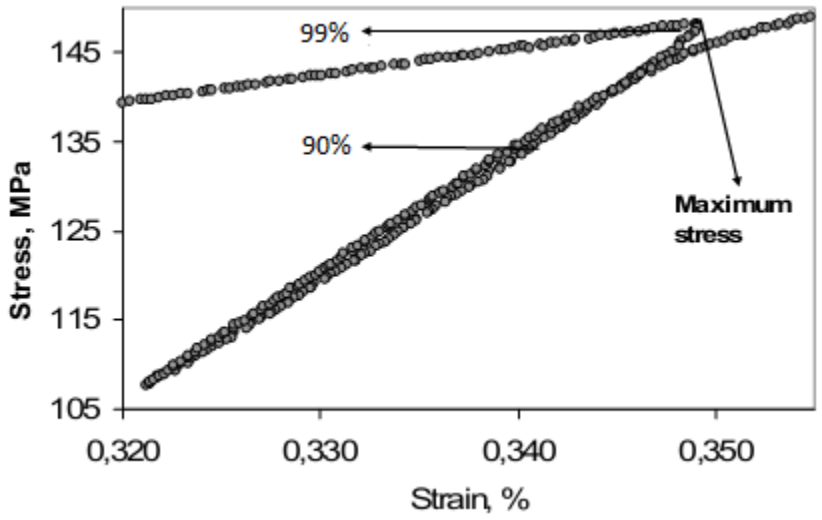

Figure 28: Unloading portion as demonstrated by IEC draft

The unloading curves created with this apparatus did not demonstrate the same sharp transition (Figure 29). Using the same stress range as the draft to calculate the Young's modulus yielded poor linearity for the linear regression line. The difference between the curve shape generated with this apparatus compared to the IEC draft will be discussed further in Section 5.4.7 – Debugging the System. Instead, the linear portion of the curve was manually determined between approximately 90-75% of the stress at unloading. Ideally, this process should be automated to prevent any user bias, however, more experiments must be done to be sure that this range will consistently yield accurate results.

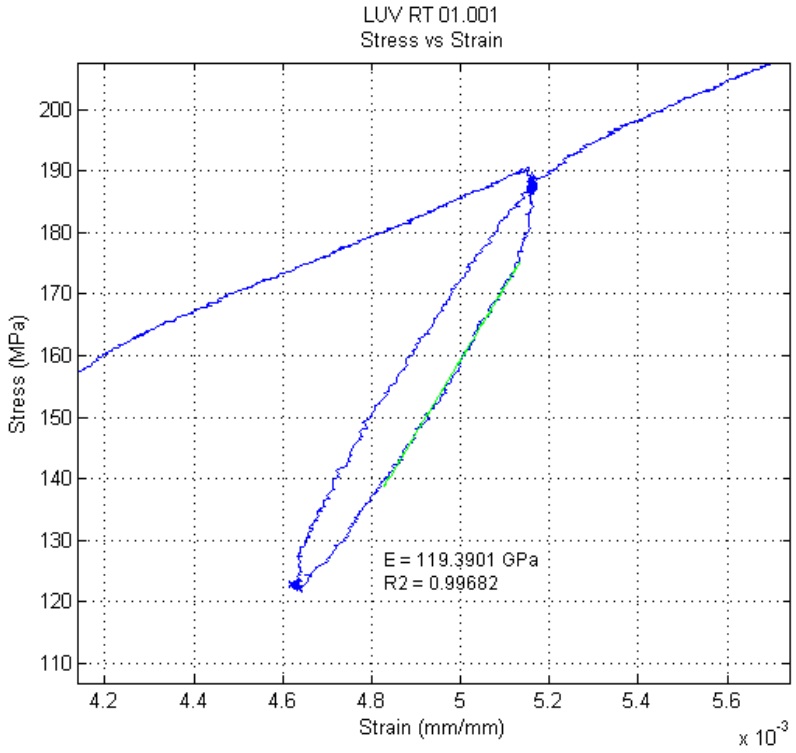

Figure 29: Unloading portion of stress-strain curve for apparatus

5.1.2 Comparing E_0 and E_U

In theory, the E_0 and E_u should be equal. However, values for E_0 can vary greatly due to various sources of error that are difficult to avoid. These sources of error can include "bedding in" of the sample material into test grips, non-linearity of the sample prior to testing, axial mismatch in the sample grips [21]. In the round-robin testing it was found that the COV % of E_0 diminished as the ratio of E_0 to E_u went to unity [14]. It was found that the COV converged to a sufficiently low level when the ratio was within 30% of unity. Therefore, the IEC draft recommends that a test is considered valid if the modulus ratio falls within the range described by Equation 1 [13] where delta, Δ, represents the percent deviation of the modulus ratio from unity. In an ideal case, where the initial modulus was unaltered by pre-strains, delta, Δ, would equal zero.

Equation 1

$$1 - \Delta < \frac{E_0}{E_U} < 1 + \Delta$$

where Δ = 0.3

5.2 Load Cell Comparison

Two load cells were used in the reference material testing; the first with 2000 lb (8.9 kN) capacity and the second with 250 lb (1.1 kN) capacity. The strongest material tested, type 316 spring stainless steel, has an ultimate tensile strength of 1640 MPa. With a diameter of approximately 1 mm, the ultimate strength corresponds to 820 N. The stainless steel material uses up to 9% of the capacity of the 2000 lb load cell and 75% of the 250 lb load cell. Readings between 10-90% of the load cell capacity are preferred for better resolution of the load cell data. Similarly, the other materials fall within a more appropriate range of the load cell

capacity with the 250 lb load cell (Table 3).

Table 3 : Load cell capacity usage

Material	% of 250 lb capacity	% of 2000 lb capacity
Aluminum	9	1
Copper	20	2
Titanium	45	5
Stainless Steel	75	9

Data collected with the 250 lb load cell did show a reduction in noise compared to that of the 2000 lb load cell, however, the relative improvement appears small. Data collected by each load cell for Titanium are shown in

Figure 30.

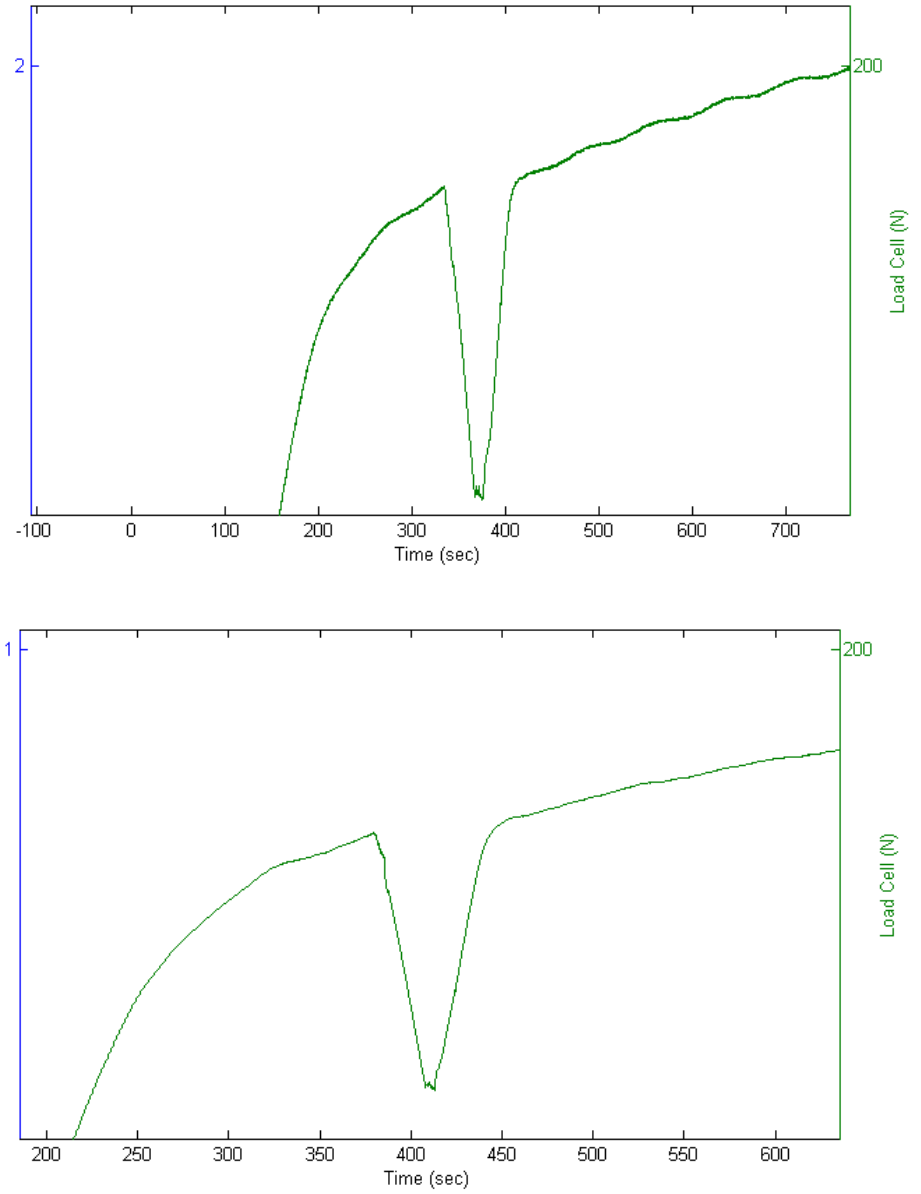

Figure 30: Load cell readings for 2000 lb capacity (above) and 250 lb capacity (below)

5.3 Reference Materials Results

The stress-strain plots developed from the reference material data are shown in Figure 31-Figure 34 for copper, Figure 35-Figure 39 for titanium, for stainless steel, and for aluminum. Strain, calculated from the measured extensometer

signal, is plotted on the abscissa and stress, calculated from the measured load cell signal, is plotted on the ordinate. The titles of these plots show the material type and the sample number associated with each test. These sample numbers may vary (i.e. skip values) because of tests that were discarded due to slipping of the sample grips and therefore incomplete data. All of these samples were tested at room temperature. All of the reference material tests used the 2000 lb capacity load cell, except for the last two titanium tests, Ti RT 05 (Figure 38) and Ti RT 06 (Figure 39), which used the 250 lb capacity load cell.

The initial loading moduli varied significantly and were much lower than the expected values. This effect is a result of how the reference materials are packaged and shipped. All the reference materials were wound on spools for shipping and therefore had significant bend along the length of the wire. The straightening required to mount the samples in the apparatus results in a significantly lower initial modulus. This effect is also demonstrated in the International RRT [14] and is important to remember while testing heat-treated Nb_3Sn samples in order to produce tests with sufficiently low Δ.

Furthermore, some of the plots (e.g. Figure 33) show a noticeable offset along the stress axis. This does not indicate pre-load being applied to the sample, but rather an error in the post-processing procedure. In any case, any adjustments in the offset do not affect the calculations for the initial and unloading modulus of the material. As the elastic modulus is the primary value of interest in this research,

any issues with the post-processing offset will be addressed in the future, but are not affecting the overall results presented in this work.

5.3.1 Copper

As previously mentioned, the initial modulus of copper showed large variation, ranging from 81 GPa to 127 Gpa, and was very far from the expected value for the modulus of copper of 117 GPa. The unloading modulus, ranging from 120 to 138 GPa, was more consistent and more closely matched the expected modulus value. Both modulus values, scattering measured by COV %, difference from the expected benchmark values, and deviation from each other (Δ) are shown in Table 4. The improvement in consistency and accuracy of the unloading modulus as compared to the initial modulus demonstrate the need for the unloading procedure during experiments. Additionally, the yield and ultimate strengths were close to the expected values, ranging from 375 to 388 MPa and 406 to 417 MPa, respectively. In light of the possible errors with the vertical offset, this value may vary by about 20 MPa, but the values obtained were still reasonable close to the expected strength values.

Table 4 : Summary of mechanical properties for copper samples

Property	Average	Std Dev	COV %	Benchmark	% Difference
E_0 (GPa)	100.47	18.66	18.6	117	14
E_u (GPa)	130.83	9.03	6.9	117	-12
Δ	0.20	0.16	81.9	-	-

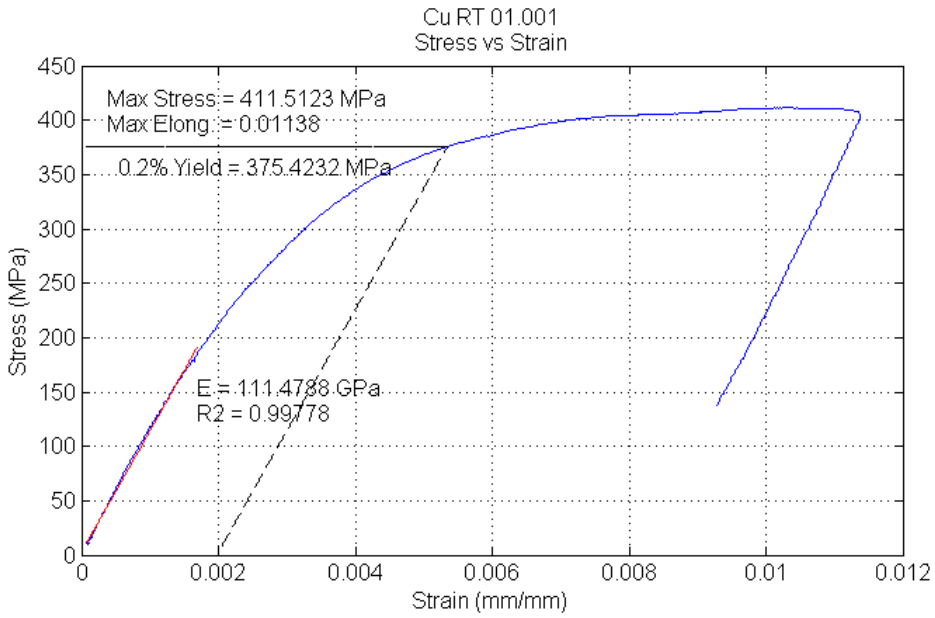

Figure 31: Stress-strain of Sample #01 of copper

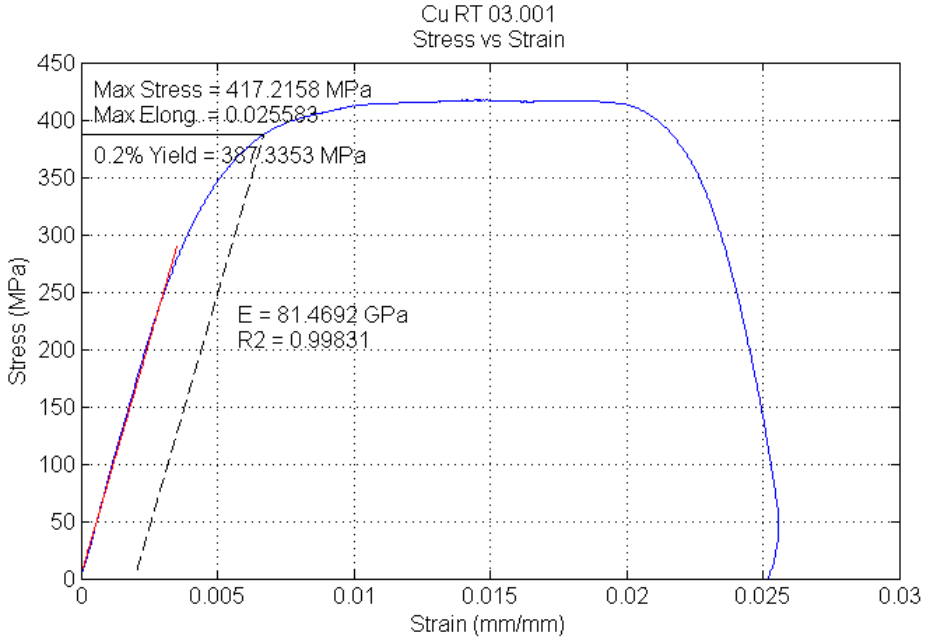

Figure 32: Stress-strain of Sample #03 of copper

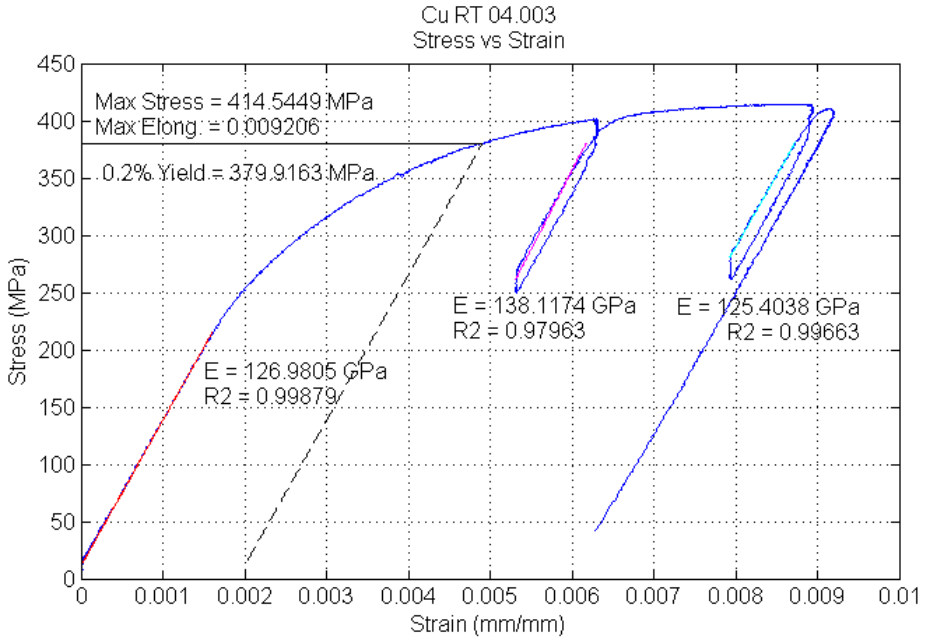

Figure 33: Stress-strain of Sample #04 of copper

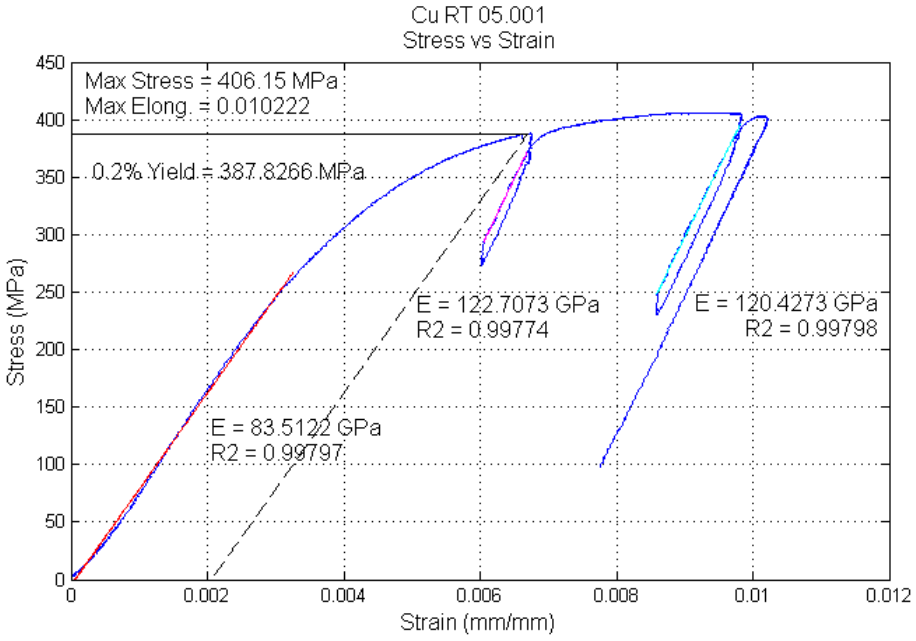

Figure 34: Stress-strain of Sample #05 of copper

5.3.2 **Titanium**

The titanium samples showed similar trends as the copper samples: decreased initial modulus, consistent unloading modulus, and close to expected values for

unloading modulus and yield and ultimate strengths. The initial modulus ranged from 68 to 89 GPa, compared to the expected value of 110 GPa. The unloading modulus ranged from 91 to 105 GPa. Both modulus values, their scattering measured by COV %, their difference from the expected benchmark values, and their deviation from each other (Δ) are shown Table 5. Additionally, a seemingly periodic disturbance signal can be seen towards the latter half of the curve. This may be due to electrical interference, vibrations, or because the load cell is operating in a small fraction of its overall capacity; however, it was significantly reduced after replacing the installed 2000 lb load cell with the smaller 250 lb load cell (Figure 38 and Figure 39). Additional investigations will be required to fully understand the source of this noise.

Table 5 : Summary of mechanical properties for titanium samples

Property	Average	Std Dev	COV %	Benchmark	% Difference
E_0 (GPa)	76.25	7.66	10.0	110	31
E_u (GPa)	99.16	3.54	3.6	110	10
Δ	0.22	0.08	36.1	-	-

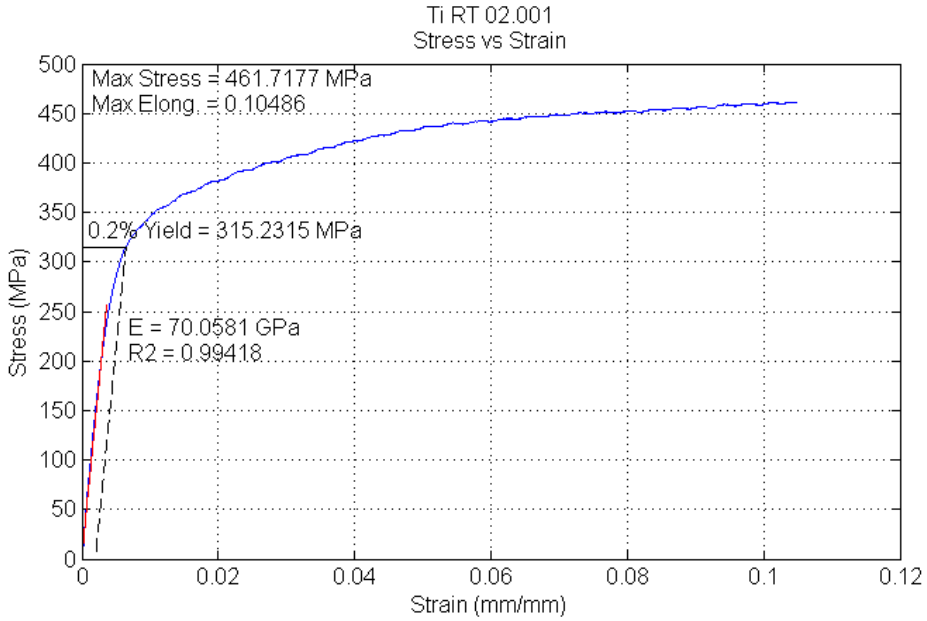

Figure 35: Stress-strain of Sample #02 of titanium

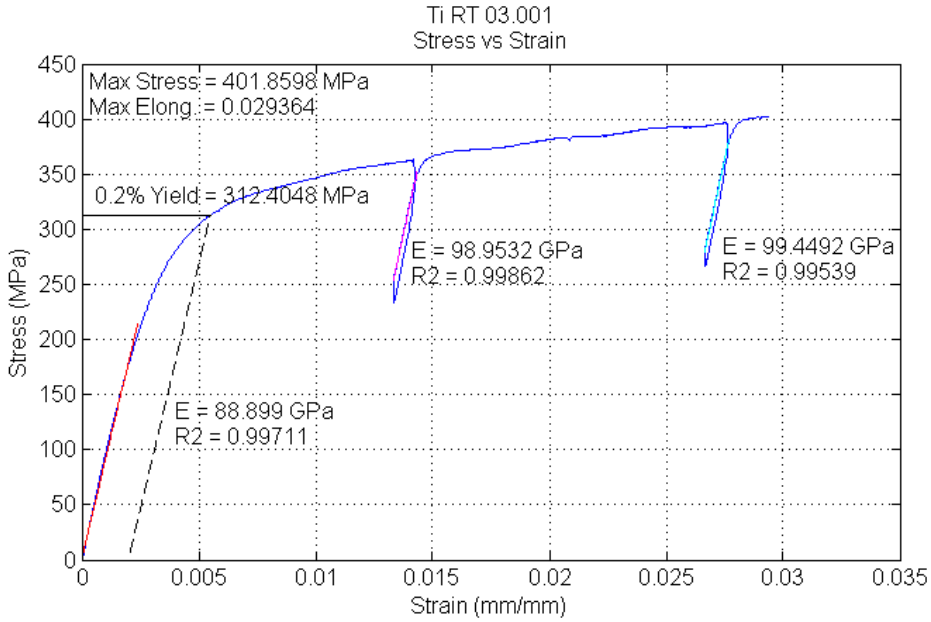

Figure 36: Stress-strain of Sample #03 of titanium

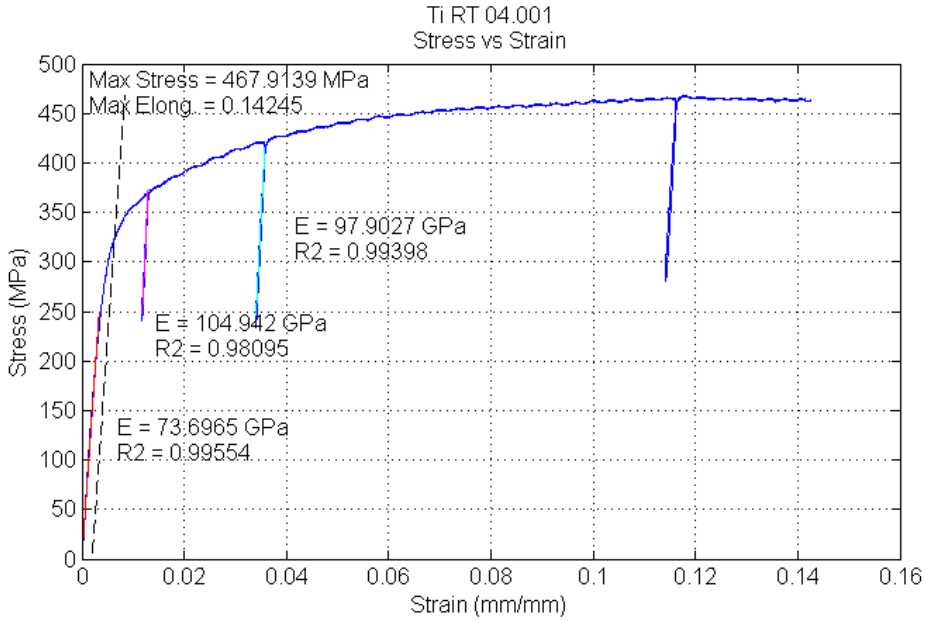

Figure 37: Stress-strain of Sample #04 of titanium

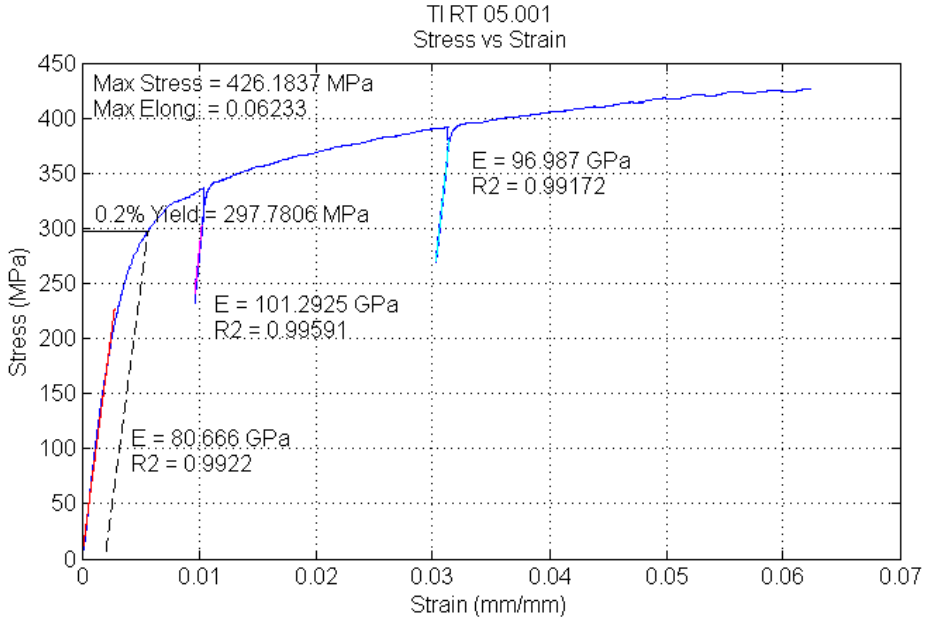

Figure 38: Stress-strain of Sample #05 of titanium

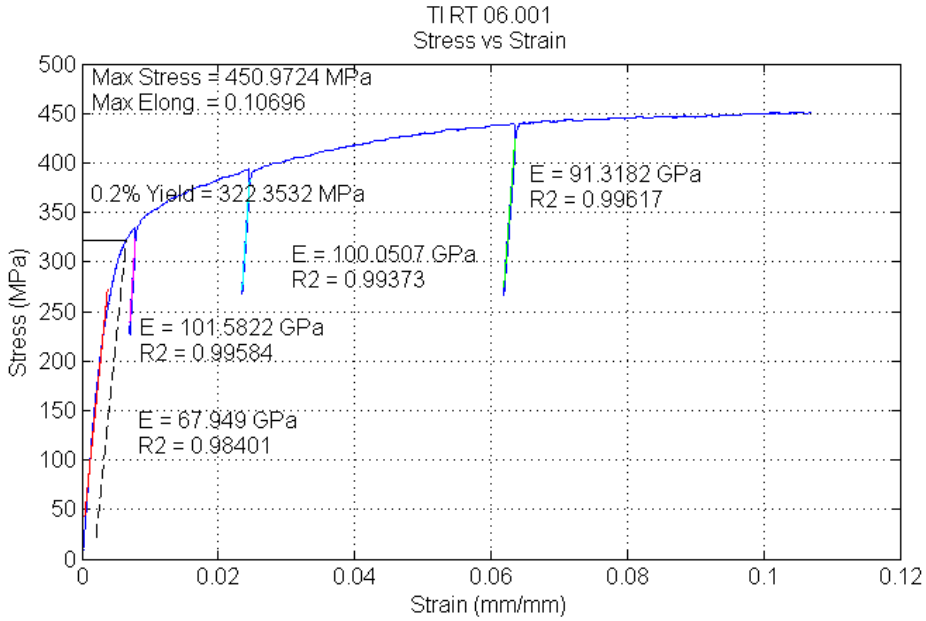

Figure 39: Stress-strain of Sample #06 of titanium

5.3.3 Stainless Steel

The stainless steel samples proved too strong to plastically deform with the sample grips designed for this apparatus. Before the stainless steel samples reached non-linear, plastic behavior and could be unloaded to generate an unloading modulus, the sample grips would begin to slip. While, this highlights the fact that the grips as they are currently designed cannot meet the required design load of 5 kN, the grips are small and relatively inexpensive components and would not be difficult to redesign for higher load. Fortunately, these tests were beneficial in showing the maximum holding capacity of the sample grips, around 770 N (around 1500 MPa for a 0.8 mm diameter wire). The average initial loading modulus and its deviation from the expected value for stainless steel is shown in Table 6.

Table 6 : Summery of the mechanical properties measured from stainless steel tests

Property	Average	Std Dev	COV %	Benchmark	% Difference
E_0 (GPa)	144.42	0.96	0.7	180	20
E_u (GPa)	-	-	-	-	-
Δ	-	-	-	-	-

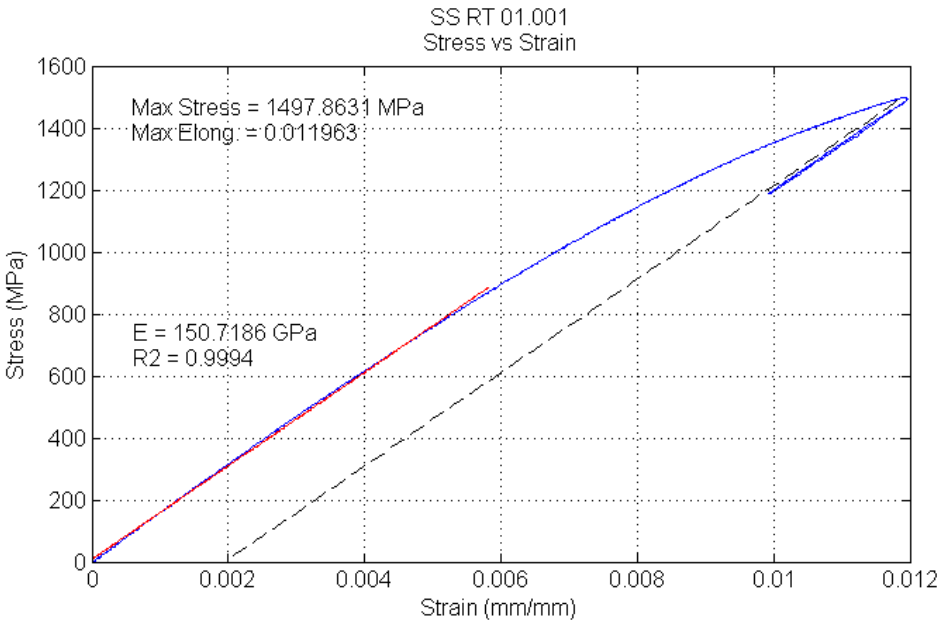

Figure 40: Stress-strain of Sample #01 of stainless steel

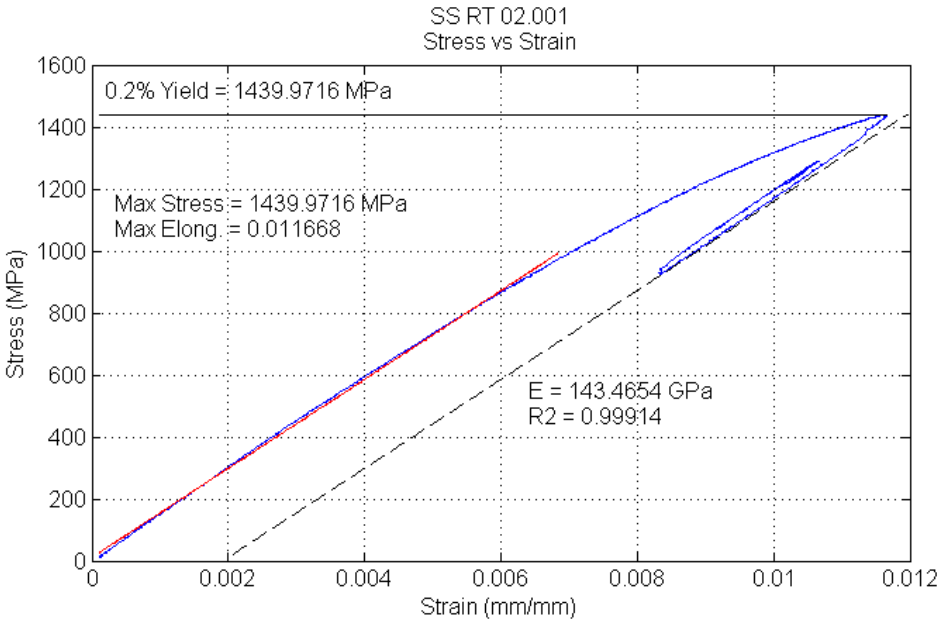

Figure 41: Stress-strain of Sample #02 of stainless steel

5.3.4 **Aluminum**

Aluminum proved to be the most difficult material to test due to its incredibly soft nature. These test samples exhibited a very low yield strength (below 60 MPa, compared to around 300 MPa for copper) and therefore it was very difficult to accurately measure the Young's modulus of the material. The initial modulus varied tremendously, ranging from 14 GPa to 50 GPa, and was much lower than expected. Additionally, the unloading modulus also ranged greatly, from 68 GPa to 145 GPa. Also, the noise from the load cell is very noticeable in these plots, adding additional uncertainty to the modulus measurements.

Due to the great difficulty in measuring the modulus of the aluminum material, a second series of testing for aluminum on an Instron tensile testing machine was attempted to attempt to duplicate the results seen on this apparatus. However, due to a lack of proper equipment to grip the small diameter wires, the modulus obtained in this second series using the Instron machine showed even greater scattering of results and the series was abandoned.

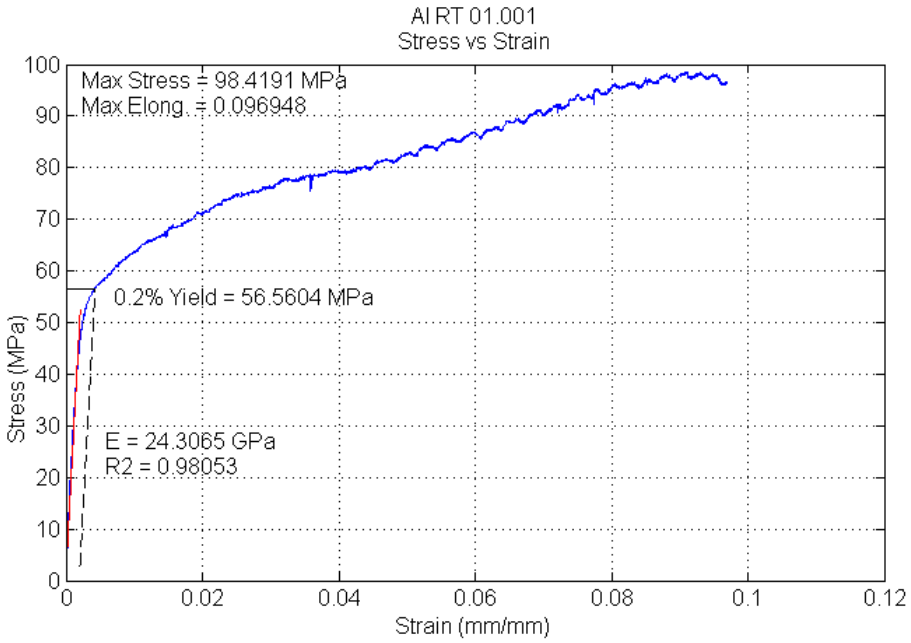

Figure 42: Stress-strain of Sample #01 of aluminum

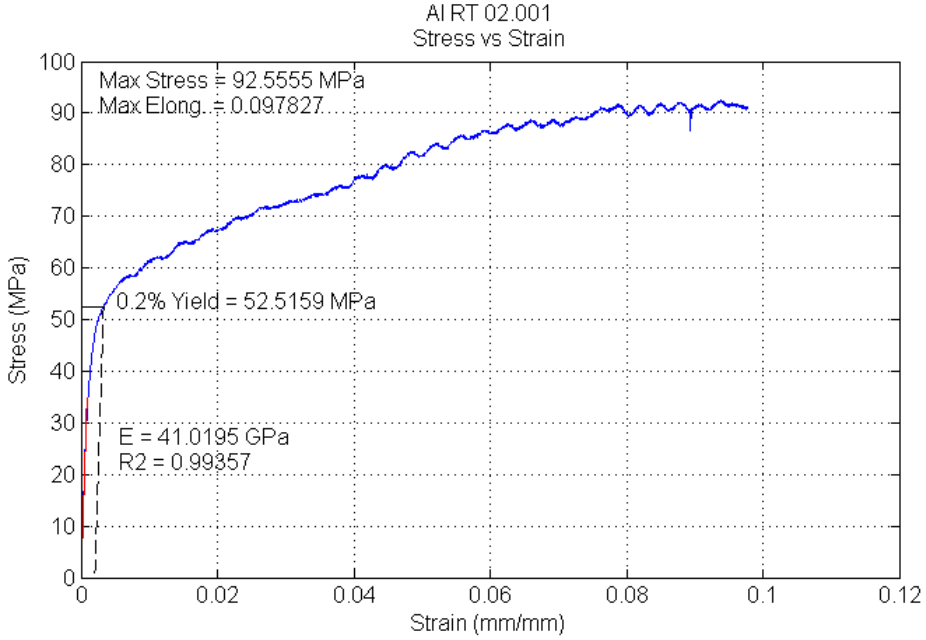

Figure 43: Stress-strain of Sample #02 of aluminum

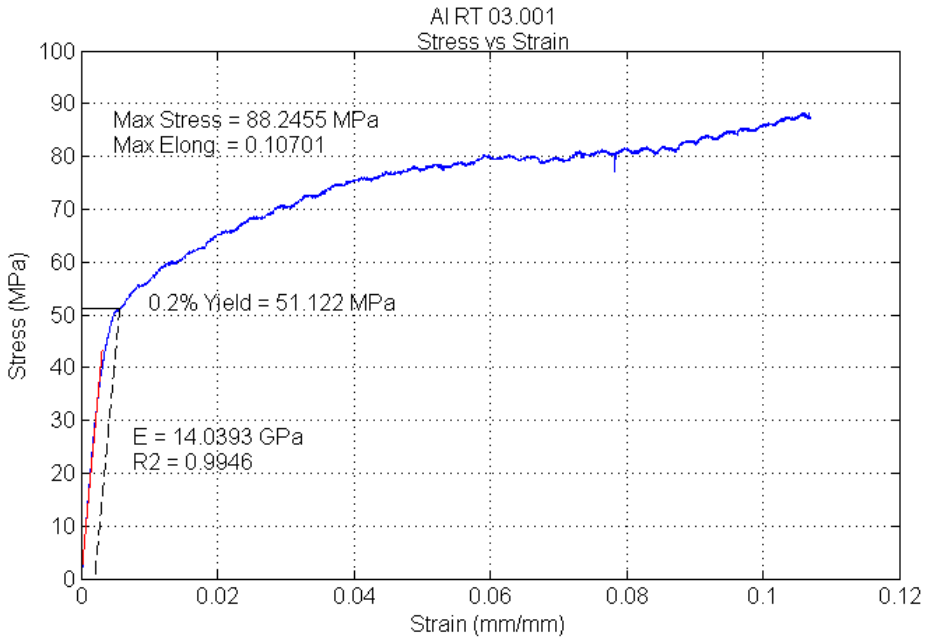

Figure 44: Stress-strain of Sample #03 of aluminum

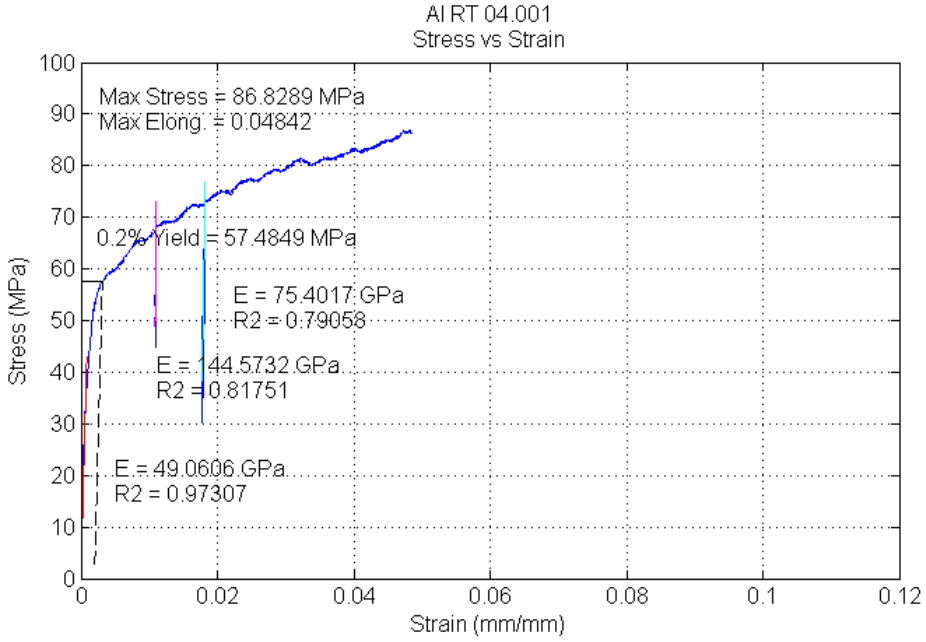

Figure 45: Stress-strain of Sample #04 of aluminum

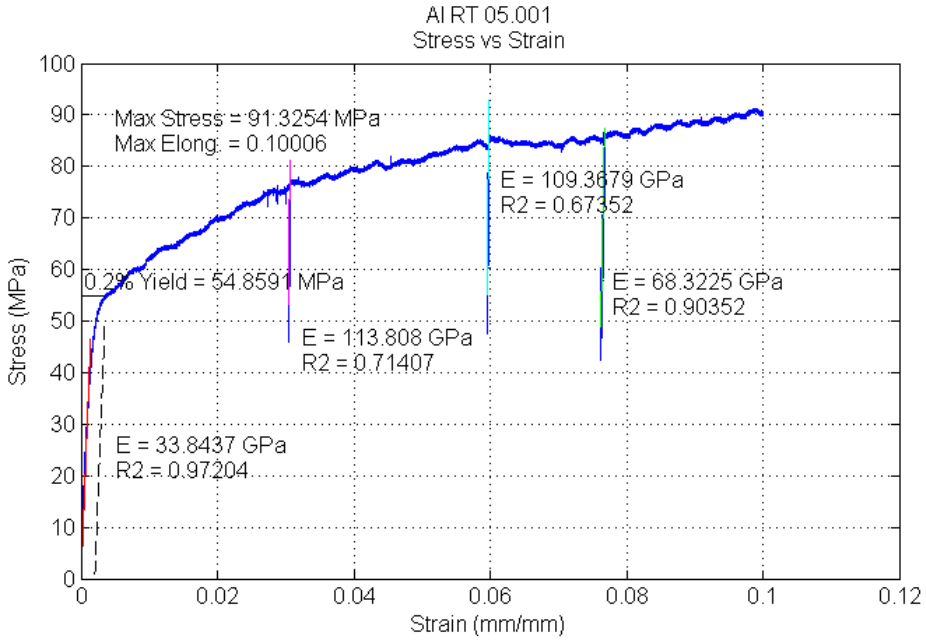

Figure 46: Stress-strain of Sample #05 of aluminum

A summary of the results for the average initial loading modulus and the average unloading modulus for each material are listed in Table 7. Only results from the tests that showed $\Delta < 0.3$ are included in this table.

The initial loading modulus for all the materials showed large amounts of scatter. This is most likely due to the initial bend of the wire samples. The unloading modulus for copper and titanium showed results very close to expected values (about 14% and 10% from expected values) with minimal scatter of data. However, aluminum proved very difficult to test accurately, with very high COV % for all measured moduli and the high yield strength of the stainless steel wire exceeded the holding force of the sample grips and therefore did not produce any unloading modulus values.

Table 7: Summary of Reference Material Results

Material	N	E_0			E_u		
		Average	COV %	% from	Average	COV	% from

		(GPa)		expected	(GPa)	%	expected
Copper	4	100.47	18.6	12.6	130.83	6.9	-13.8
Titanium	5	76.25	10.0	30.7	99.16	3.6	9.9
Stainless Steel	2	144.42	0.7	19.8	-	-	-
Aluminum	5	32.45	37.9	53.0	102.29	27.1	-48.3

5.4 Superconducting Materials Results

Four manufacturers of Nb_3Sn wire were tested to characterize their mechanical properties: Oxford, Luvata, Hitachi, and European Advanced Superconductors (EAS). Both unreacted and heat-treated samples were tested. First, the heat-treated sample tests will be discussed. The stress-strain plots developed from these tests are shown in Figure 48 through Figure 51 for Oxford, Figure 52 through Figure 55 for Luvata, Figure 56 through Figure 58 for Hitachi, and Figure 59 through Figure 61 for EAS. The Oxford and Luvata wires are manufactured with the internal tin type method and the Hitachi and EAS wires are manufactured with the bronze-route type method (Figure 47).

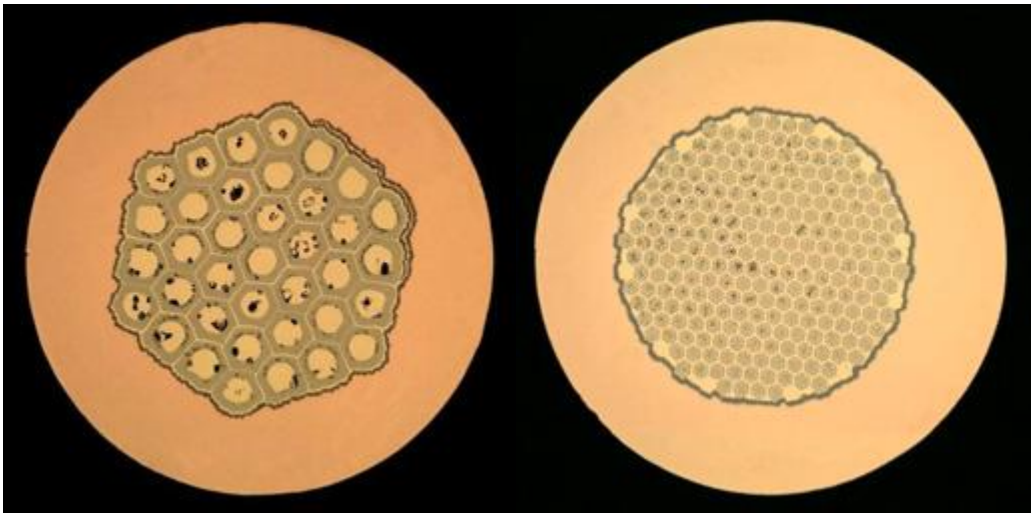

Figure 47: Cross section of wire for internal tin method (left) and bronze-route method (right)

Features to note in the plots of the heat-treated samples include:

- A much smaller range of strain compared to that of the reference materials
- A very small and slightly non-linear elastic region
- An absence of a purely plastic region as seen in the reference material tests (This demonstrates the brittle nature of the heat-treated material)

5.4.1 Oxford Samples

The three features just previously mentioned (small strain range, small elastic region, non-linear elastic region, brittle behavior) can be seen in the Oxford stress-strain plots. The Oxford samples failed under much less strain (and stress) compared to the reference materials (highest strain reached was just over 0.5%). The initial loading line is very small, ending before 20 MPa in some cases, and the modulus measured on this line varied considerably, with up to 20 GPa difference between the maximum and minimum initial modulus measured. On the other hand, the unloading modulus values differed by at most 10 GPa between the maximum and minimum values measured.

It should also be noted that the yield strength taken at the 0.2% offset point follows the standard procedure for reporting yield strength, however, this procedure is clearly inappropriate for this material. Yielding can be seen to occur much sooner than 0.2%, closer to 0.02%. However, for the purposes of consistency of the experimental procedure and because the primary goal of this

work is to obtain the Young's modulus, these tests still reported the yield strength taken at the 0.2% offset.

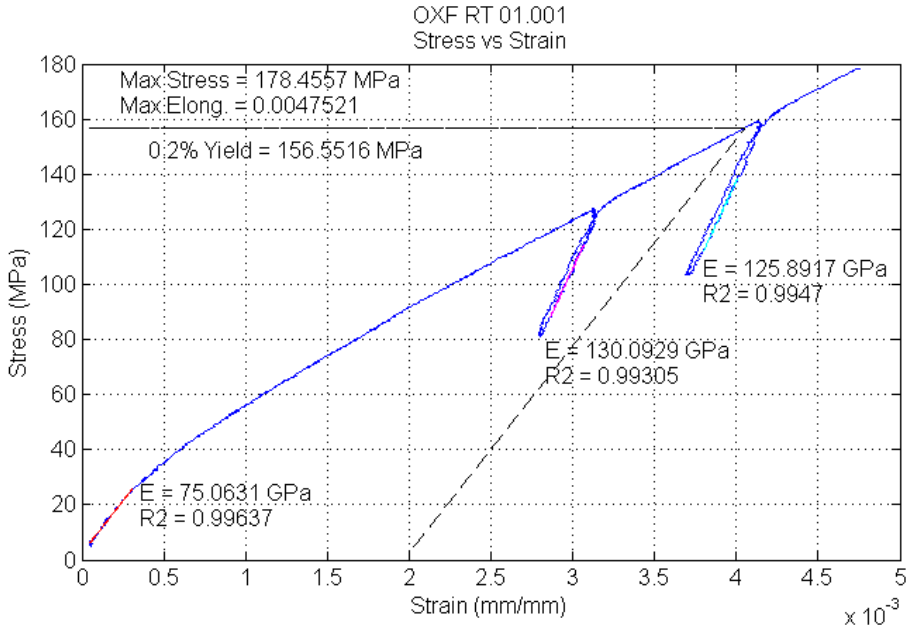

Figure 48: Stress-strain plot of Sample #01 for Oxford wire

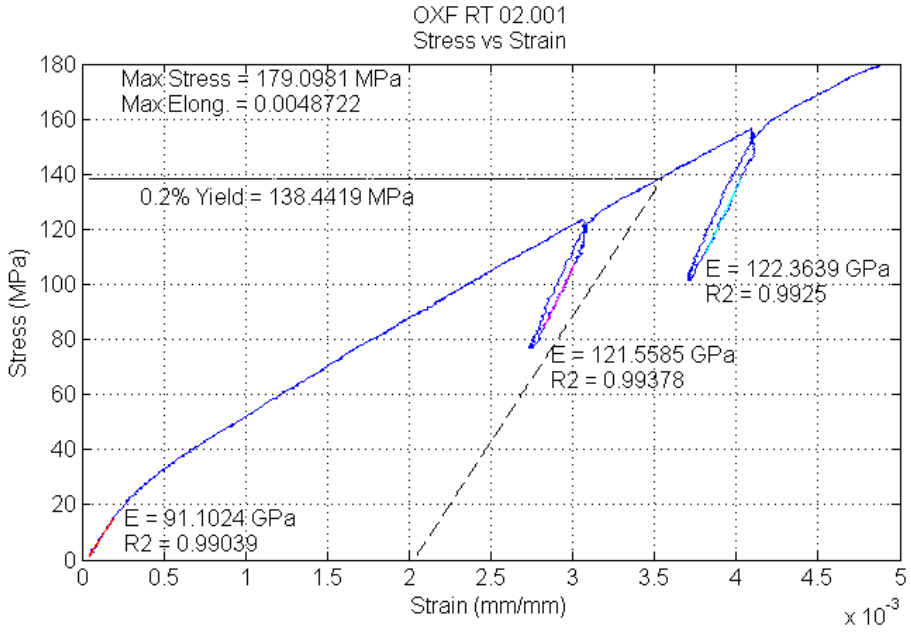

Figure 49: Stress-strain plot of Sample #02 for Oxford wire

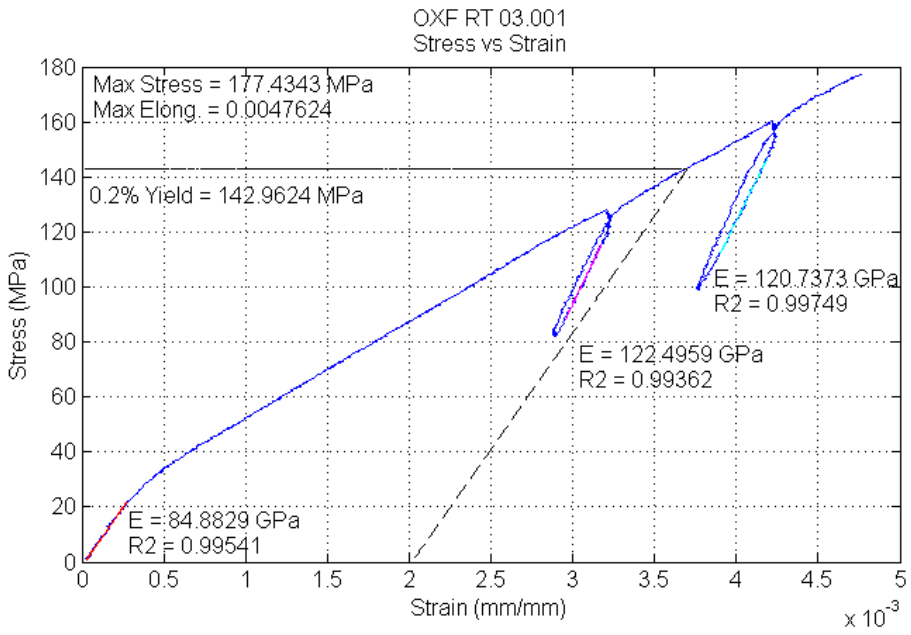

Figure 50: Stress-strain plot of Sample #03 for Oxford wire

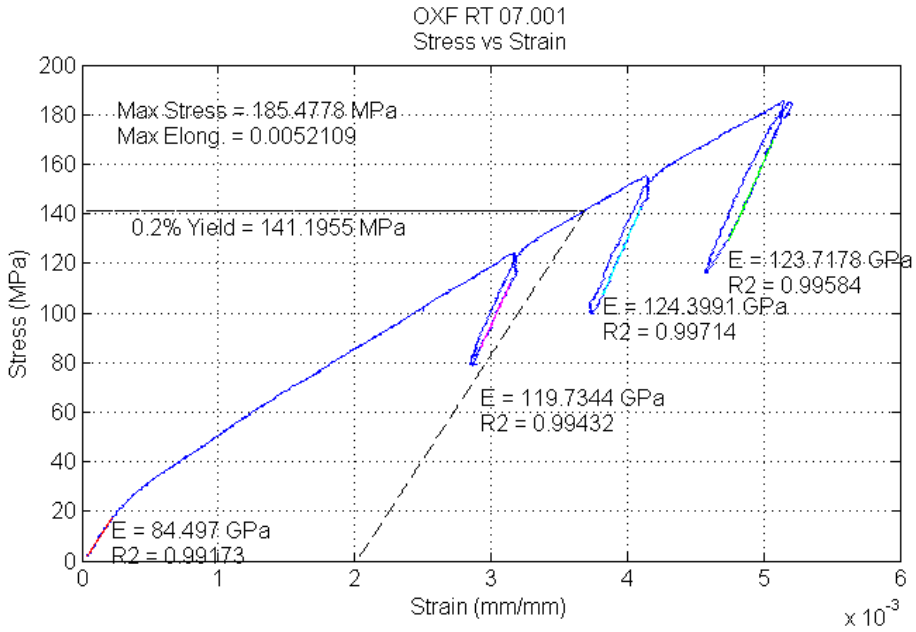

Figure 51: Stress-strain plot of Sample #07 for Oxford wire

5.4.2 Luvata Wire

The Luvata samples showed very similar results as those of the Oxford wire. The unloading modulus was around 120 GPa and the results showed a large delta, Δ. Both the Oxford and Luvata wires are manufactured with the internal-tin method.

The similar results produced by the Oxford and Luvata wires may be related to the manufacturing process used for both and the resulting structure of the cross-section.

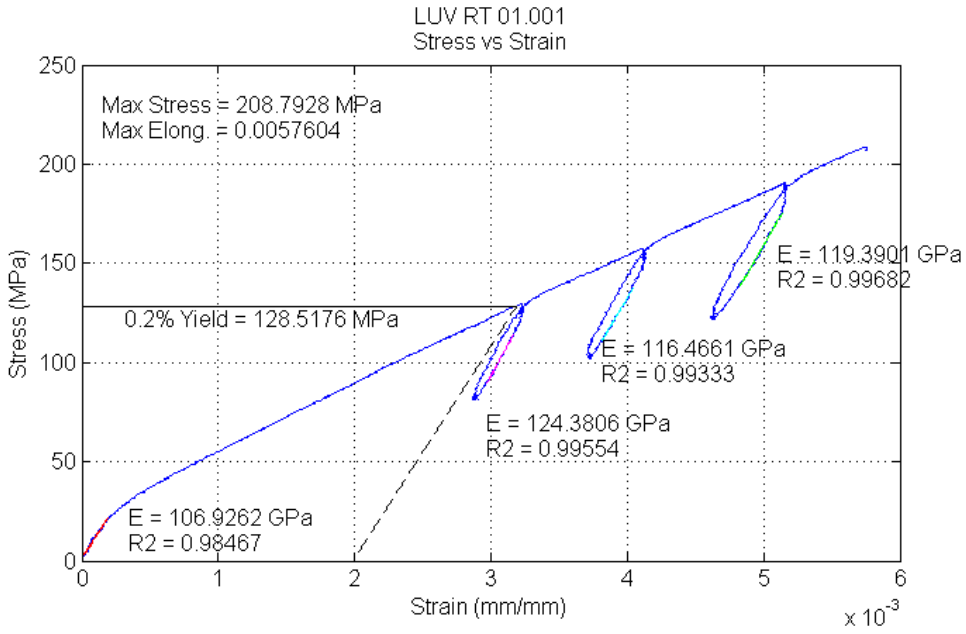

Figure 52: Stress-strain plot of Sample #01 for Luvata wire

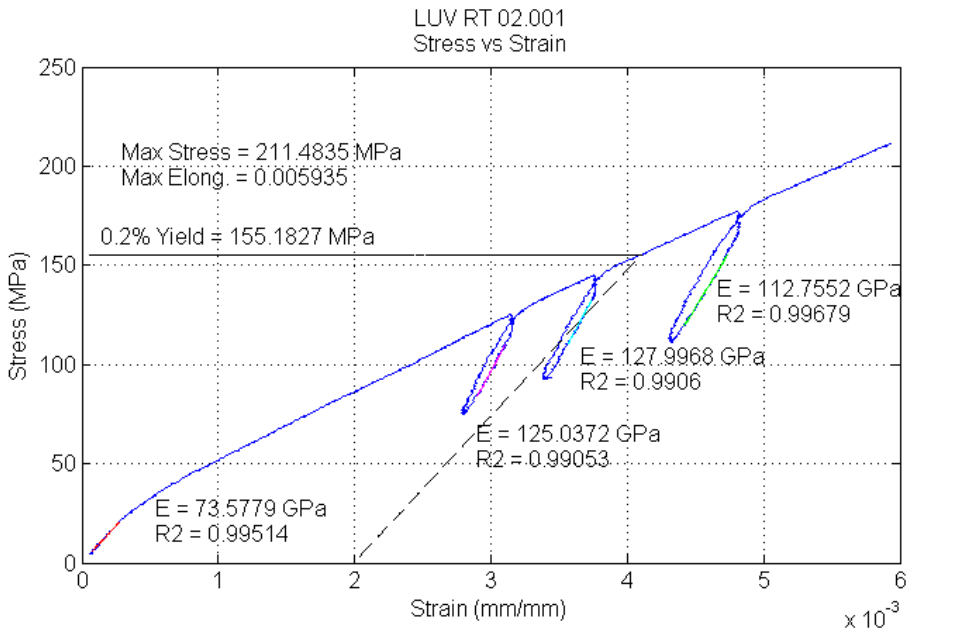

Figure 53: Stress-strain plot of Sample #02 for Luvata wire

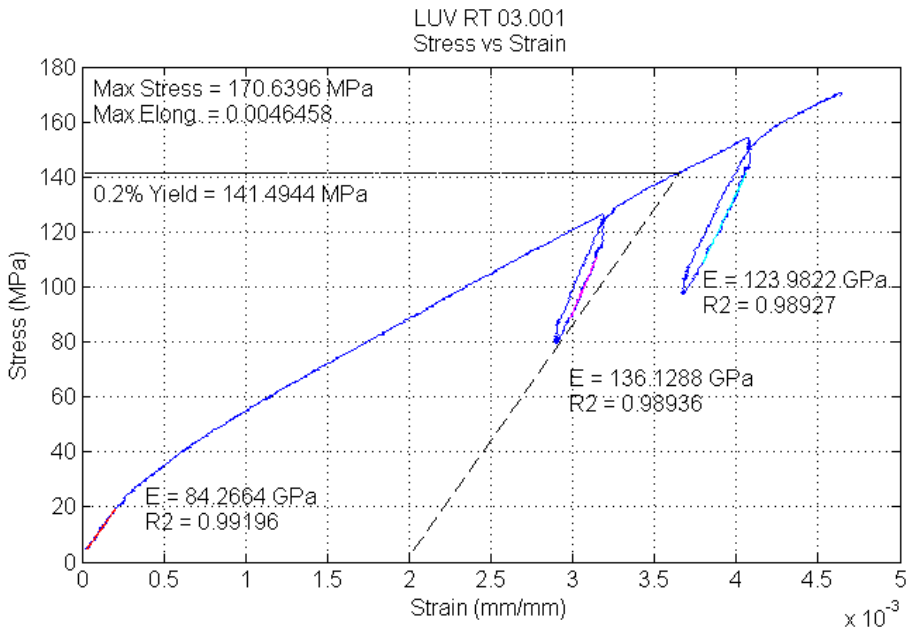

Figure 54 : Stress-strain plot of Sample #03 for Luvata wire

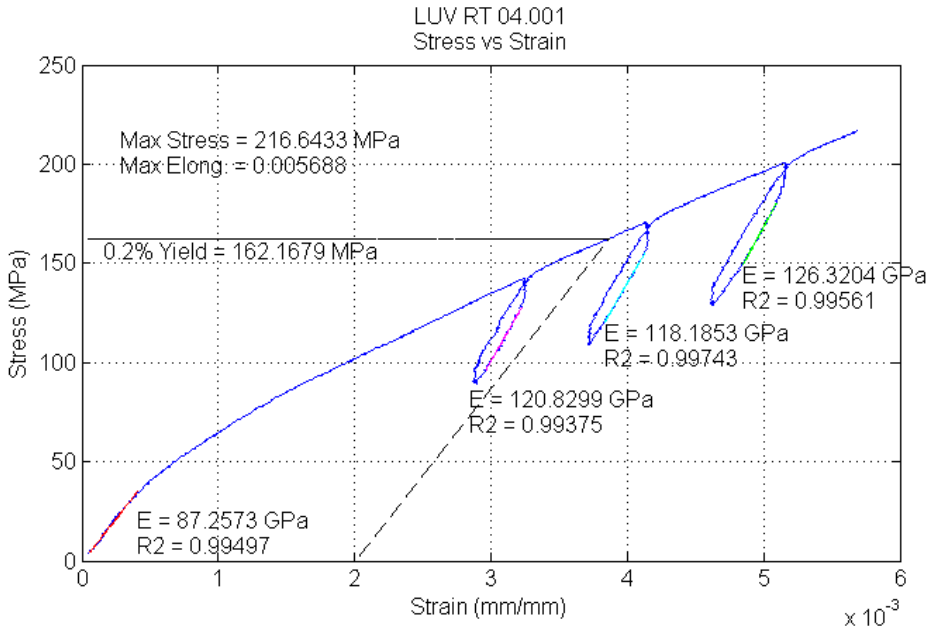

Figure 55: Stress-strain plot of Sample #04 for Luvata wire

5.4.3 Hitachi Wire

Unlike the Oxford and Luvata wires, the Hitachi wire samples showed a slightly lower modulus and significantly lower delta, Δ. The latter point resulted in no tests invalidated for the Hitachi wire, as opposed to the Oxford and Luvata

samples that both had 50% invalid tests. Unlike the other two wires mentioned, the Hitachi wire is manufactured with the bronze-route method (Figure 47, right). This further supports the suggestion that the manufacturing method and the resultant cross-section of the wire may have an influence over the modulus values and its delta value during testing.

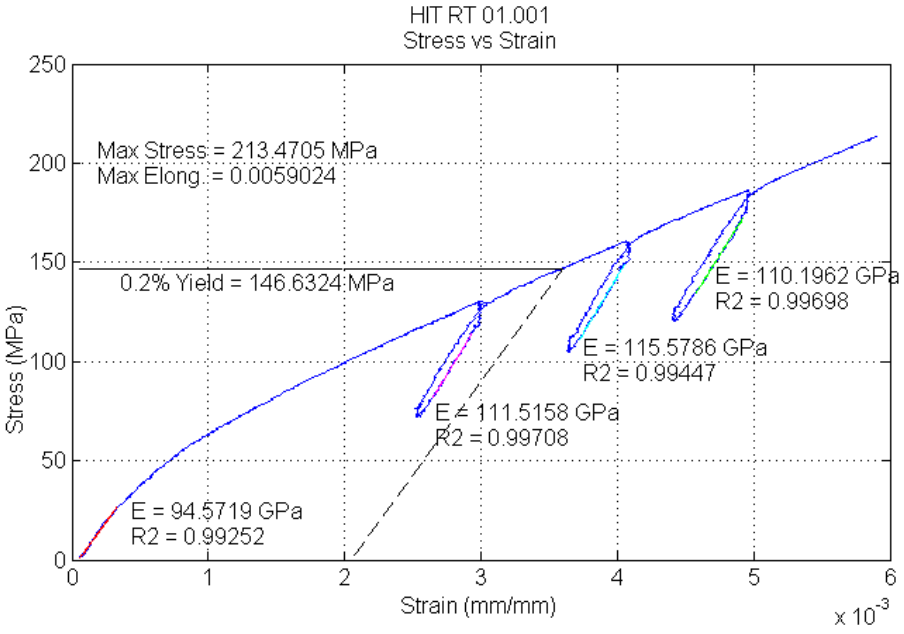

Figure 56: Stress-strain curve for Sample #01 of Hitachi wire

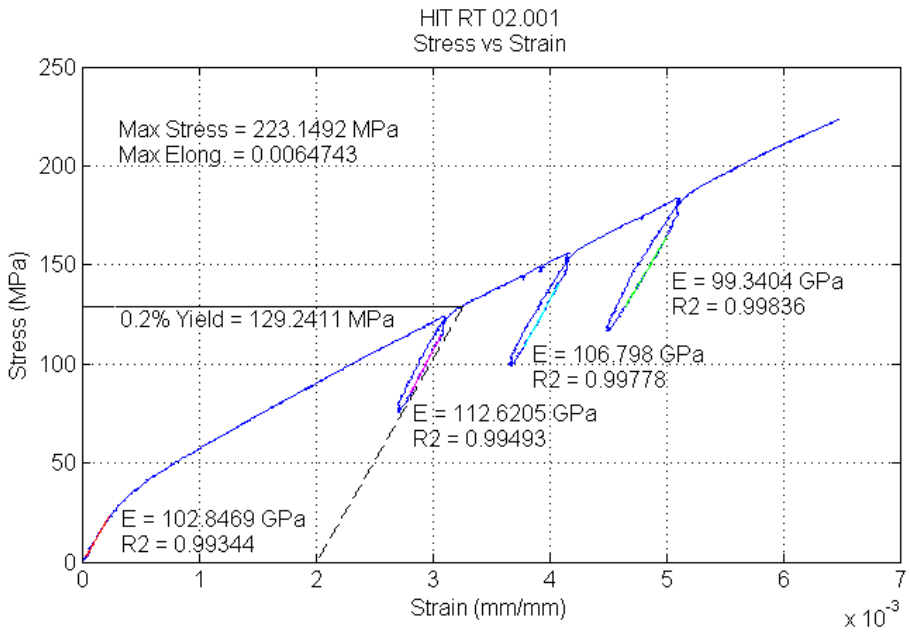

Figure 57: Stress-strain curve for Sample #02 of Hitachi wire

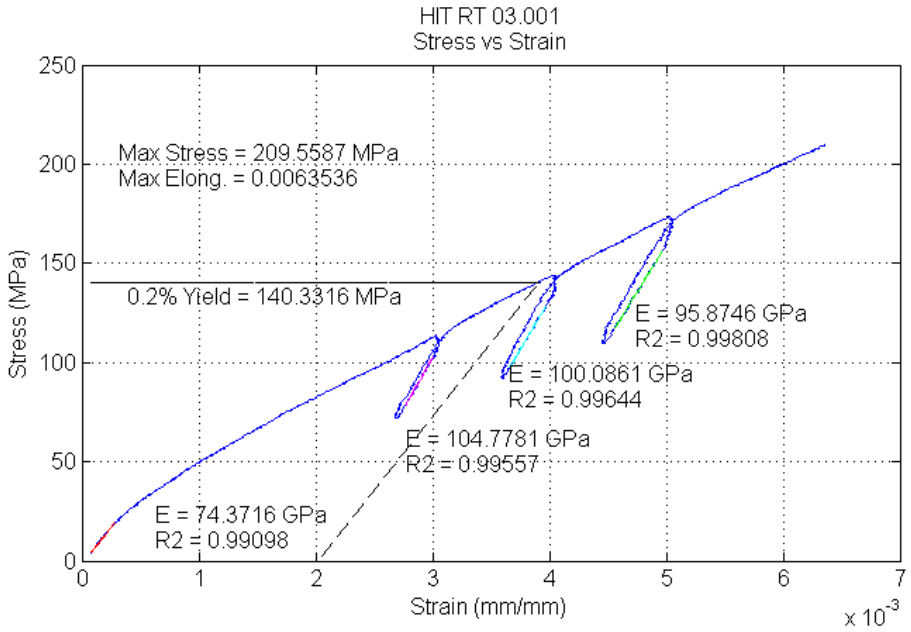

Figure 58: Stress-strain curve for Sample #03 of Hitachi wire

5.4.4 European Advanced Superconductor (EAS) Wire

The EAS wires showed very similar results to those of the Hitachi wires; unloading modulus values of about 110 GPa and low delta, Δ, values (all tests were valid). Again, like the two internal tin type wires, the two bronze-route types

(Hitachi and EAS) performed very similarly and differences of the properties between the two manufacturing methods are visible.

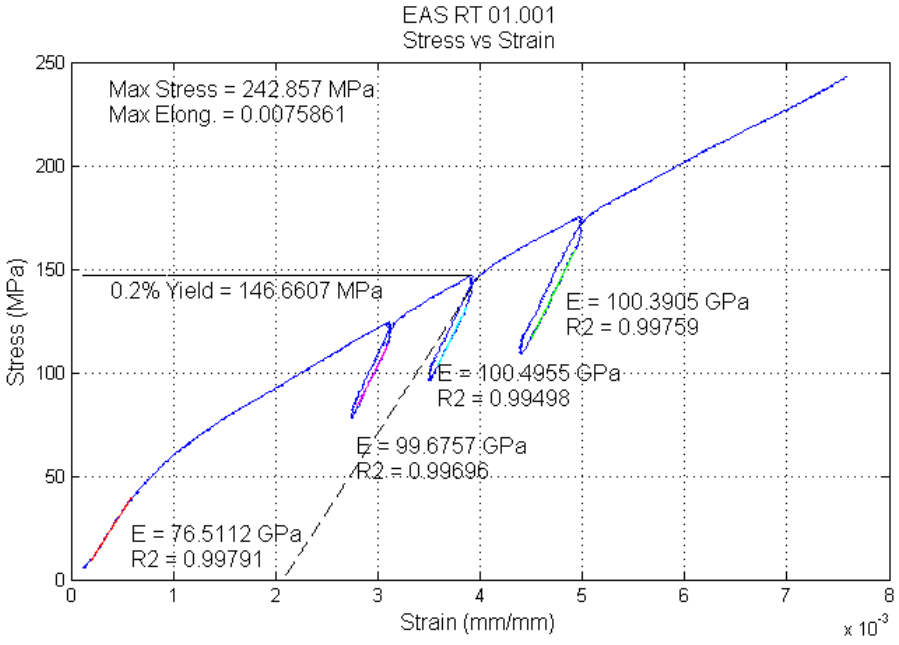

Figure 59: Stress-strain curve for Sample #01 of EAS wire

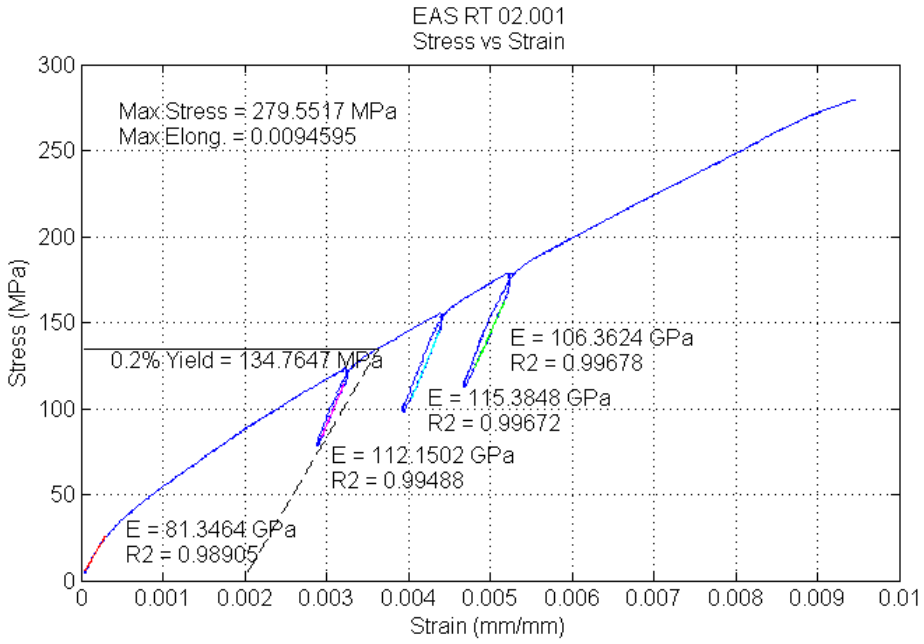

Figure 60: Stress-strain curve for Sample #02 of EAS wire

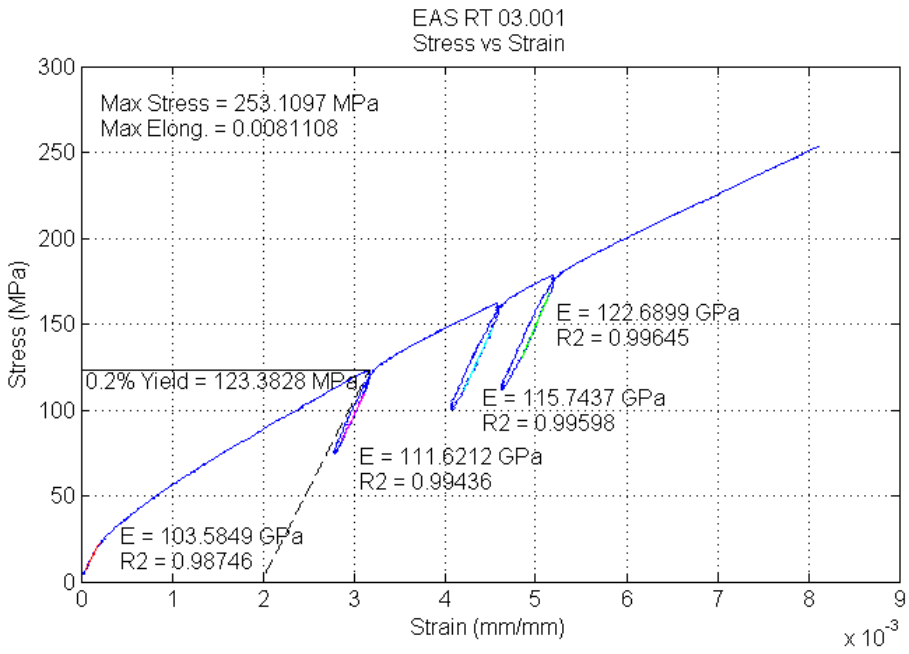

Figure 61: Stress-strain curve for Sample #03 of EAS wire

5.4.5 Heat Treatment Effect on Nb_3Sn wires

In addition to the heat-treated samples, unreacted samples from each manufacturer were also tested to investigate the effect that heat-treatment has on the material properties of the wire. In Figure 62, stress-strain curves for both an unreacted and heat-treated sample are shown.

Both curves overlap in the initial loading region, both with Young's modulus around 80 GPa. Once outside the initial loading region, the heat-treated sample separates from the unreacted sample and demonstrates more plasticity than the latter. The unloading moduli for both samples are all very similar in value, around 110 GPa, indicating that heat-treatment does not affect the elastic properties of the material. The effect on the material's plastic properties, however, is very evident. The unreacted sample shows much greater ductility, elongating over three times as much as the heat-treated sample.

Figure 63 through Figure 73 show the stress-strain plots for the remaining unreacted samples. All of these samples demonstrated the same trends as the previously mentioned EAS sample #06 compared to their corresponding wire manufacturer. The modulus values remained relatively constant for both initial modulus and unloading modulus, while the plastic properties changed greatly, indicating partial plasticity from heat-treatment as well as brittle behavior.

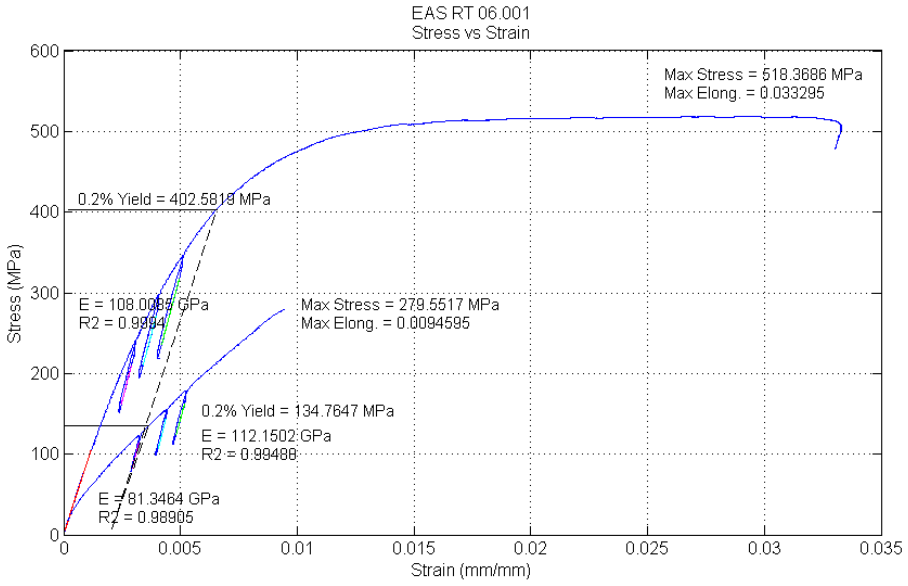

Figure 62: Stress-strain curve for heat treated and unreacted EAS Samples #02 & #06

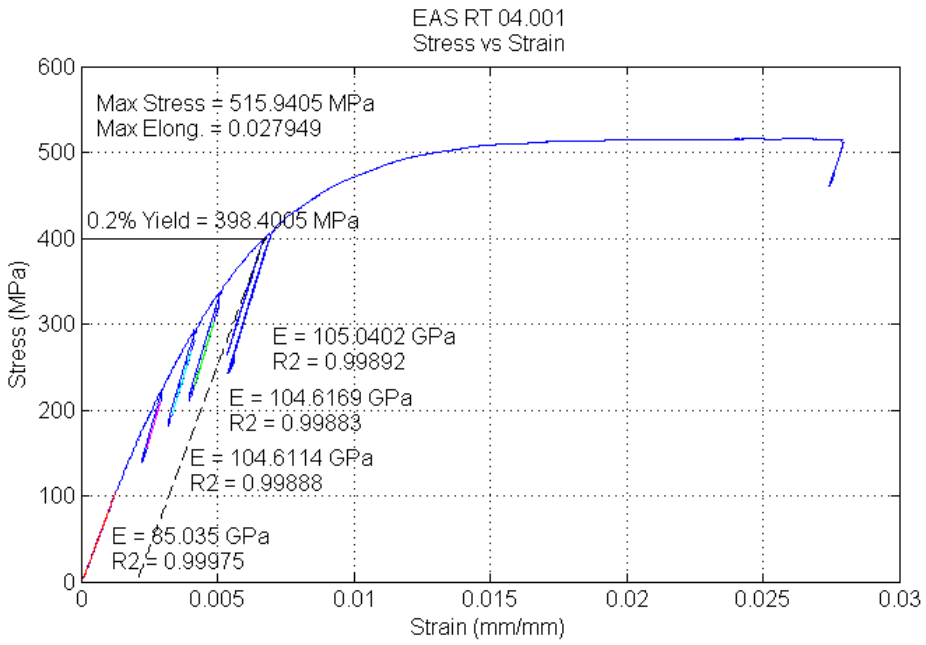

Figure 63: Stress-strain curve for unreacted EAS Sample #04

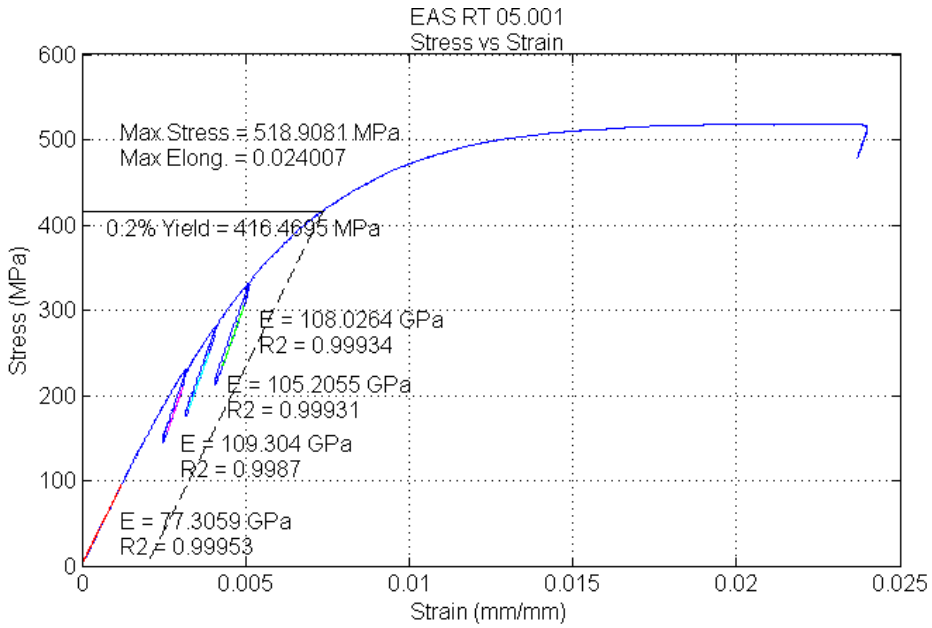

Figure 64: Stress-strain curve for unreacted EAS Sample #05

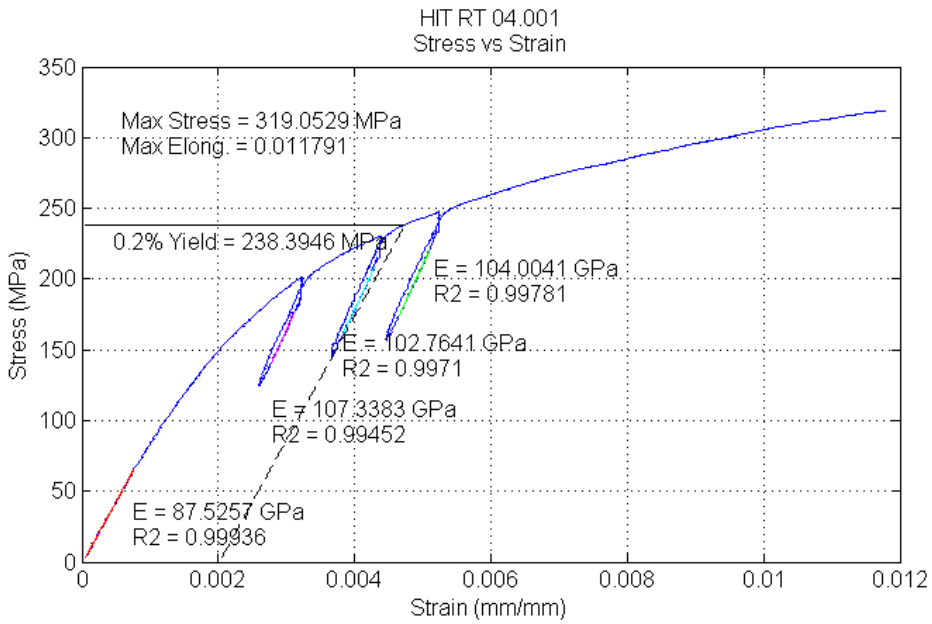

Figure 65: Stress-strain curve for unreacted HIT Sample #04

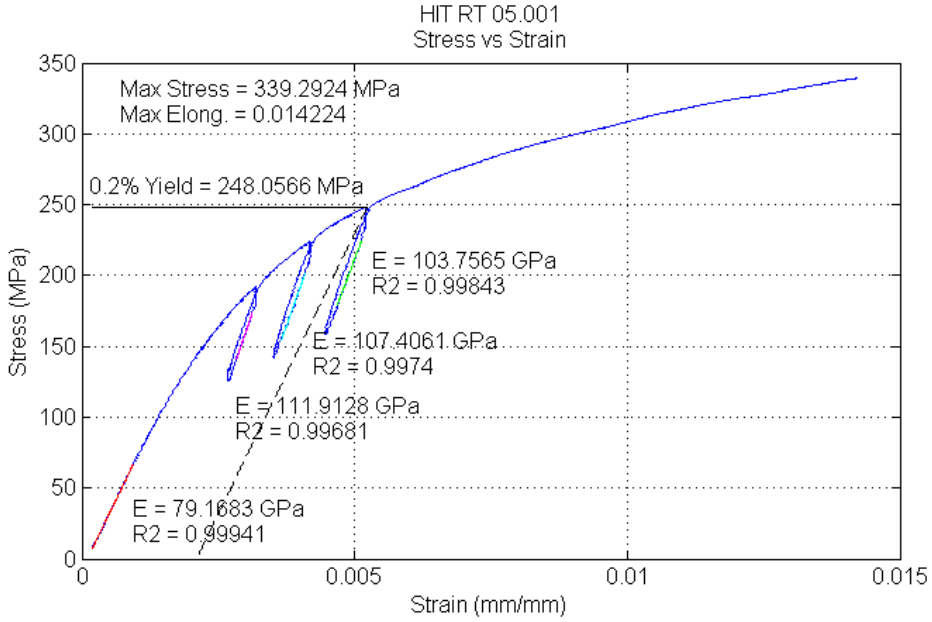

Figure 66: Stress-strain curve for unreacted HIT Sample #05

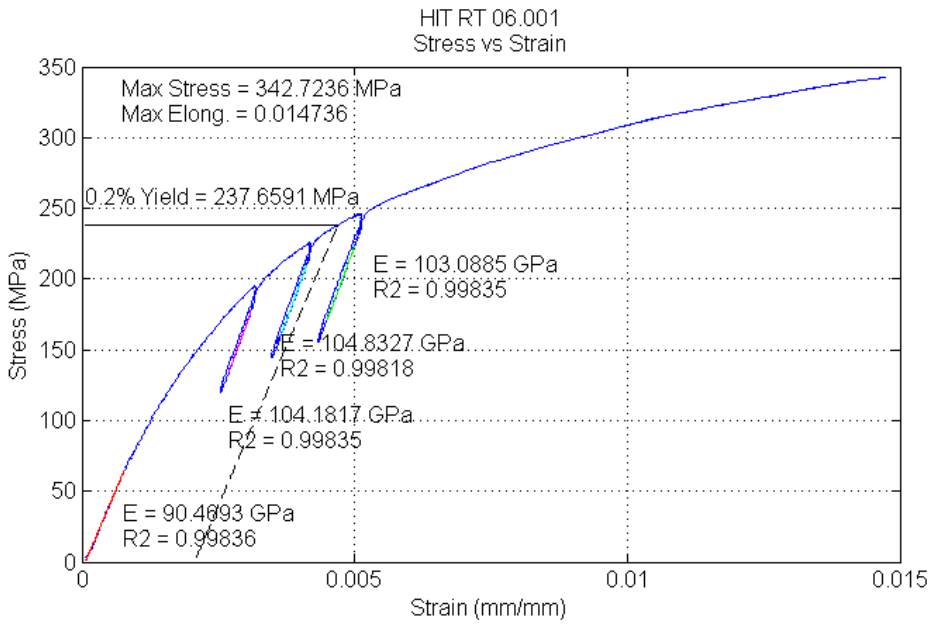

Figure 67: Stress-strain curve for unreacted HIT Sample #06

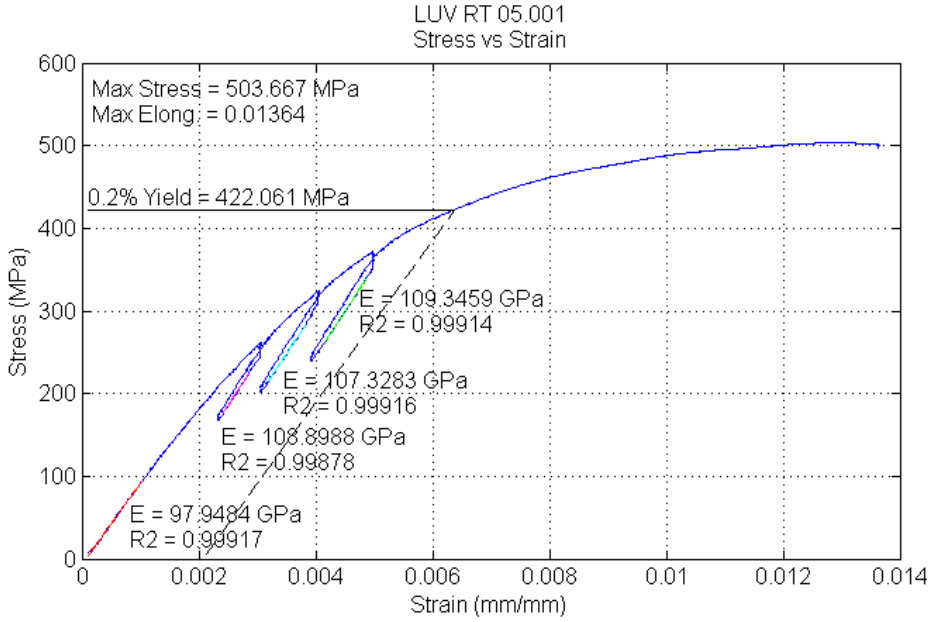

Figure 68: Stress-strain curve for unreacted LUV Sample #05

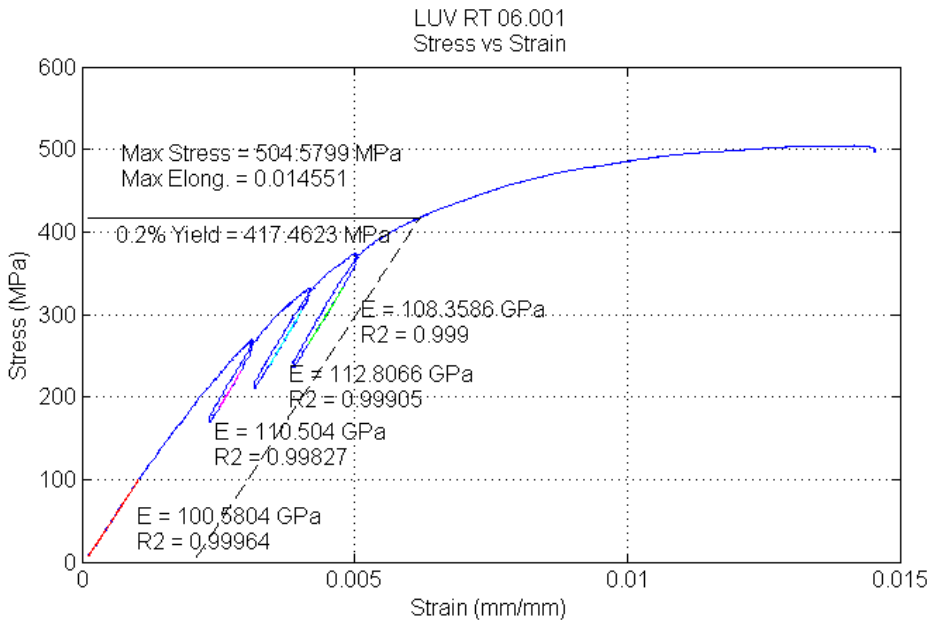

Figure 69: Stress-strain curve for unreacted LUV Sample #06

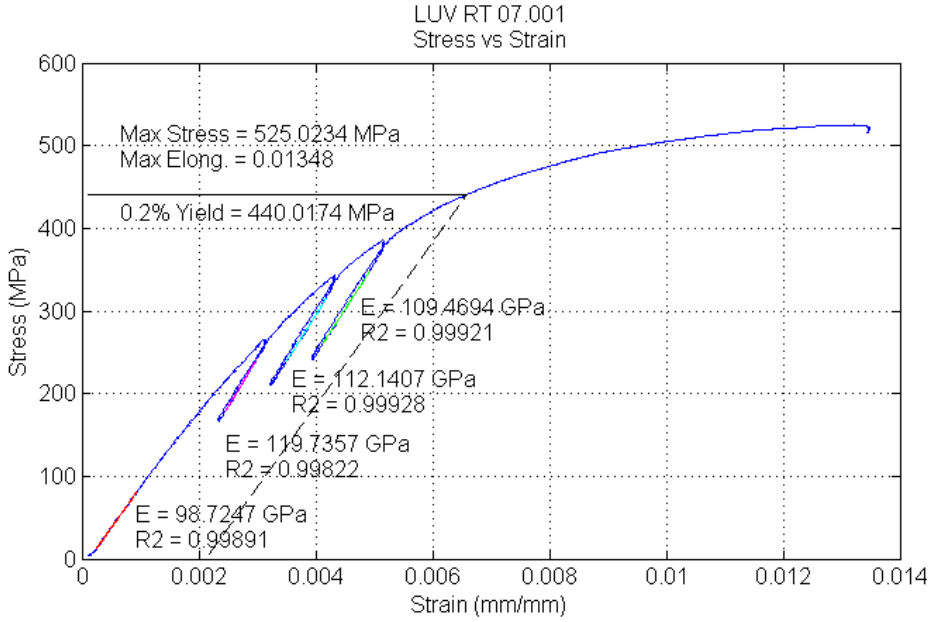

Figure 70: Stress-strain curve for unreacted LUV Sample #07

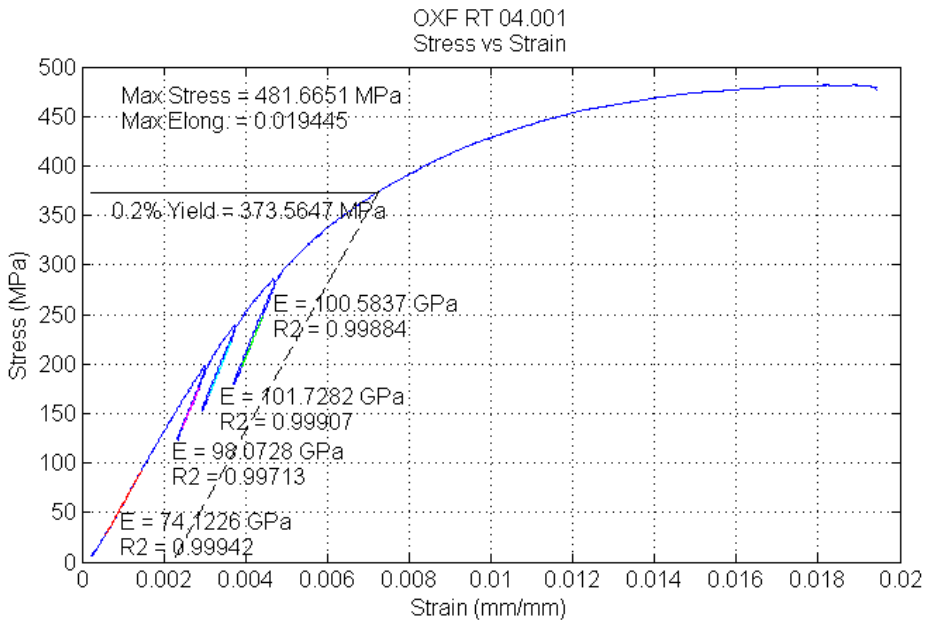

Figure 71: Stress-strain curve for unreacted OXF Sample #04

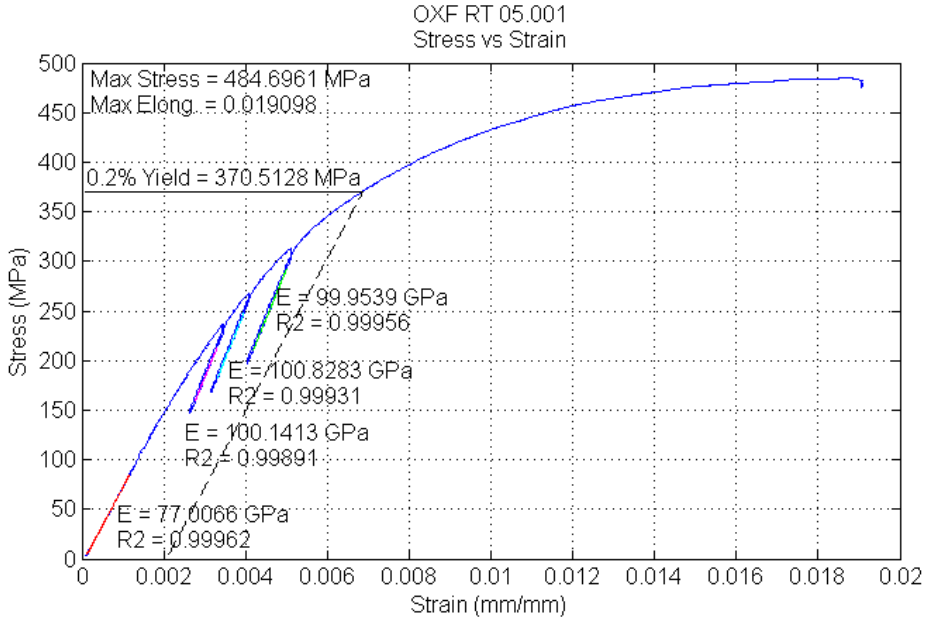

Figure 72: Stress-strain curve for unreacted OXF Sample #05

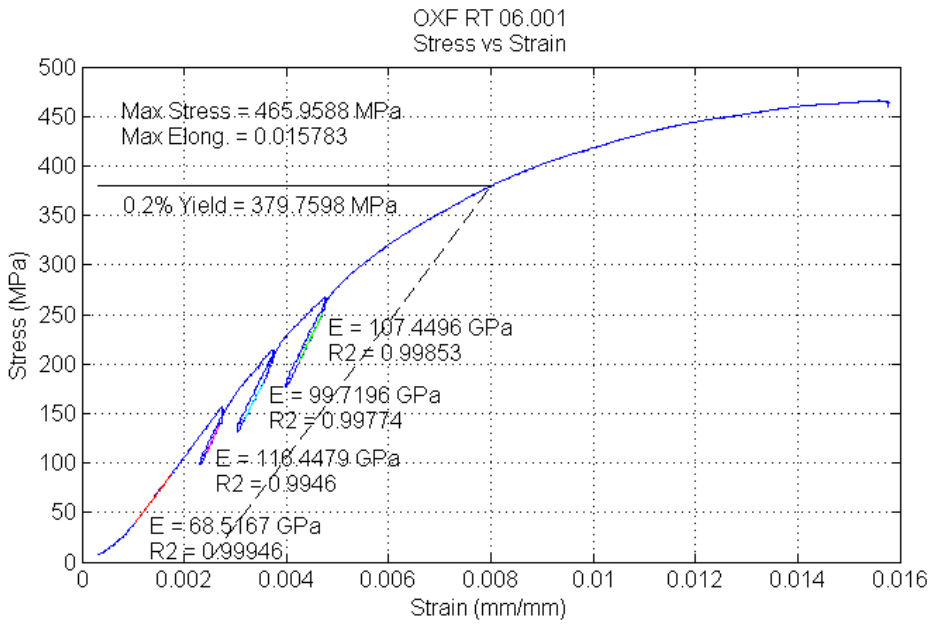

Figure 73: Stress-strain curve for unreacted OXF Sample #06

5.4.6 **Results Summary**

The results for the superconducting wire tests are listed in Table 8 by manufacturer and heat-treatment. Only the results with $\Delta<0.3$ are included in the summary. The Young's modulus values are very similar across all the wire manufacturers and are similar to the results found by the International Round Robin testing. It should be noted though, that the Round Robin testing series tested many more samples (approximately 30 samples per wire type) than were tested in these experiments. Additionally, wires manufactured by Hitachi show the smallest values of Δ while those manufactured by Oxford show the highest.

Table 8: Summary of superconducting wire tests

Manufacturer	Heat-treated	Un-reacted		Manufacturer	Heat-treated	Un-reacted
OXF				**LUV**		
N	2	2		N	2	3
E0 (GPa)	88	76		E0 (GPa)	97	99
EU0.3 (GPa)	122	99		EU0.3 (GPa)	123	113
EU0.4 (GPa)	122	101		EU0.4 (GPa)	117	111
EU0.5 (GPa)		100		EU0.5 (GPa)	123	109
EU Avg.	122	100		EU Avg.	121	111
Δ Avg.	0.28	0.25		Δ Avg.	0.20	0.11
Sy0.2%	141	372		Sy0.2%	145	427
Su	178	483		Su	213	511
elong. (%)	0.49	1.93		elong. (%)	0.57	1.39
HIT				**EAS**		
N	3	3		N	3	3
E0 (GPa)	91	86		E0 (GPa)	87	83
EU0.3 (GPa)	110	108		EU0.3 (GPa)	108	109
EU0.4 (GPa)	107	105		EU0.4 (GPa)	111	106
EU0.5 (GPa)	102	104		EU0.5 (GPa)	110	107
EU Avg.	106	106		EU Avg.	109	107
Δ Avg.	0.15	0.19		Δ Avg.	0.21	0.22
Sy0.2%	139	241		Sy0.2%	135	406
Su	215	334		Su	259	518
elong. (%)	0.63	12.87		elong. (%)	0.84	2.84

The COV for E_0 is significantly higher than $E_{u_}$across all the manufacturers, as shown in

Figure 74. The ranges for the COV of E_0 and E_u are similar to those found in the measurements of the International Round Robin [14] test series (

Figure 75). Moreover, many of the values show a reduced COV compared to those of the round robin tests. This may be an indication that the apparatus is generating consistent results, but may also be influenced by the materials selected for the tests.

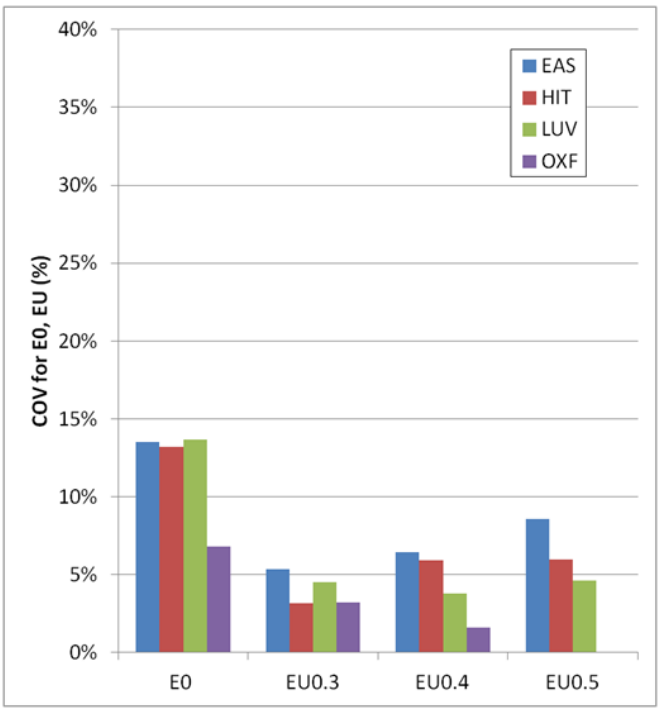

Figure 74 : COV for E0, Eu of heat-treated Nb_3Sn samples

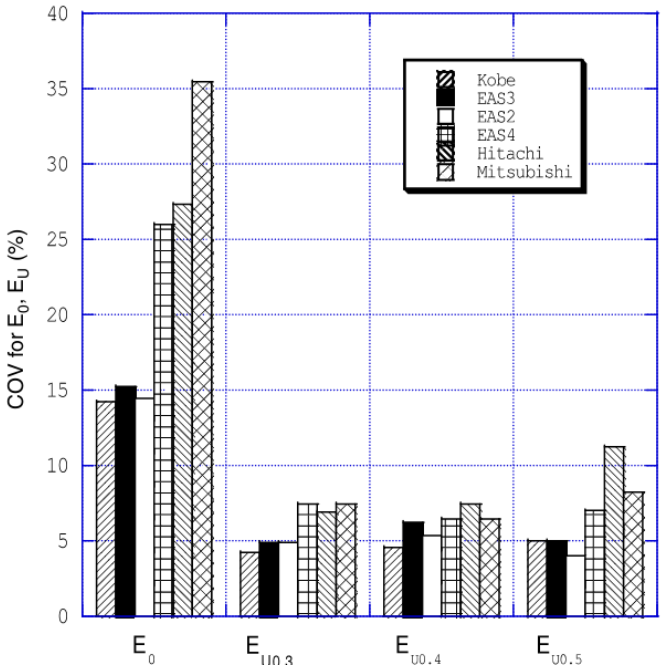

Figure 75 : COV for E0, Eu from International Round Robin test series [14]

5 CONCLUSION

5.3 Tensile Testing Apparatus

The apparatus was designed with all of the requirements listed in Section 3.1, including recommendations by the IEC draft, and has returned consistent mechanical property values for single strand Nb_3Sn superconducting wires at room temperature.

Reference materials copper, titanium, stainless steel, and aluminum were used to confirm the validity of the apparatus. The unloading modulus measured form the copper and titanium reference materials had low scatter and were close to expected values. Stainless steel was too strong to be yielded in this setup, however, the test with this material provided a measure of the maximum holding force of the sample grips. The aluminum proved very difficult to measure and the results were inconclusive. All in all, these tests demonstrated the limits of the apparatus difficulty in testing very strong and very soft materials, but also proved that it would return accurate and consistent results for materials with a modest modulus.

Wire types of four different Nb_3Sn manufacturers were tested and characterized. All the samples demonstrated small elastic zones, brittle behavior, and relatively similar Young's modulus. The manufacturing process appeared to cause noticeably different behaviors between the samples. The two wires manufactured with the internal-tin method, Oxford and Luvata, showed large variation between the initial and unloading modulus values (high Δ). Meanwhile, those

manufactured with the bronze method, Hitachi and EAS, showed considerably lower variation between the initial and unloading modulus (low Δ) and slightly higher unloading modulus (about 10 GPa higher).

Overall, the Young's modulus values from Nb_3Sn tests showed a COV of less than 15% for E_0 and less than 10% for E_u, which compared well against previous tests conducted for the International RRT series. This suggests that this apparatus is working appropriately and generating results with similar precision as those conducted in the RRT series. Unfortunately, the wire manufactures tested in the RRT series and in this experiment did not overlap much and so the modulus values collected from each experiment could not be compared.

5.4 Recommendations for Future Work

5.4.7 Debugging the system

In Figure 28 & Figure 29, several differences can be observed between the two stress-strain curves during unloading. These differences include:

- The sharpness of the transition point from loading to unloading
- A drop in stress at the moment of unloading for this apparatus
- The separation between the unloading and reloading curves

These issues could be caused by the material behavior, measurement devices, actuator, or overall apparatus compliance. It is important to determine the factors involved in causing these discrepancies with the IEC draft plots to ensure that this

apparatus is not adding additional errors and so that experiments can be made more repeatable and accurate.

Some steps that can be taken to debug the system include:

- Adapt grips to mount to commercial Instron machine to confirm results
- Use optical extensometer to compare measured strain against that measured with the double extensometer system to confirm that the extensometers are not slipping
- Adjust the anti-backlash nut spacing on the linear actuator to investigate any slack that may exist between the machine threads
- Investigate whether the noise observed in the load cell is produced by the electrical wall outlet and which components are picking up the noise
- Determine whether the motor is slowing under load or taking time to slow down or speed up during running and braking

5.4.8 Confirm apparatus works for 3-strand samples and at cryogenic temperatures

In the scope of this thesis, the apparatus has been designed with the goal of testing up to 3-strand samples at liquid nitrogen and liquid helium cryogenic temperatures, but it has only been confirmed to work for single strands at room temperature. At cryogenic temperatures it would be most important to ensure that thermal contraction of the materials does not impart any stress on the sample prior

to testing. For multi-strand samples, the sample grips will likely require a redesign to accommodate the larger overall diameter and non-circular nature of the bundle.

5.4.9 Closed-loop feedback for motor control

While the current motor setup meets all the design requirements for the tensile testing, a closed-loop system for the motor control that included computer control and feedback on crosshead position and motor speed would add more accuracy and autonomy to the apparatus. The current method for setting the crosshead speed does not account for any slowing of the motor under load, although it has not been determined how much of an effect this has on the system. This problem could be corrected with a feedback system that measures the speed of rotation of the actuator input shaft, such as an encoder, or a linear variable differential transformer (LVDT) to track the displacement of the actuator crosshead.

Additionally, the input shaft could be used to provide an indication of the crosshead position based on the displacement per rotation of the actuator. Position indication linked to computer motor control would allow the operator to automatically return the crosshead to the exact starting position needed for an experiment instead of watching and waiting for the actuator to traverse to the correct position. Furthermore, this control system could be used to automatically apply unloading at specified amounts of displacement.

5.4.10 Multi-geared motor for positioning flexibility

To meet the speed requirements of the experiments, the motor needed to be geared down significantly; the linear actuator has a 20:1 gear ratio and the motor

has a gearbox with a 702:1 ratio. While this gearing does provide efficient motor operation during testing, it also limits the maximum speed of the motor output to 2.6 rpm or a crosshead speed of 0.65 mm/min. Practically speaking, this means that it becomes time-consuming to reset the sample grip position for a new test or change sample lengths.

A solution might be to have multiple gearing systems, one for testing and the other for quick position adjustment. The linear actuator is fitted with two linked input shafts. A system that allowed for quickly connecting and disconnecting the two input shafts would allow for high and low gear operation of the linear actuator and could provide more flexibility for repositioning the crosshead.

5.4.11 Automated Analysis Processing

The current method of manually selecting the linear range of the loading and unloading lines was adequate for the preliminary testing under the scope of this thesis, but it introduces some bias error and would take significant amounts of time for more rigorous testing. An automated process for determining the starting and ending points of the Young's modulus calculation range would eliminate any bias error and would reduce processing time. This code might identify regions where the load decreases over a given threshold that would distinguish between general noise and an unloading line. The Young's modulus could then be calculated between an upper stress limit and lower stress limit set as proportions of the stress at the point of unloading. Additionally, feedback from the automated

motor control would provide this system with known unloading start and end points as well.

6 REFERENCES

[1] Bruzzone P., 2006, "30 Years of Conductors for Fusion: A Summary and Perspectives," IEEE Transactions on Applied Superconductivity, **16**(2), pp. 839-844.

[2] Wysokinski K. I., 2011, "Superconductivity-the first 100 years," Physics World, **24**(4).

[3] Ridge O., 1995, "Twenty Years of Cable-in-Conduit Conductors : 1975-1995," Most, **14**(1).

[4] Nijhuis a, Ilyin Y., and Abbas W., 2008, "Axial and transverse stress–strain characterization of the EU dipole high current density Nb 3 Sn strand," Superconductor Science and Technology, **21**(6), p. 065001.

[5] Eijnden N. C. V. D., Nijhuis a, Ilyin Y., Wessel W. a J., and Kate H. H. J. T., 2005, "Axial tensile stress–strain characterization of ITER model coil type Nb 3 Sn strands in TARSIS," Superconductor Science and Technology, **18**(11), pp. 1523-1532.

[6] Harris D. L., 2005, "Characterization of Nb 3 Sn Superconducting Strand Under Pure Bending by," Science, (2003).

[7] Mallon P., 2011, "Characterization of Nb3Sn Superconducting Strands under Wide Range Pure-Bending Strain," Tufts University.

[8] Takayasu M., Chiesa L., Harris D. L., Allegritti A., and Minervini J. V., 2011, "Pure bending strains of Nb 3 Sn wires," Superconductor Science and Technology, **24**(4), p. 045012.

[9] Wang T., 2010, "Stress analysis of transverse load on superconducting Nb 3 Sn strand(s)," Tuft.

[10] Chiesa L., 2009, "Mechanical and electromagnetic transverse load effects on superconducting niobium-tin performance," Massachusetts Institute of Technology.

[11] Chiesa L., 2011, "ME-149 Cryogenics and Superconductivity Fall 2011 LECTURE 14 : London ' s equations and some quantum mechanics effects Type I and Type II superconductors," Cryogenics, pp. 1-20.

[12] Chiesa L., 2011, "ME-149 Cryogenics and Superconductivity Fall 2011 - Lecture 18," Cryogenics.

[13] International Electrotechnical Commission, “WG5 - Nb3Sn – FINAL GNC DRAFT – (080602),” Practice, pp. 1-33.

[14] Osamura K., Nyilas a, Thoener M., Seeber B., Fluekiger R., Ilyin Y., Njihuis a, Ekin J., Clickner C., Walsh R. P., Toplosky V., Shin H., Katagiri K., Ochiai S., Hojo M., Kubo Y., and Miyashita K., 2008, “International round robin test for mechanical properties of Nb 3 Sn superconductive wires at room temperature,” Superconductor Science and Technology, **21**(4), p. 045006.

[15] Katagiri K., Kasaba K., Hojo M., Osamura K., Sugano M., and Kimura A., 2001, “Tensile testing methods of Cu / Nb 3 Sn superconducting wires at room temperature,” Physica C, **360**, pp. 1302-1305.

[16] Nyilas A., Weiss K., Thoener M., Hojo M., and Osamura K., 2012, “On the Measurement of Tensile Properties of Superconducting NB3Sn Wires at Ambient Temperature and at Cryogenic Environment,” **582**(2006).

[17] Ekin J. W., 2006, Experimental Techniques for Low-Temperature Measurements: Cryostat Design, Material Properties, And Superconductor Critical-Current Testing (Google eBook), Oxford University Press.

[18] Nyilas A., 2005, “Strain sensing systems tailored for tensile measurement of fragile wires,” Superconductor Science and Technology, **18**(12), p. S409-S415.

[19] Nyilas A., Engineering C., and Expertise M., 2007, “Documentation of manufacturing practice of high resolution extensometers with working range between 300 K and 1 . 8 K Document 21-11-07 Design The design incorporates the know-how about the materials test procedure . Two examples are given about the diffe,” Advances in Cryogenic Engineering, (November).

[20] Bauer P., Bruzzone P., Portone A., Roth F., Vogel M., Vostner A., and Weiss K., 2007, Review of material properties, past experiences, procedures, issues and results for a possible solder filled cable as Plan B conductor for the EFDA dipole magnet (Draft Vs 1).

[21] Lord J. D., and Morrell R. M., 2010, “Elastic modulus measurement—obtaining reliable data from the tensile test,” Metrologia, **47**(2), p. S41-S49.

Appendix A

The following Appendix shows the shop drawings generated for all the manufactured components of the tensile testing apparatus. The components include both those used for the 2000 lb load cell configuration and the 250 lb load cell configuration.

The shop drawings shown here include those for the following components:

- Connector A
- Connector B
- Dewar Top Plate
- G10 Plate (bottom)
- Pull Rod
- Sample Holder A
- Sample Holder B
- Sample Holder C
- Sample Holder D
- Standoffs
- Support Rods
- Connector B2
- Middle G10 Plate

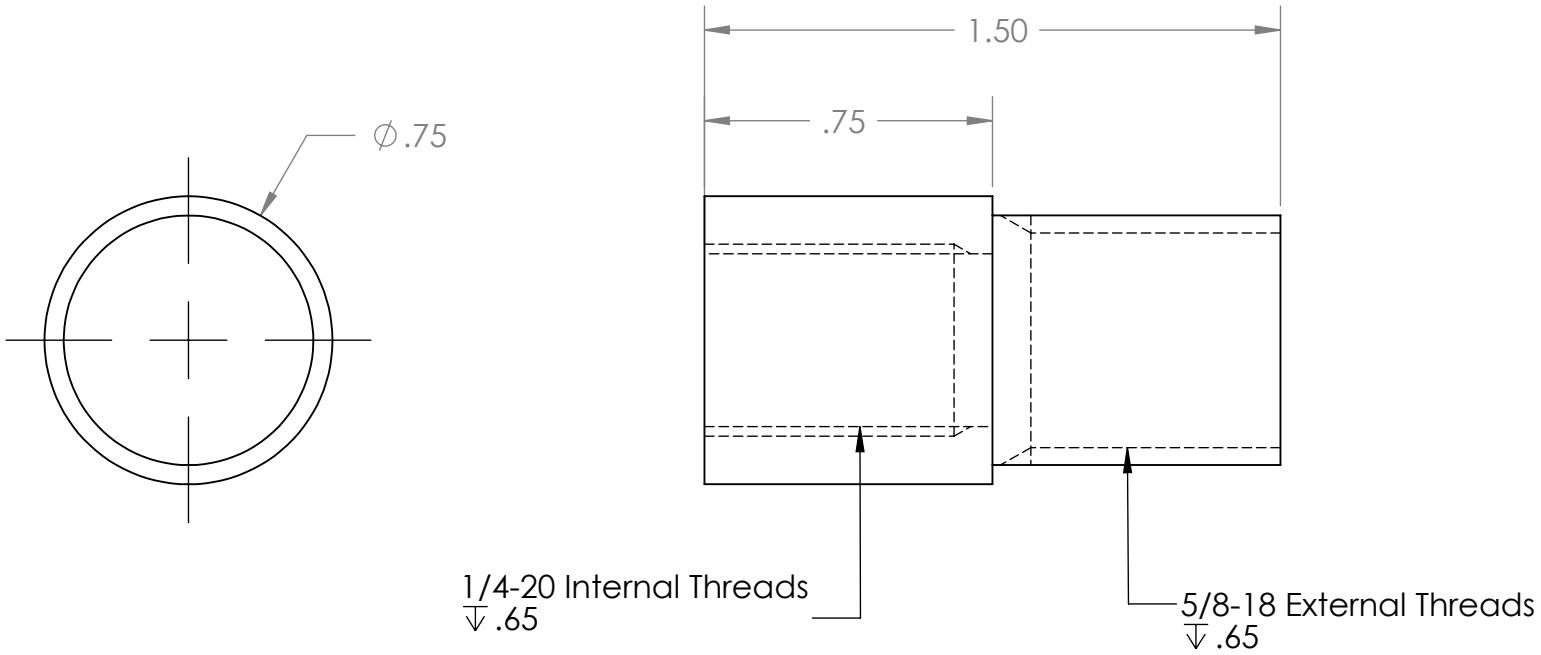

		UNLESS OTHERWISE SPECIFIED:		NAME	DATE
		DIMENSIONS ARE IN INCHES TOLERANCES: FRACTIONAL ± ANGULAR: MACH ± BEND ± TWO PLACE DECIMAL ± THREE PLACE DECIMAL ±	DRAWN		
			CHECKED		
			ENG APPR.		
			MFG APPR.		
		INTERPRET GEOMETRIC TOLERANCING PER:	Q.A.		
		MATERIAL SS 316	COMMENTS:		
NEXT ASSY	USED ON	FINISH			
APPLICATION		DO NOT SCALE DRAWING			

TITLE:

SIZE	DWG. NO.	REV
A	Connector_A	
SCALE: 2:1	WEIGHT:	SHEET 1 OF 1

5 4 3 2 1

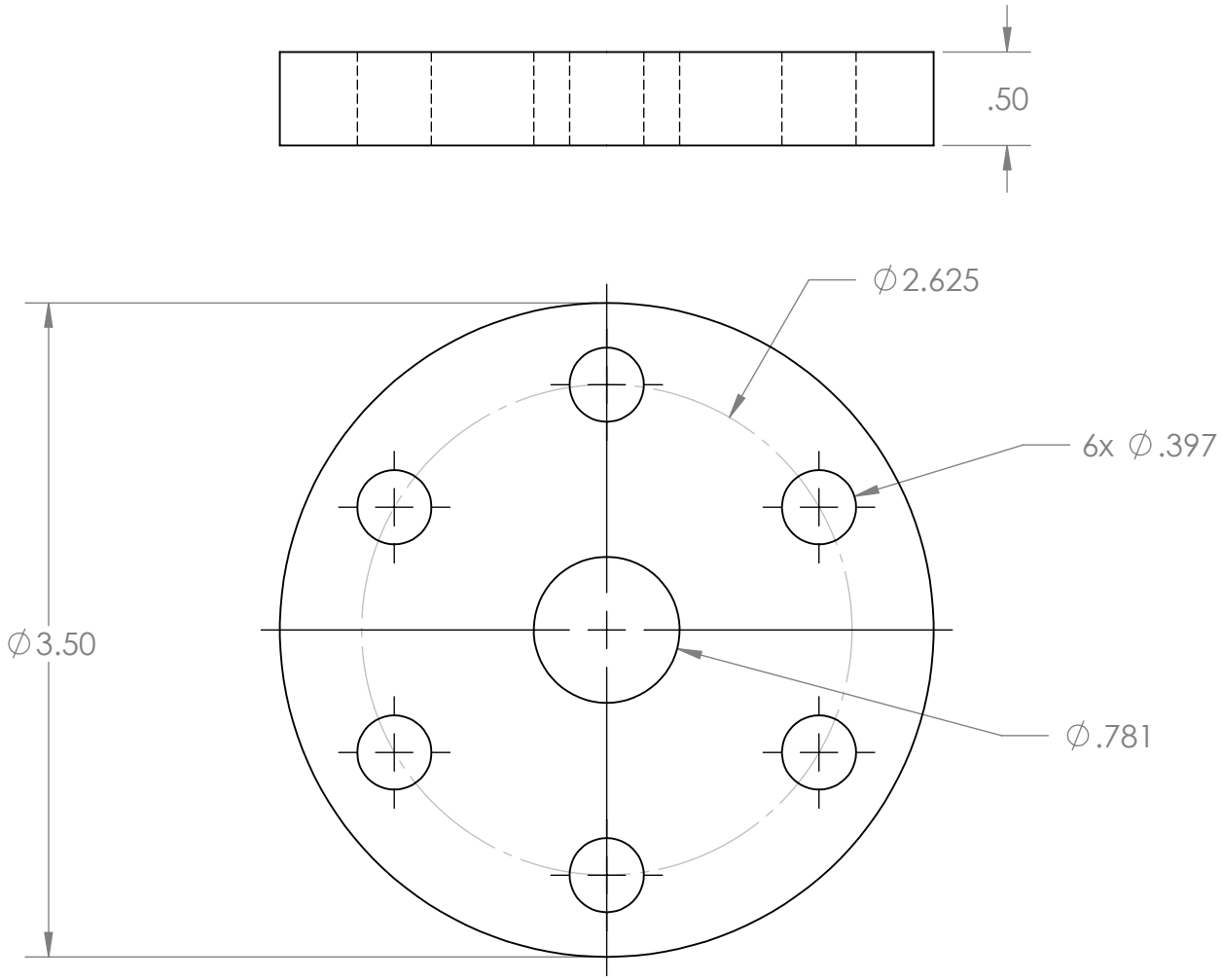

		UNLESS OTHERWISE SPECIFIED:		NAME	DATE
		DIMENSIONS ARE IN INCHES TOLERANCES: FRACTIONAL ± ANGULAR: MACH ± BEND ± TWO PLACE DECIMAL ± THREE PLACE DECIMAL ±	DRAWN		
			CHECKED		
			ENG APPR.		
			MFG APPR.		
		INTERPRET GEOMETRIC TOLERANCING PER:	Q.A.		
		MATERIAL G10 Epoxy	COMMENTS:		
NEXT ASSY	USED ON	FINISH			
APPLICATION		DO NOT SCALE DRAWING			

TITLE:

SIZE	DWG. NO.	REV
A	Connector_B	1

SCALE: 1:2	WEIGHT:	SHEET 1 OF 1

5 4 3 2 1

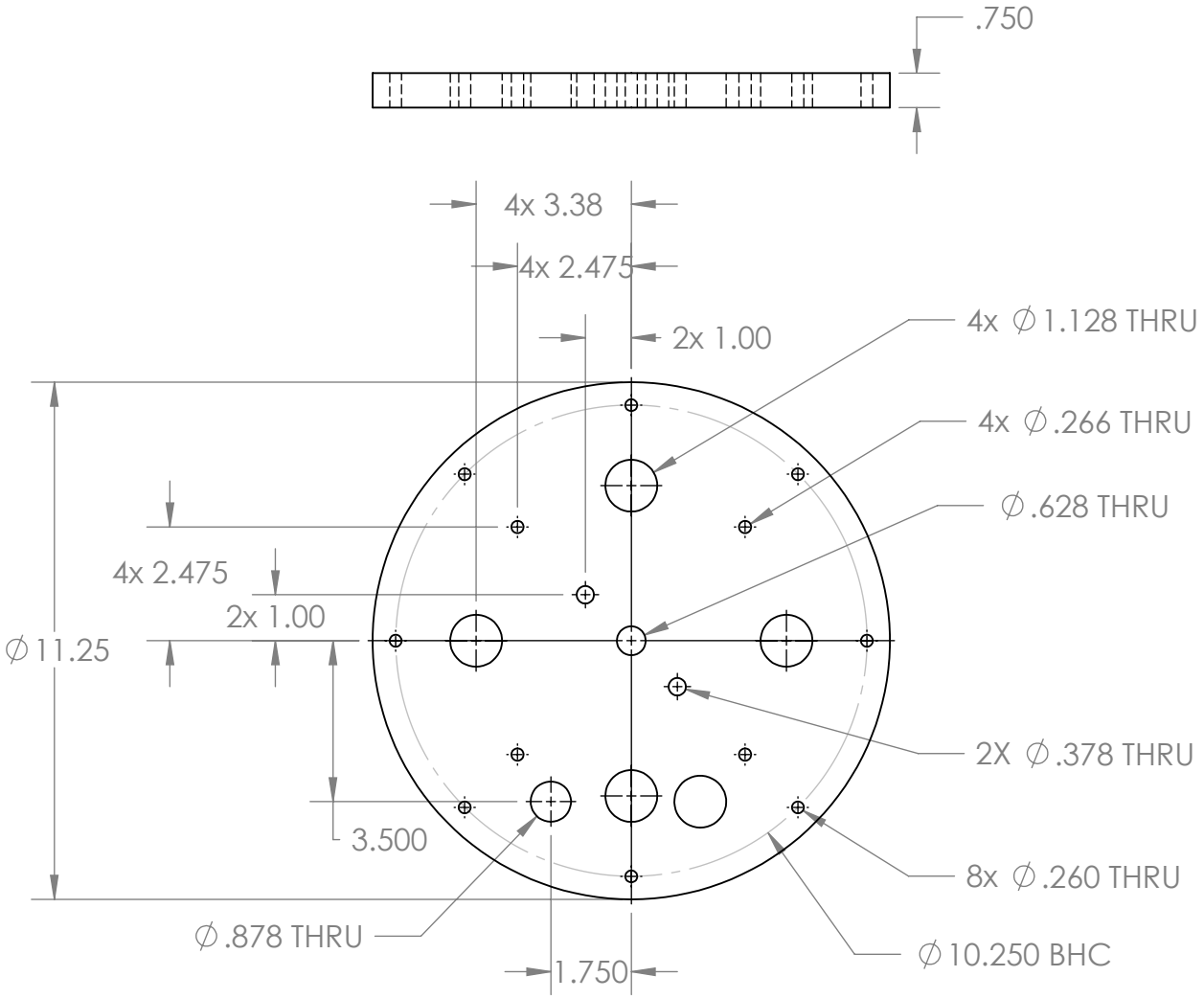

		UNLESS OTHERWISE SPECIFIED:		NAME	DATE
		DIMENSIONS ARE IN INCHES TOLERANCES: FRACTIONAL ± ANGULAR: MACH ± BEND ± TWO PLACE DECIMAL ± THREE PLACE DECIMAL ±	DRAWN		
			CHECKED		
			ENG APPR.		
			MFG APPR.		
		INTERPRET GEOMETRIC TOLERANCING PER:	Q.A.		
		MATERIAL G10 Epoxy	COMMENTS:		
NEXT ASSY	USED ON	FINISH			
APPLICATION		DO NOT SCALE DRAWING			

TITLE:

SIZE	DWG. NO.	REV
A	Dewar Top Plate	2

SCALE: 1:5 | WEIGHT: | SHEET 1 OF 1

5 4 3 2 1

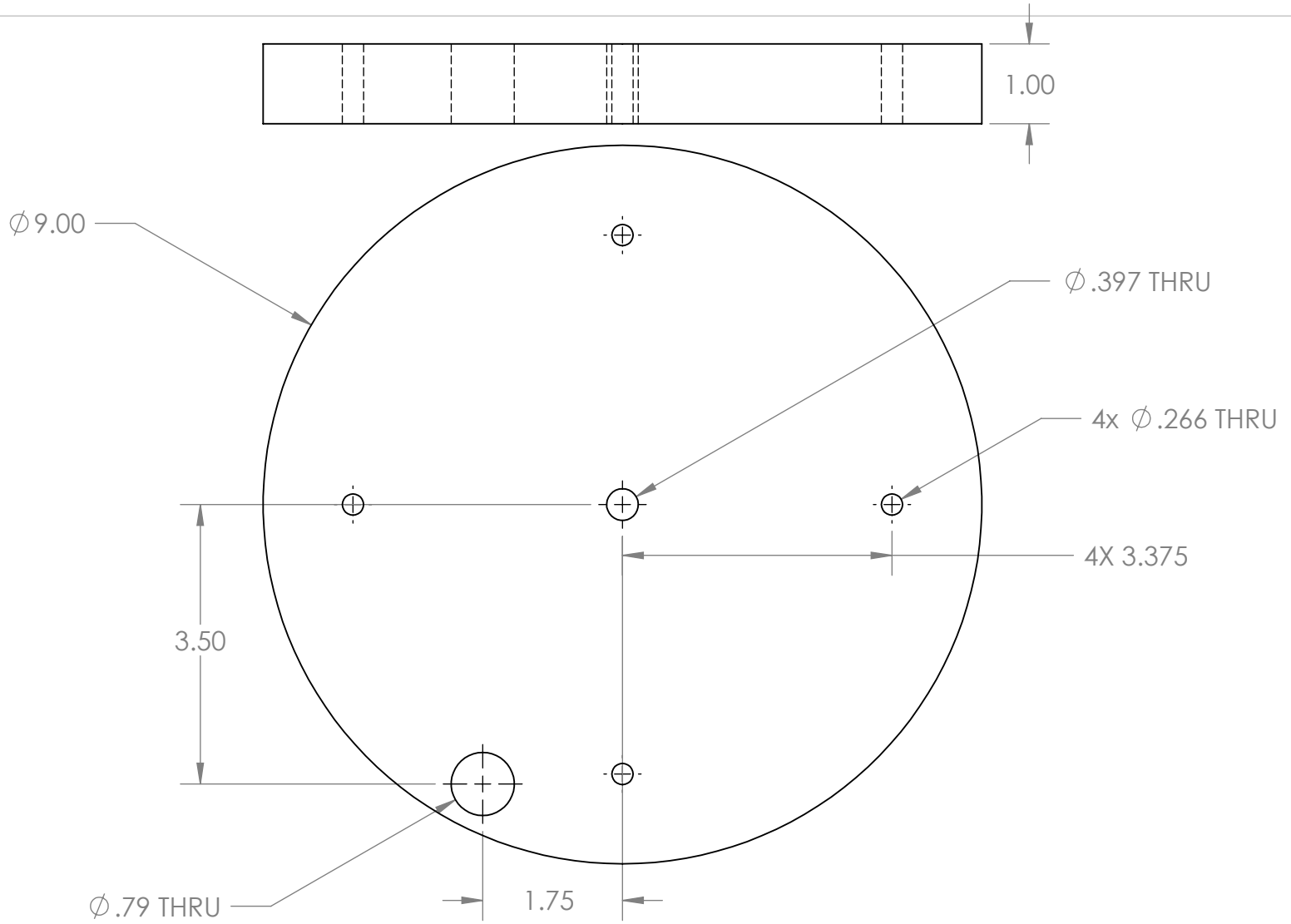

		UNLESS OTHERWISE SPECIFIED:		NAME	DATE
		DIMENSIONS ARE IN INCHES TOLERANCES: FRACTIONAL ± ANGULAR: MACH ± BEND ± TWO PLACE DECIMAL ± THREE PLACE DECIMAL ±	DRAWN		
			CHECKED		
			ENG APPR.		
			MFG APPR.		
		INTERPRET GEOMETRIC TOLERANCING PER:	Q.A.		
		MATERIAL G10 Epoxy	COMMENTS:		
NEXT ASSY	USED ON	FINISH			
APPLICATION		DO NOT SCALE DRAWING			

TITLE:

SIZE	DWG. NO.	REV
A	G10 Plate	2
SCALE: 1:2	WEIGHT:	SHEET 1 OF 1

5 4 3 2 1

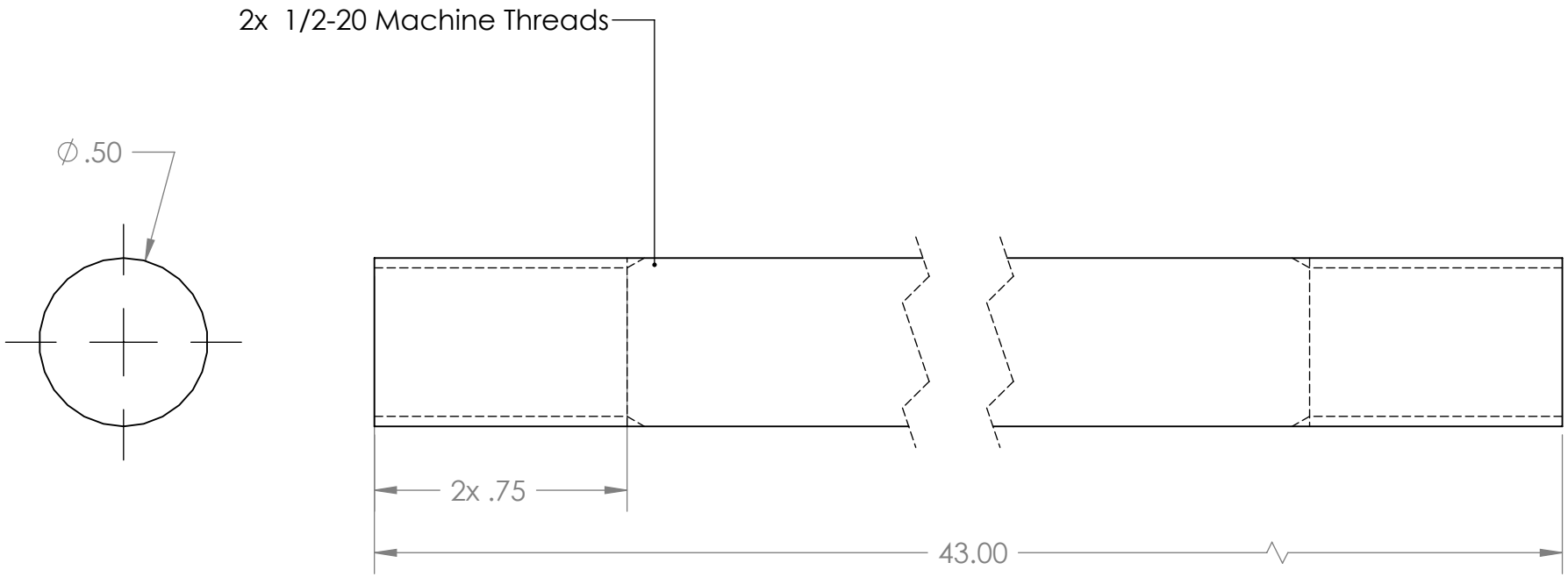

		UNLESS OTHERWISE SPECIFIED:		NAME	DATE
		DIMENSIONS ARE IN INCHES TOLERANCES: FRACTIONAL ± ANGULAR: MACH ± BEND ± TWO PLACE DECIMAL ± THREE PLACE DECIMAL ±	DRAWN		
			CHECKED		
			ENG APPR.		
			MFG APPR.		
		INTERPRET GEOMETRIC TOLERANCING PER:	Q.A.		
		MATERIAL SS 316	COMMENTS:		
NEXT ASSY	USED ON	FINISH			
APPLICATION		DO NOT SCALE DRAWING			

TITLE:

SIZE	DWG. NO.	REV
A	Pull Rod	1
SCALE: 1:10	WEIGHT:	SHEET 1 OF 1

5 4 3 2 1

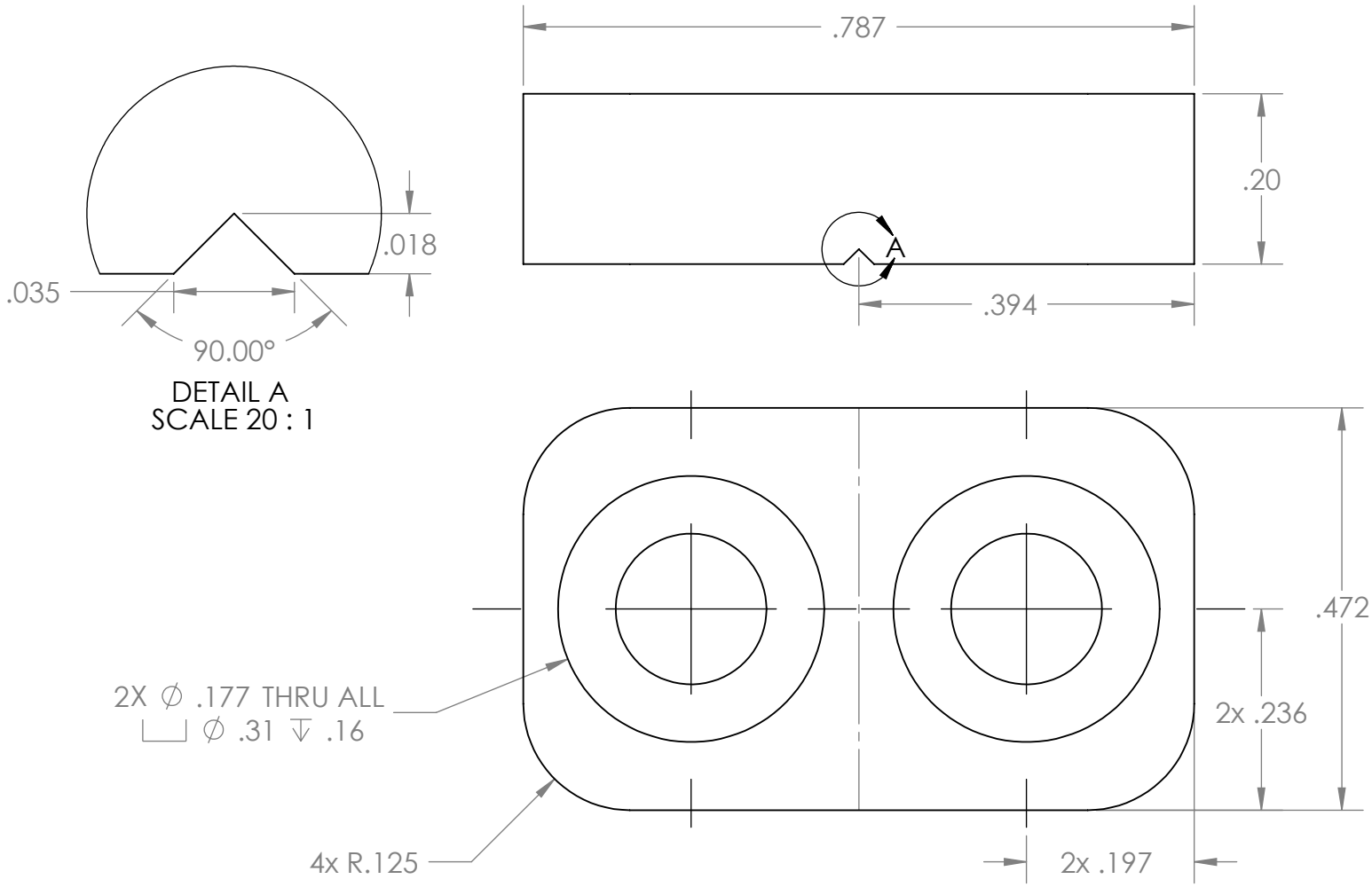

		UNLESS OTHERWISE SPECIFIED:		NAME	DATE
		DIMENSIONS ARE IN INCHES TOLERANCES: FRACTIONAL ± ANGULAR: MACH ± BEND ± TWO PLACE DECIMAL ± THREE PLACE DECIMAL ±	DRAWN		
			CHECKED		
			ENG APPR.		
			MFG APPR.		
		INTERPRET GEOMETRIC TOLERANCING PER:	Q.A.		
		MATERIAL SS 316	COMMENTS: Qty: 2		
NEXT ASSY	USED ON	FINISH			
APPLICATION		DO NOT SCALE DRAWING			

TITLE:

SIZE	DWG. NO.	REV
A	Sample Holder A	2
SCALE: 5:1	WEIGHT:	SHEET 1 OF 1

5 4 3 2 1

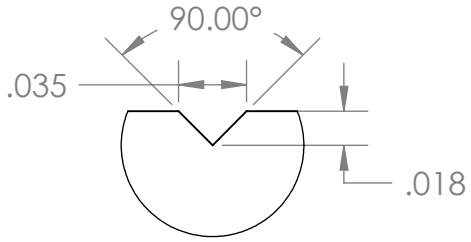

DETAIL A
SCALE 10 : 1

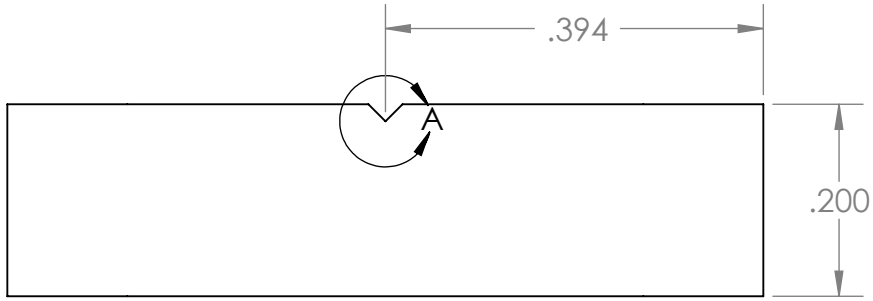

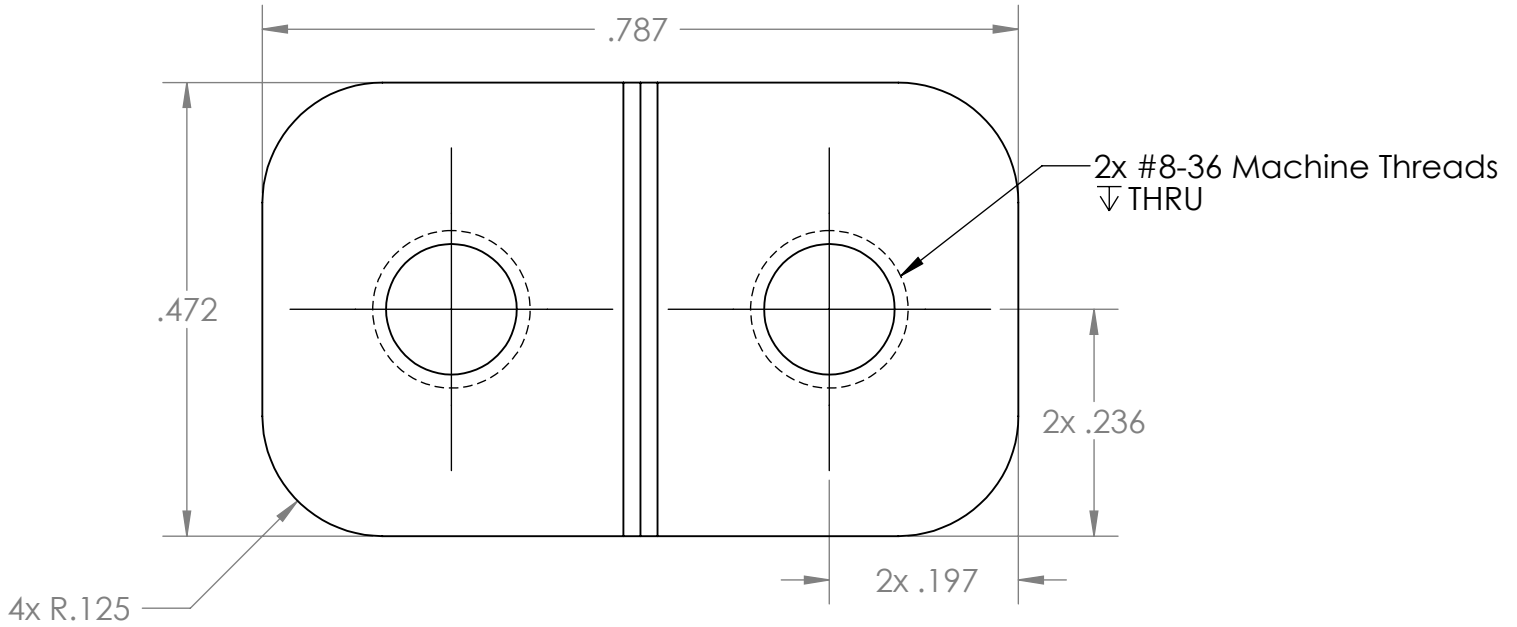

		UNLESS OTHERWISE SPECIFIED:		NAME	DATE
		DIMENSIONS ARE IN INCHES TOLERANCES: FRACTIONAL ± ANGULAR: MACH ± BEND ± TWO PLACE DECIMAL ± THREE PLACE DECIMAL ±	DRAWN		
			CHECKED		
			ENG APPR.		
			MFG APPR.		
		INTERPRET GEOMETRIC TOLERANCING PER:	Q.A.		
		MATERIAL SS 316	COMMENTS:		
NEXT ASSY	USED ON	FINISH			
APPLICATION		DO NOT SCALE DRAWING			

TITLE:

SIZE	DWG. NO.	REV
A	Sample Holder B	1

SCALE: 5:1	WEIGHT:	SHEET 1 OF 1

5 4 3 2 1

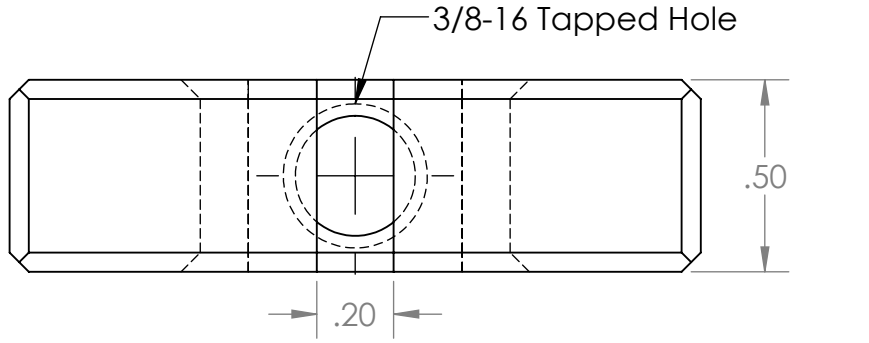

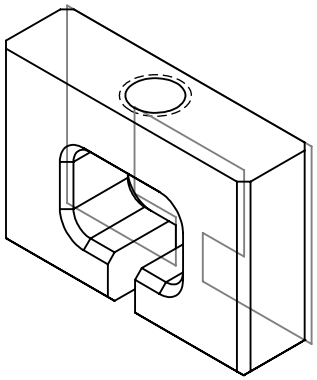

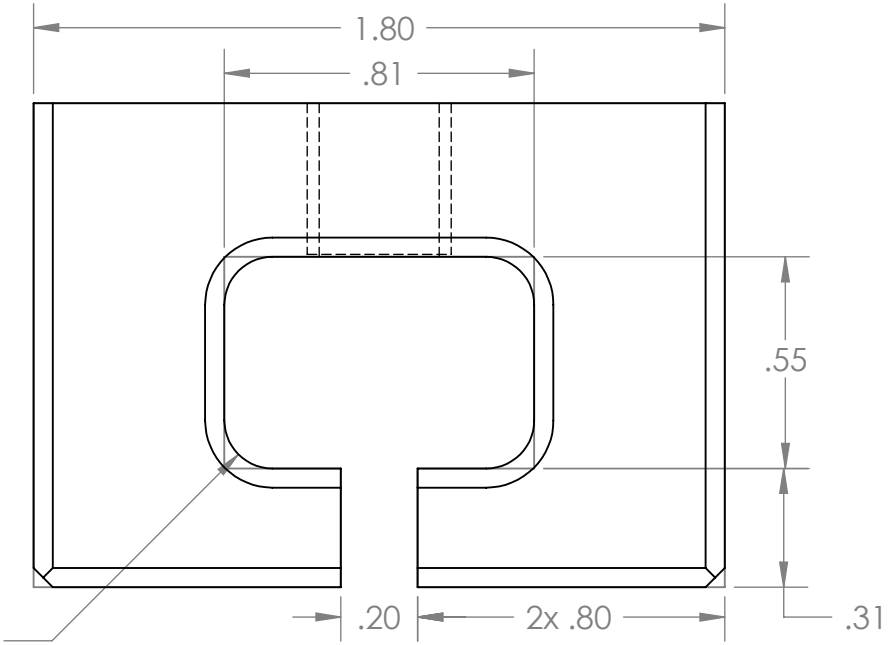

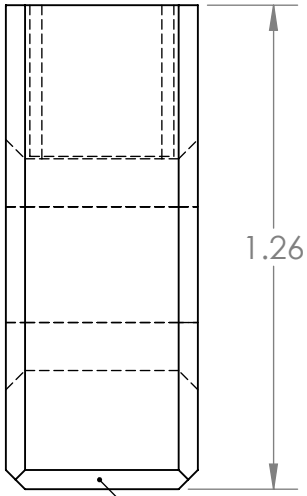

		UNLESS OTHERWISE SPECIFIED:		NAME	DATE
		DIMENSIONS ARE IN INCHES TOLERANCES: FRACTIONAL ± ANGULAR: MACH ± BEND ± TWO PLACE DECIMAL ± THREE PLACE DECIMAL ±	DRAWN		
			CHECKED		
			ENG APPR.		
			MFG APPR.		
		INTERPRET GEOMETRIC TOLERANCING PER:	Q.A.		
		MATERIAL SS 316	COMMENTS:		
NEXT ASSY	USED ON	FINISH			
APPLICATION		DO NOT SCALE DRAWING			

TITLE:

SIZE	DWG. NO.	REV
A	Sample Holder C	1
SCALE: 2:1	WEIGHT:	SHEET 1 OF 1

5 4 3 2 1

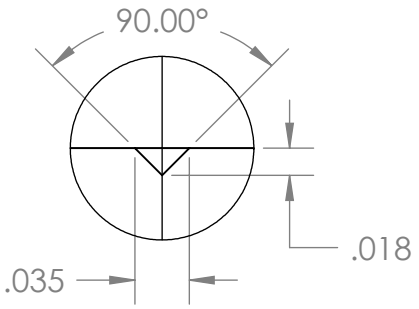

DETAIL A
SCALE 8 : 1

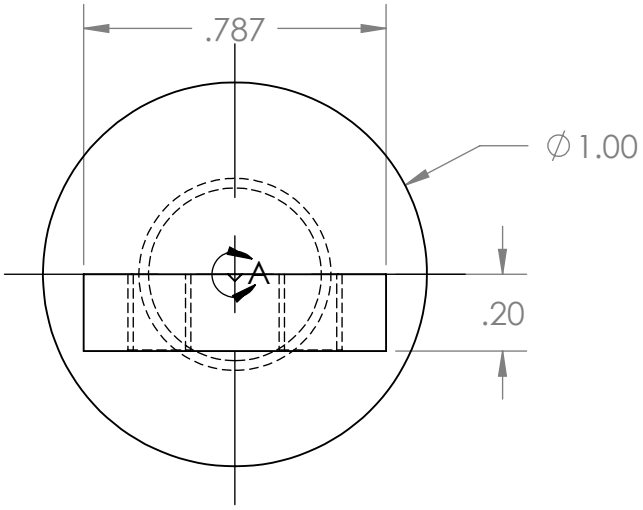

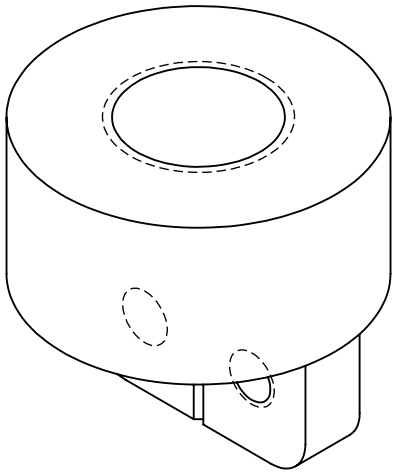

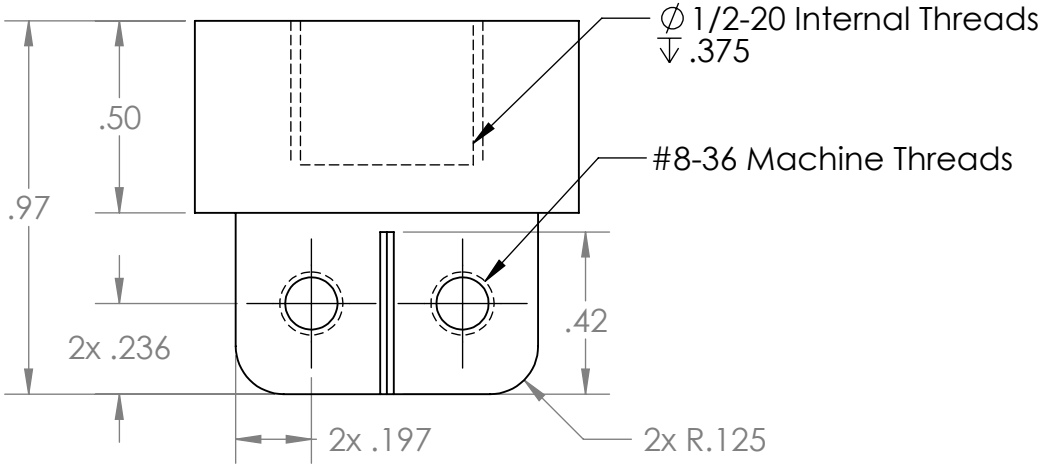

		UNLESS OTHERWISE SPECIFIED:		NAME	DATE
		DIMENSIONS ARE IN INCHES TOLERANCES: FRACTIONAL ± ANGULAR: MACH ± BEND ± TWO PLACE DECIMAL ± THREE PLACE DECIMAL ±	DRAWN		
			CHECKED		
			ENG APPR.		
			MFG APPR.		
		INTERPRET GEOMETRIC TOLERANCING PER:	Q.A.		
		MATERIAL SS 316	COMMENTS:		
NEXT ASSY	USED ON	FINISH			
APPLICATION		DO NOT SCALE DRAWING			

TITLE:

SIZE	DWG. NO.	REV
A	Sample Holder D	1
SCALE: 2:1	WEIGHT:	SHEET 1 OF 1

5 4 3 2 1

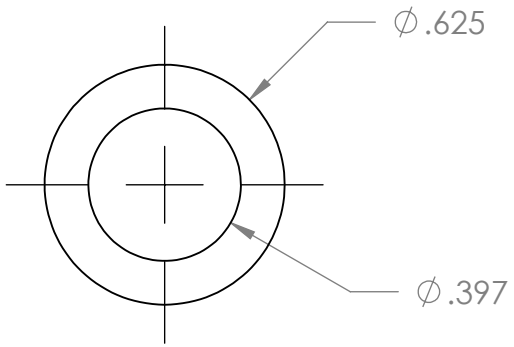

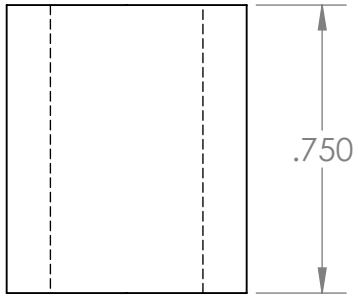

		UNLESS OTHERWISE SPECIFIED:		NAME	DATE
		DIMENSIONS ARE IN INCHES TOLERANCES: FRACTIONAL ± ANGULAR: MACH ± BEND ± TWO PLACE DECIMAL ± THREE PLACE DECIMAL ±	DRAWN		
			CHECKED		
			ENG APPR.		
			MFG APPR.		
		INTERPRET GEOMETRIC TOLERANCING PER:	Q.A.		
		MATERIAL SS 316	COMMENTS: Qty: 6		
NEXT ASSY	USED ON	FINISH			
APPLICATION		DO NOT SCALE DRAWING			

TITLE:

SIZE	DWG. NO.	REV
A	Standoff	
SCALE: 2:1	WEIGHT:	SHEET 1 OF 1

5 4 3 2 1

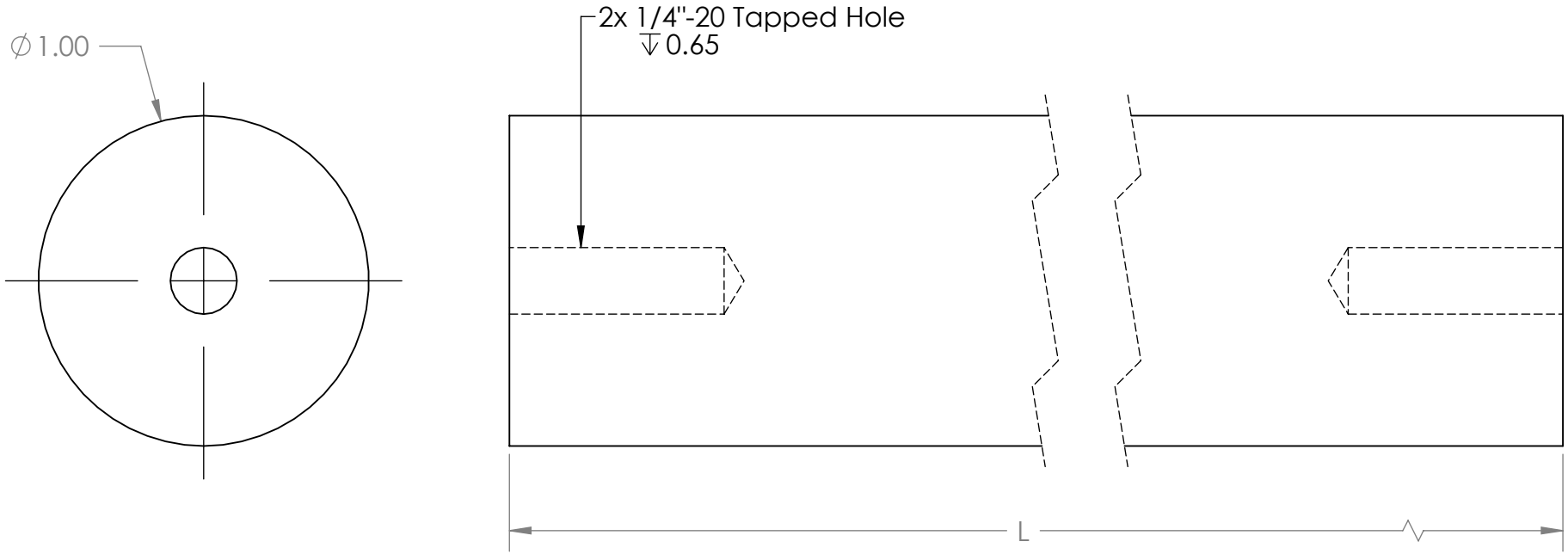

L [in.]	
Configuration 1	9.5
Configuration 2	58.0

		UNLESS OTHERWISE SPECIFIED:		NAME	DATE
		DIMENSIONS ARE IN INCHES TOLERANCES: FRACTIONAL ± ANGULAR: MACH ± BEND ± TWO PLACE DECIMAL ± THREE PLACE DECIMAL ±	DRAWN		
			CHECKED		
			ENG APPR.		
			MFG APPR.		
		INTERPRET GEOMETRIC TOLERANCING PER:	Q.A.		
		MATERIAL SS 316	COMMENTS: Qty: 4 ea.		
NEXT ASSY	USED ON	FINISH			
APPLICATION		DO NOT SCALE DRAWING			

TITLE:

SIZE	DWG. NO.	REV
A	Support Rod	1
SCALE: 1:5	WEIGHT:	SHEET 1 OF 1

5 4 3 2 1

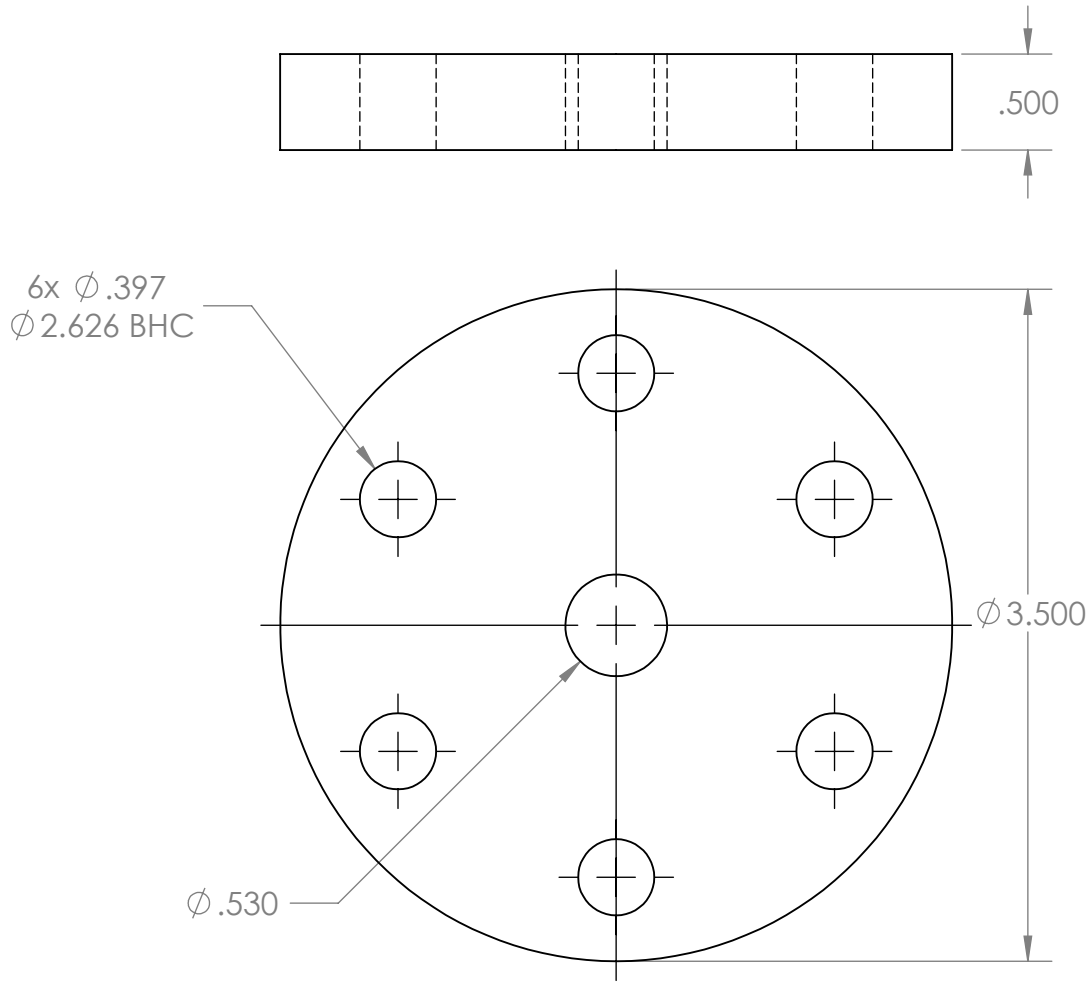

		UNLESS OTHERWISE SPECIFIED:		NAME	DATE
		DIMENSIONS ARE IN INCHES TOLERANCES: FRACTIONAL ± ANGULAR: MACH ± BEND ± TWO PLACE DECIMAL ± THREE PLACE DECIMAL ±	DRAWN		
			CHECKED		
			ENG APPR.		
			MFG APPR.		
		INTERPRET GEOMETRIC TOLERANCING PER:	Q.A.		
		MATERIAL G10 Fiberglass Epoxy	COMMENTS:		
NEXT ASSY	USED ON	FINISH			
APPLICATION		DO NOT SCALE DRAWING			

TITLE:

SIZE	DWG. NO.	REV
A	Connector_B2	
SCALE: 1:2	WEIGHT:	SHEET 1 OF 1

5 4 3 2 1

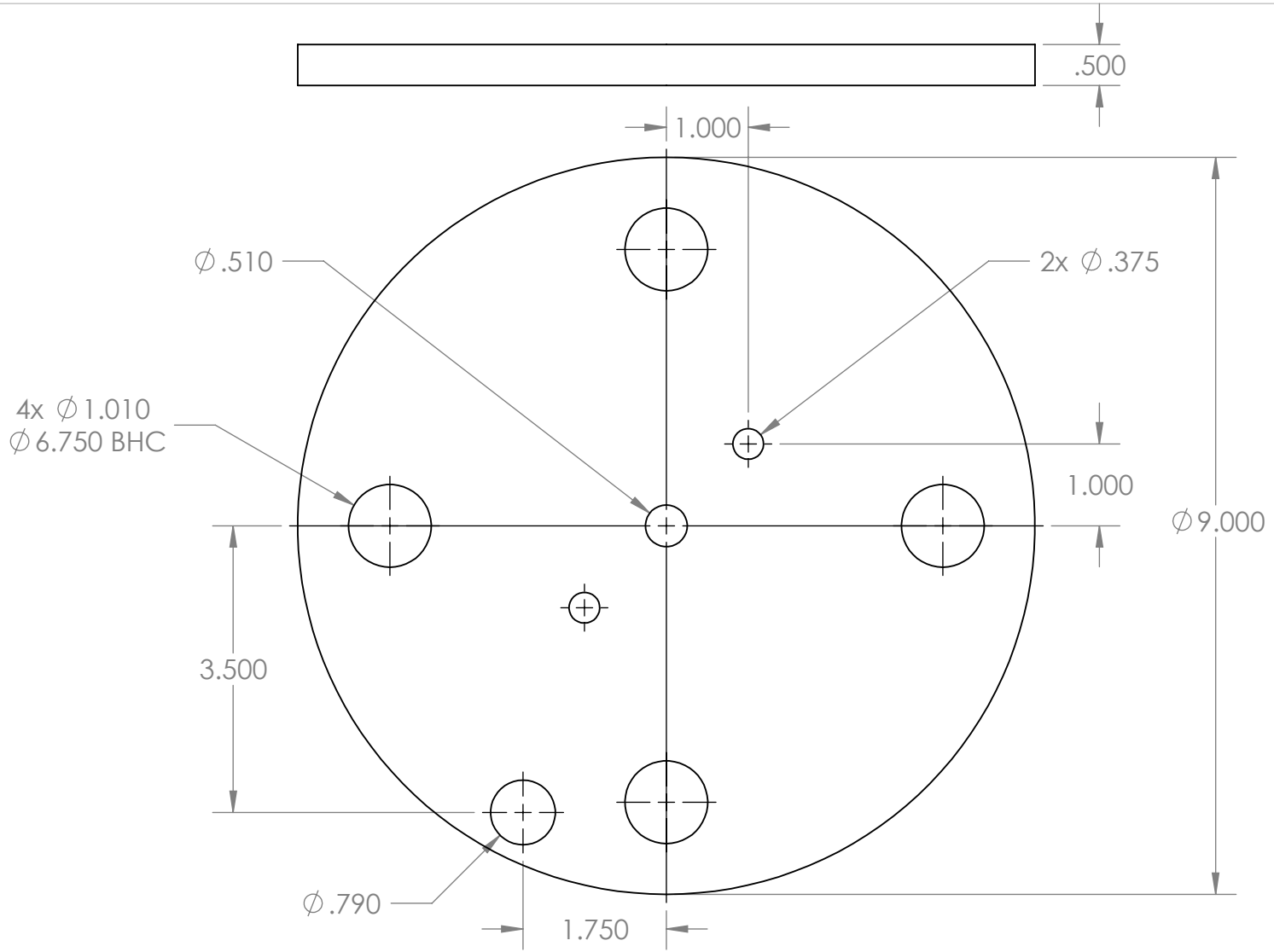

		UNLESS OTHERWISE SPECIFIED:		NAME	DATE
		DIMENSIONS ARE IN INCHES TOLERANCES: FRACTIONAL ± ANGULAR: MACH ± BEND ± TWO PLACE DECIMAL ± THREE PLACE DECIMAL ±	DRAWN		
			CHECKED		
			ENG APPR.		
			MFG APPR.		
		INTERPRET GEOMETRIC TOLERANCING PER:	Q.A.		
		MATERIAL G10 Fiberglass Epoxy	COMMENTS:		
NEXT ASSY	USED ON	FINISH			
APPLICATION		DO NOT SCALE DRAWING			

TITLE:

SIZE **A** | DWG. NO. Mid. G10 Plate | REV

SCALE: 1:5 | WEIGHT: | SHEET 1 OF 1

5 4 3 2 1